THE UNIVERSITY
OF QUEENSLAND
AUSTRALIA

MINE4123:

Mining Research Project II

Final Thesis (Revised):

Influence of Geotechnical Properties on the Run-out Process at Bingham Canyon Slope Failure

Commissioned by: Prof. Marc Ruest

Course Coordinator: Dr. Christopher Leonardi

Date of Submission: 08th November 2016

Submitted by: Alfred Septian

UQ Supervisor: Marcelo Llano Serna

ACKNOWLEDGEMENTS

I would like to express the deepest gratitude to my advisor Marcelo Llano Serna for his full dedication, to support, commit, expert guidance, understanding and encouragement throughout my study and research. Without his incredible patience, commitment, and timely wisdom and counsel, my thesis work would have been a frustrating, time consuming, and overwhelming pursuit. Also, I express my appreciation to Prof. Marc Ruest for providing me with this astounding thesis project, for the potential breakthrough of the thesis that I undertake this year. His time was valued greatly.

Finally, I would like to thank my parents, and peers for their unconditional love and support during this year upon completing my thesis. I would not have been able to complete this thesis without their constant love and encouragement.

SUMMARY

The Bingham Canyon Mine is located approximately 30 km south-west of Salt Lake City in Utah, USA. Bingham Canyon mine is located at Oquirrh Mountains at late Palaeozoic period (between 260 and 320 million years ago). Bingham Canyon Mine dependent on hydrothermally altered and mineralised plutonic body referred to as Bingham Stock. The mineralisation that formed the deposit is mainly chalcopyrite and bornite.

The Kennecott failure occurred on the 10th of April 2013. The first event happened at 03:30 am UT from the middle bench of the mine, where infrastructures located. The second event occured at 05:56 am UT from the top bench of the pit. There are no casualties in both events. However, there are damaged trucks even with the predicted run-out before the event take place. This project covers mainly on numerical analysis using a tridimensional limit equilibrium method to define suitable failure surfaces and later the Material Point Method (MPM) to describe the kinematics of the landslide.

The relevance of this analysis relies on the potential of defining a framework of actions that may give insights on the preparation to attend the operative needs in a failed slope and mitigate its adverse effects. The volumes of the first failure are approximately 24Mm3 volumes with 0.98 for FOS with 3D Bishop's search method. The volumes of the second failure are approximately 22Mm3 volumes with 0.89 for FOS with 3D Bishop's search method. In comparison, the second failure gives lower FOS rather than the first one due to some of the mass that move from the first failure acted as support for the mass that moved at the second failure.

Kinetic energy of the first slide shows a decrease value at t=40s. It is suspected that the failure material points hit the pit wall that causes the material points to change direction throughout the run-out. The kinetic energy of the second slide is constant throughout the event due to the path that created by the first slide cause the failure path to be smoother. Same behaviour occurred with the velocity analysis for both first and second failure, and it is in close agreement with two-dimensional and LFH past research. Sensitivity analysis was conducted by changing the geotechnical properties of the failure surfaces to observed the changes that will affect the run-out of the landslide. A tridimensional approach is able to describe better due to complex topography than two-dimensional simplifications. The numerical analysis used to give insight in predicting the possible failure that might occur on site, to help assess the risk assessment and safety.

STATEMENT OF ORIGINALITY

I hereby declare that this research project proposal is my own work and that it contains, to the best of my knowledge and belief, no material previously published or written work by another person nor material which to a substantial extent has been submitted for another course, except where due acknowledgement is made in the report.

Signed,

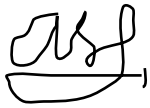

Alfred Septian

TABLE OF CONTENTS

LIST OF FIGURES

LIST OF TABLES

1. INTRODUCTION

1.1. AIMS AND OBJECTIVES

Numerical simulation of the run-out process observed on the 10th of April 2013 due to two slope failures in the pit wall failures at Bingham Canyon mine. The specific aims and objectives of this project derived from the following:

- comprehensive understanding of the historical background of Bingham Canyon mine;
- understand the mechanism and consequences of the landslides that occurred in Bingham Canyon mine;
- gathering the necessary geological and geotechnical information of Bingham Canyon mine;
- literature review;
- define a suitable geotechnical model of the Bingham Canyon failed slope;
- calculate tridimensional failure surface using the software Scoops3D and compare the results with available technical and scientific results;
- using the output from Scoop3D, define a Material Point Method model to simulate the run-out process;
- calibration of the numerical model to improve the accuracy;
- measurement of the kinetic energy that released in the numerical model; and
- study of the geotechnical properties and its influence in the kinematics of the landslide.

1.2. SCOPE

This project will cover mainly on numerical analysis using a tridimensional limit equilibrium method to define suitable failure surfaces and later the Material Point Method (MPM) to describe the kinematics of the landslide. MPM methods mainly derived from a continuum mechanics framework that allows the use of conventional geotechnical constitutive models. The idea is to model the large deformations produced in the run-out process at the Bingham Canyon slope

failure to quantify run-out distance, energy release, and maximum velocity. Furthermore, we will analyse the influence of geotechnical conditions of the slope and its influence in the kinematics of the failure.

1.3. SIGNIFICANCE AND RELEVANCE TO INDUSTRY

A sophisticated network of geotechnical monitors showed the instability at the mine. Later, the monitors showed an increasing displacement and all employees were evacuated from the mine. However, the underestimation of the effects brought, therefore, the loss of important excavation equipment as shown in Figure 1. The relevance of this kind of analysis relies on the potential of defining a framework of actions that may give insights on the preparation to attend the operative needs in a failed slope and mitigate its negative effects.

Figure 1. After effect on excavation equipment

1.4. BACKGROUND

The Bingham Canyon Mine is located approximately 30 km south-west of Salt Lake City in Utah, USA. The location of the mine can be depicted in Figure 2.

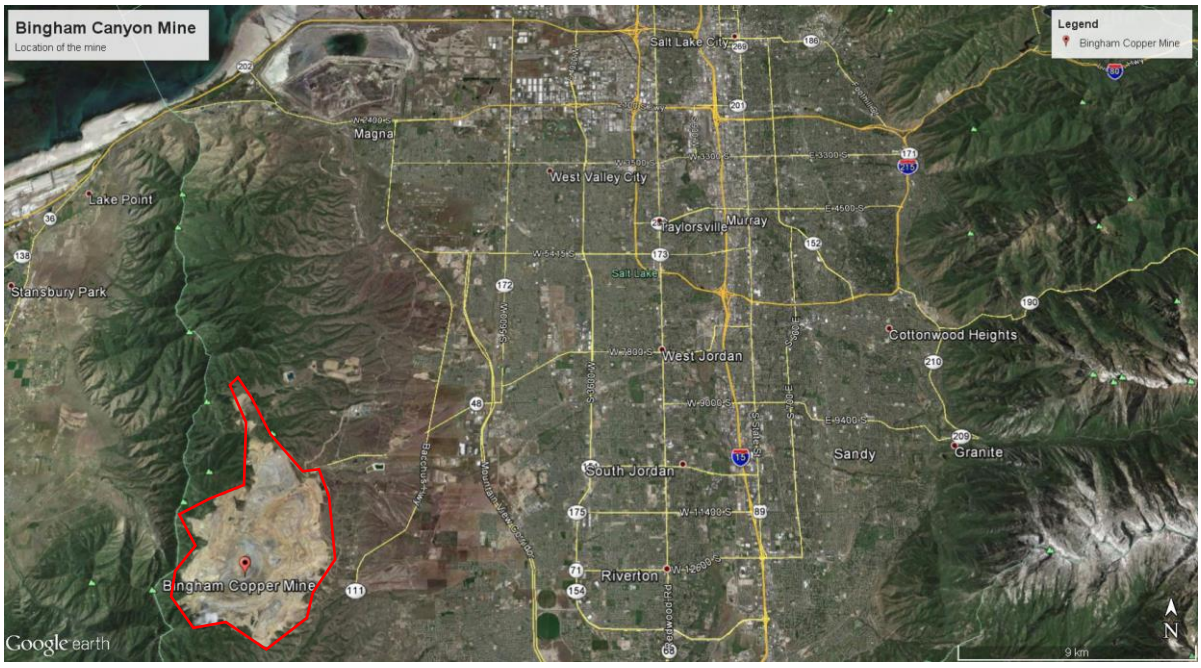

Figure 2. Location of Bingham Canyon mine (Google Earth, 2016)

Rio Tinto (2009) has summarised the brief history of the Bingham Canyon Mine as the following:

- Bingham Canyon was founded in 1848 by the Bingham brothers, Thomas and Sanford with no mining experience;
- Utah first mining district was established the soldiers who were stationed and explored the Canyon in 1863;
- In 1903, the Utah Copper Company was formed to develop the mine, based on the recommendations of Mr. Jackling and Mr. Gemmell and;
- The first steam shovels began operation at the main Canyon in 1906.

1.4.1. Geology

Bingham Canyon mine is located at Oquirrh Mountains at late Palaeozoic period (between 260 and 320 million years ago). Bingham Canyon Mine dependent on hydrothermally altered and mineralised plutonic body referred to as Bingham Stock (Lanier et al, 1978). The deposit that formed is the porphyry deposit that forms many important resources such as copper, gold, and silver. The mineralisation that formed the deposit is mainly chalcopyrite and bornite. The igneous rocks formed in Bingham Canyon is a product of an epizonal intrusion, which gives a maximum cover of approximately 2700 m (Gruen, Heinrich & Shroeder, 2010). Many intrusions are vented showing give volcanic materials on the eastern side of Oquirrh range. Consequently, the configuration is mainly composed by monzonitic and quartz.

At the southern part, sedimentary rocks are being formed and can be categorised by the forming of large feldspathic orthoquartzites and calcaneous quartzites at the host rock. At the upper members, many quartzite compositions are also formed with fewer limestone compositions as shown in Figure 3. Faults, fractures, joints, are abundant in Bingham Canyon Mine (Hume, 1983). The oldest fault in the district is west to north-west striking normal faults. Furthermore, there is folding occurrence at the southern part of Oquirrh Mountains. These folds can be characterised by large, open, asymmetric anticlines, and synclines striking north-west.

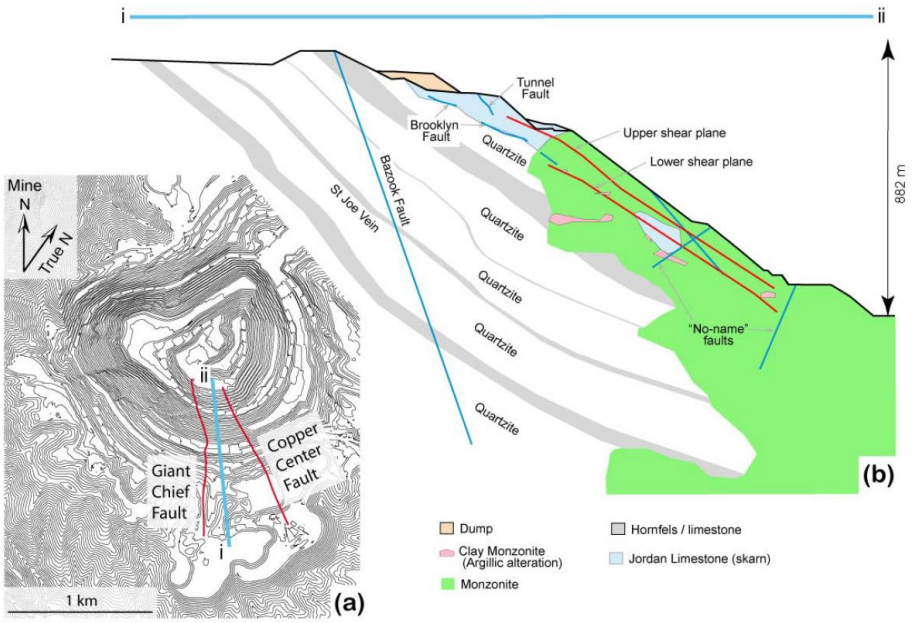

Figure 3. CROSS-SECTION of Bingham Canyon mine (Styles et al, 2011)

As shown in Figure 4, the syncline is more dominant that strikes at 310º, plunging at 12º, and in direction of 315º (Landtwing et al, 2010). As the main aim of this project is not on the geological perspectives, further research is recommended for the further understanding of the geology.

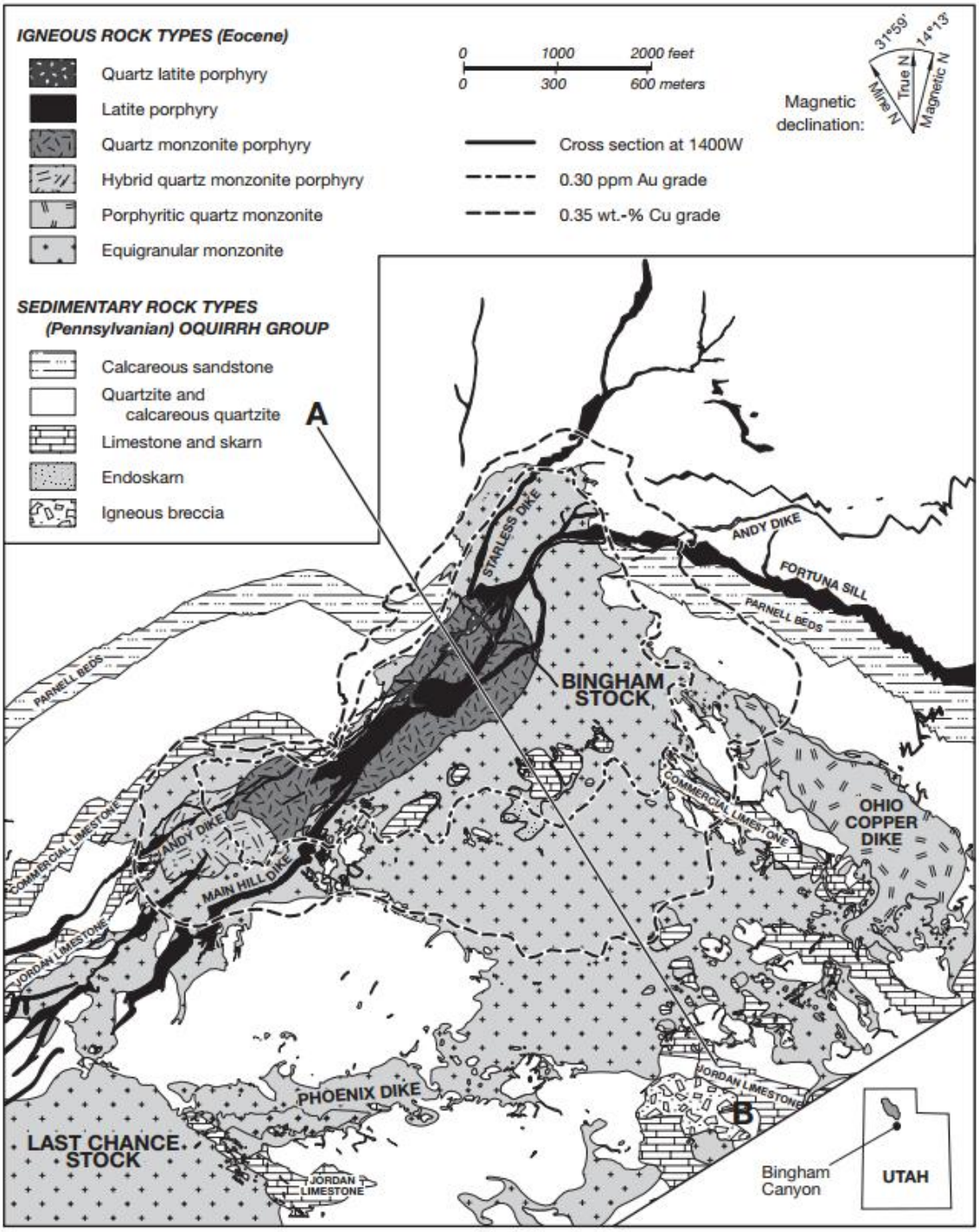

Figure 4. General structural geology and location of Bingham Canyon mine (Landtwing et al, 2010)

Northwest-southeast cross section gives more detailed information on the geological and deposits information at Bingham Canyon mine as shown in Figure 5.

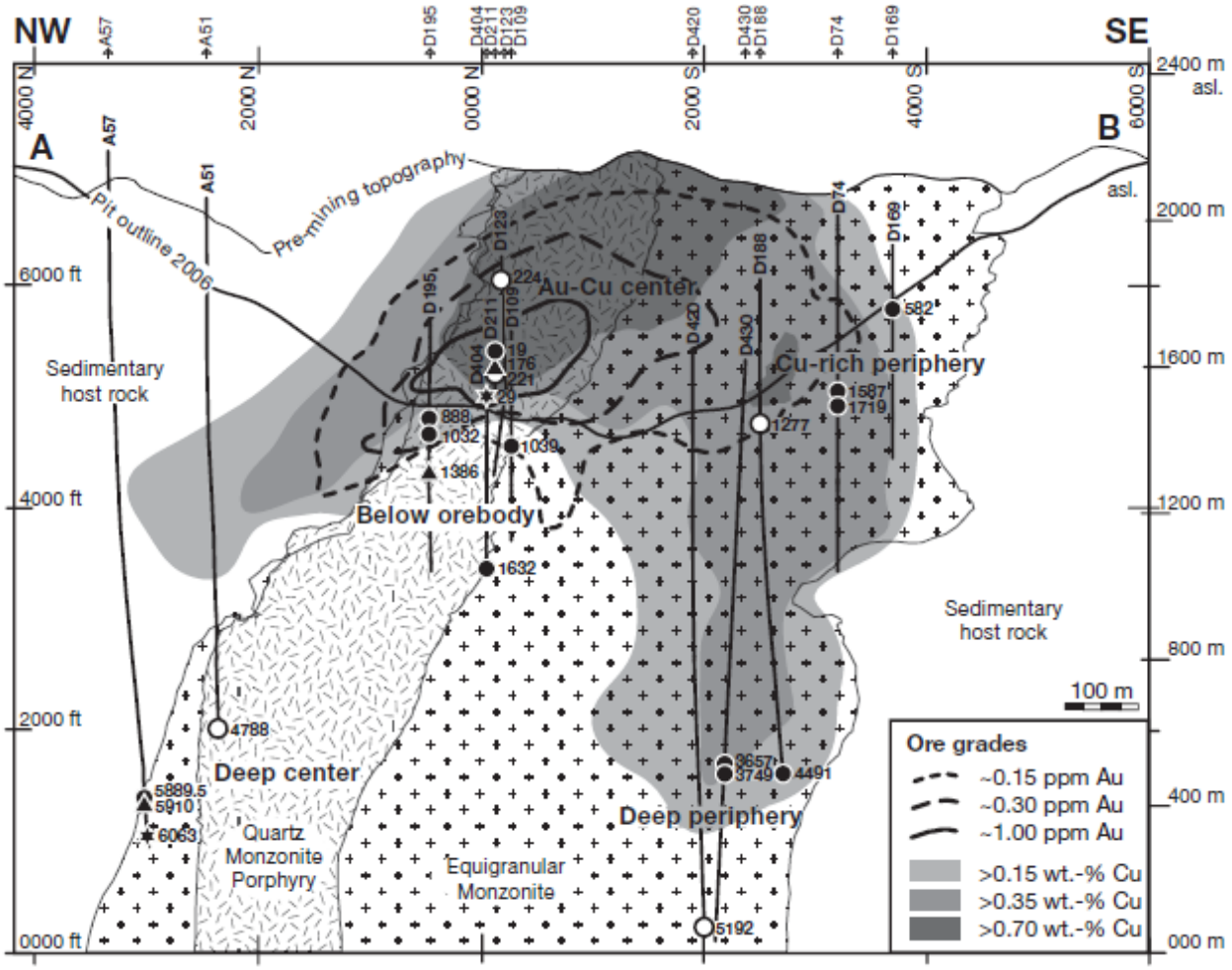

Figure 5. Northwest-Southwest cross section (Landtwing et al, 2010)

1.4.2. Geotechnical properties

The geotechnical properties are the important aspect in every case scenarios involving slope stability. The advantage of having the geotechnical information in every case study will increase further the investigation that conducted in most of the case scenarios. From a comprehensive geotechnical study, soil parameters assessed for further analysis of a case study such as needed in numerical analysis. However, the difficult on retreating significant sampling in most case studies shows that the possibility of finding geotechnical properties reduced.

A valuable tool used by researchers and practitioners rely on the geology of the area involved. Additionally, it is also useful the investigation of past records or any event that

took place in the study area. Accordingly, Bingham Canyon Mine has a very limited geotechnical information, which makes the analysis of Kennecott failure a challenge for this project (Pierce, Gaida & DeGagne, 2009). Based on the geology as mentioned above, we can infer that the rock is present in the mine pit may be classified as fine-grained, with high hardness, sedimentary rock. This information explained because of its background in Oquirrh Mountain, which ranks as non-volcanic mountains.

Geological studies also identify that there are many joints and fracturing caused by the weathering of the rocks. The initial numerical analysis to determine the location of the failure surface in Bingham Canyon mine will use parameters such as friction angle, and cohesion as shown in Table 1. The other material properties that used is the discontinuity properties around that area as shown in Table 2. However, as mentioned above, this project will focus on the numerical analysis of Kennecott failure to simulate and analyse the kinematics of the failure by using the Material Point Method (MPM). Thus, a calibration based on simple deformability and residual strength parameters conducted to give an insight into the influence of the rock properties on the event kinematics.

Table 1.

Preliminary geotechnical properties of Bingham Canyon mine (Styles et al, 2011)

Parameter	**Monzonite**	**Clay Monzonite**	**Limestone**	**Altered Limestone**	**Quartzite**
Young's Modulus, E, (GPa)	27.5	12	34	14	23.5
Poisson's Ratio, ν	0.2	0.12	0.25	0.23	0.27
Porosity, μ, (%)	1	50	30	20	10
Density, ρ, (t/m^3)	2.88	2.64	2.8	2.78	2.6
Density with porosity (t/m^3)	2.86	1.82	2.26	2.42	2.44
Bulk Modulus, K, (GPa)	15.3	5.2	22.6	8.65	17.0
Cohesion, c, (MPa)	1.8	0.59	2.9	1.1	0.65
Friction Angle, ϕ, (°)	37	35	40	32	35
Tensile Strength, σ_t (MPa)	0.2	0.35	0.87	0.35	0.27
Fracture Toughness, K_{IC} (MPa/$\sqrt{m}$)*	2.7	0.2	0.82	0.52	2.25

Table 2.

Discontinuity properties of Bingham Canyon mine (Styles et al, 2011)

Discrete Feature	Friction Angle (°)	Cohesion (kPa)	Normal Penalty (GPa)	Tangential Penalty (GPa)
Brooklyn Fault	16	3	1.5	0.08
Tunnel Fault	30	70	1.5	0.08
No Name faults	26	53	1.5	0.08
*Shear Zones**	30	100	1	0.1
*DFN and default properties**	30	0	0.2	0.02

1.4.3. Mining activities

Bingham Canyon Mine is the largest mine that producing copper. Approximately 18.4 million tonnes in the Unites States. The significant size of the open pit depicted by the fact that astronauts in the space shuttle at bird view can see mine. They produce approximately 55 million tons of copper and about 120 million tonnes of overburden in the 80's. By 2009, the mine had eight drills, performing 200 boreholes each day and using approximately 550 kg pounds of ANFO for blasting (Rio Tinto, 2009).

Now of the failure, there were about 12 electric shovels and one hydraulic shovel operating at the mine, with 100 haulage trucks that can carry approximately 300 tonnes of material in a single trip. The in-pit crusher reduces ore to less than 10 inches in diameter. Chalcopyrite, bornite, chalcocite, and molybdenite are the typical ores that mined in Bingham Canyon Mine (Rio Tinto, 2009). The average ore grade is about 0.6% copper with a cut-off around 0.35%.

1.4.4. Massive pit wall failures

The Kennecott failure occurred on the 10th of April 2013. There were two separate events happened in Bingham Canyon Mine. The first event occured at 03:30 am UT from the middle bench of the mine, where infrastructures located. The first event suggested rock planar slide followed by debris flow. The second event happened at 05:56 am UT from the top bench of the mine. The second event suggested rock rotational slide followed by debris flow. Both events happens at night with moderate to extremely rapid travel velocity. There are no casualties on both events (Hilbert, Ekstrom & Stark, 2014).

The amount of total displaced mass volume is roughly 165 Mt, which calibrated with Scoop3D. The event gives 3 shovels and 14 haul trucks destroyed as results of the landslide event. Geophysical monitoring had observed that the mass has displaced at 5 cm/day, with approximately 270 km/h velocity of the slide movement (Pankow et al, 2014). Geophysical data has reported that the earthquake magnitude of the first rock avalanche calculated to be 2.5 and 4.2. The earthquake magnitude of the second rock avalanche calculated to be 2.4 and 3.5. The second rock avalanche event gives smaller magnitude compare to the first one. However, the second event gives more run-out distance compare to the first event (Hilbert, Ekstrom & Stark, 2014). The seismic waveforms of both events seen in Figure 6.

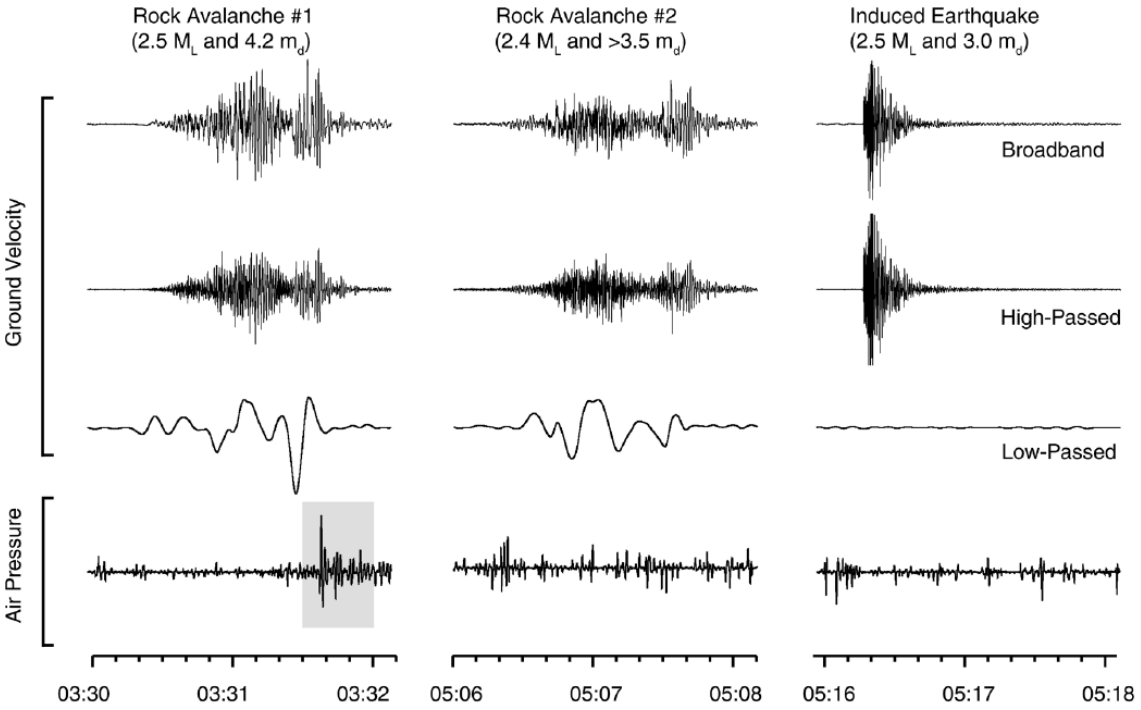

Figure 6. Seismic waveforms recorded in Bingham Canyon mine (Pankow et al, 2014)

1.5. PROBLEM DEFINITION

A landslide defined as the movement of mass down the slope due to surrounding factors that cause an increase in the shear stress due to gravity with decreasing the shear strength of the material. Furthermore, landslides are one of the most common problems that gives a sophisticated understanding of the environment around the event (Highland & Bobrowsky, 2008). Bingham Canyon Mine is the largest non-volcanic landslide event that took place in April 2013 as shown in Figure 7.

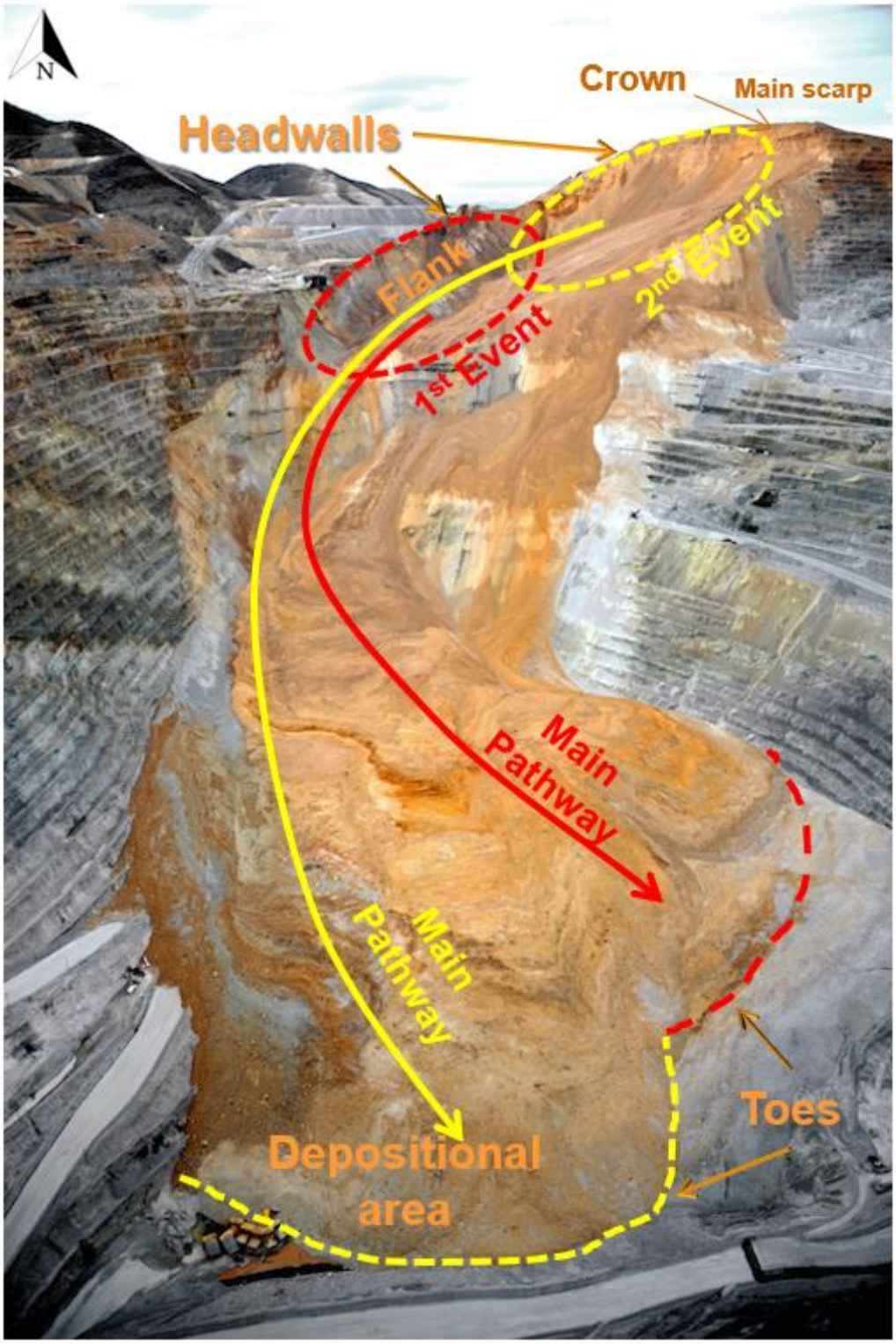

Figure 7. Landslide at Bingham Canyon mine (AGU Blogosphere, 2013)

Furthermore, landslides such as the Manefay slide have proven to be catastrophic events producing great economic and environmental losses. The Manefay failure zone shown in Figure 8.

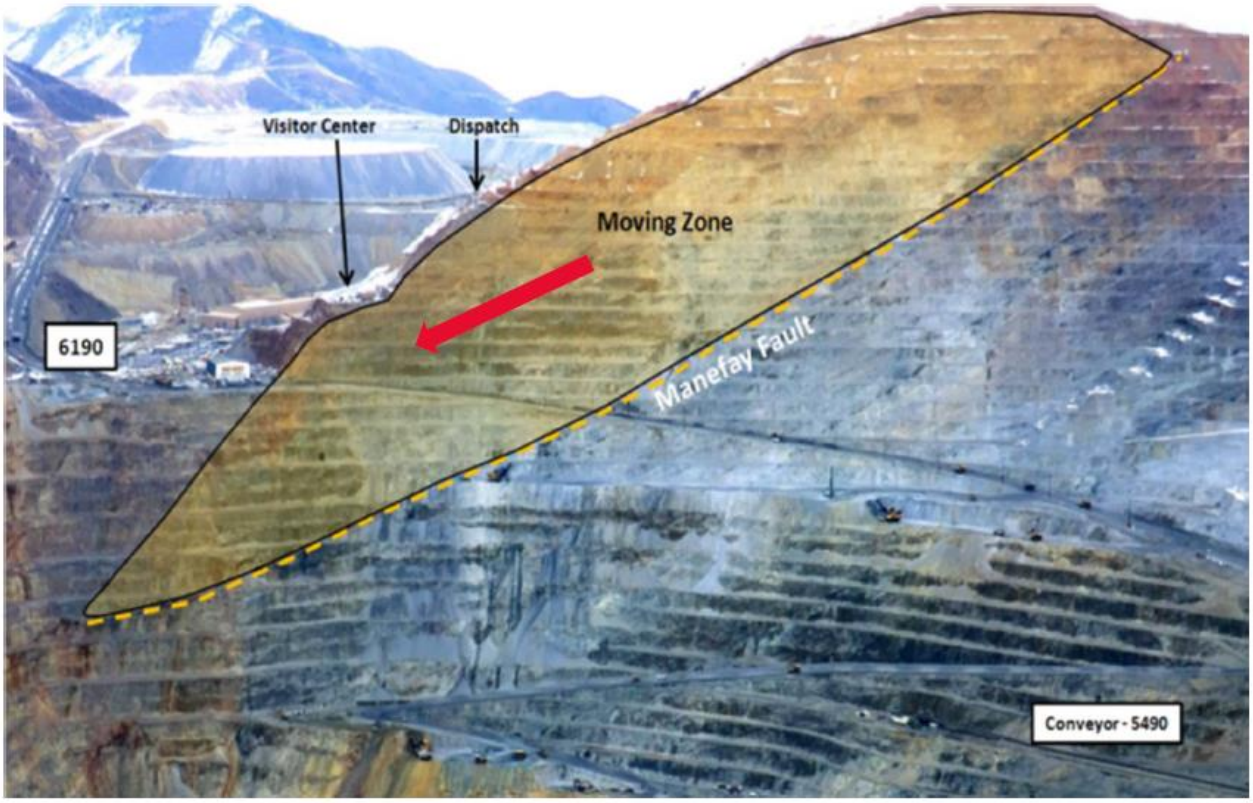

Figure 8. Manefay failure moving zone (Sutherlin, 2014)

Traditionally, the slope stability addressed is by calculating the Factor of Safety (FOS) or more recently by calculating the probability of failure. However, the area that potentially is affected or the kinetic energy released during a landslide is rarely calculated. The relevance of these quantities that easily recognised in events in which the consequences of a slope failure were neglected or miss predicted. The objective of this project is to show the result of applying new techniques is the numerical simulation of landslides. To this end, a series of numerical tools were used to replicate the run-out process as seen in the well-known Bingham Canyon Mine slope failure.

1.6. METHODOLOGY

The method of this project will be the following:

- gather the basic academic information of Kennecott failure;
- gather the necessary technical information of Kennecott failure;
- create a 3D topography model for geotechnical modelling;
- create a 3D failure surface to simulate the run-out process;
- define a suitable geotechnical model to describe the regions affected by the Bingham Canyon failure;
- set 3D MPM model for simulation through the geotechnical model;
- calibration of the numerical model to improve the accuracy;
- measurement of the kinetic energy that released in the numerical model; and
- study of the geotechnical properties and its influence in the kinematics of the landslide.

2. PROJECT MANAGEMENT

2.1. INTRODUCTION

Project management is an integral component of completing a high standard research project. Managing time effectively will ensure the project is delivered within the scheduled completion date with all aims and objectives achieved. To ensure delivery within the completion date, a Gantt chart was established could be seen in Table 3. The Gantt chart clearly outlines a timeline for a different component of the project should be completed.

Table 3.

Gantt chart on project milestones

	March				April				May				June				July				August				September				October			
Research proposal																																
Literature review																																
3D limit equilibrium analysis																																
Project progress report																																
3D MPM model set up																																
Project plan agreement																																
3D MPM model calibration																																
Report																																
Sensitivity analysis																																
Thesis completion																																

2.2. KEY TASKS

The key tasks that are required for the completion of the research project are as follows:

- Literature review on relevant topic of MPM analysis at Bingham Canyon mine
    - Complete project proposal;
    - Complete annotated bibliography; and
    - Write literature review.

- Data collection and analysis
    - Collect raw coordinates from Bingham Canyon mine by using google earth;
    - Collect DEM file of failure surfaces topography from QGIS;
    - Plot 3D interpretation of the failure surfaces topography of Bingham Canyon mine; and
    - Consult with supervisor regarding MPM analysis and modelling.
- Further review of literature review, numerical analysis and write final research project

2.3. CURRENT STATUS OF RESEARCH PROJECT

At this stage, the research project contains no MPM result analysis due to completion time, numerical error, and lack of experience on using the software. The authors have obtained the geotechnical modelling and FOS analysis at the failure surfaces at Bingham Canyon mine. However, there are difficulties in obtaining the input files for numerical analysis with MPM. Comprehensive calibration of the data is required, with consultation with the supervisor to be able to analyse MPM on both failures. A mixed review of relevant literature has been completed on the topic and is included in this progress report.

2.4. FUTURE WORK

Research is to continue for the remainder of the project with updated literature to be reviewed in the final research project submission. This continued research will work concurrently with MPM analysis and interpretation of the run out landslide behaviours in semester two.

2.5. PROJECT BUDGET

There is no budget required in this project due to most of the works is done on computation work. Most of the software that used for this project is open and free.

3. LITERATURE REVIEW

3.1. LANDSLIDE

3.1.1. Definition

Landslide defined as the movement of mass down the slope due to surrounding factors that cause an increase in the shear stress due to gravity with decreasing the shear strength of the material. Landslide is one of the most common problems that gives a complex understanding on the environment around the event (Highland & Bobrowsky, 2008). Bingham Canyon Mine is the largest non-volcanic landslide event that took place in April 2013 as shown in Figure 7.

3.1.2. Landslide parameters

As mentioned above, there are two basic parameters in most landslide event as the following;

- Increasing shear stress that caused by the increasing load, removal of lateral and underlying support, increasing lateral pressure, and regional tilting; and
- Decreasing shear strength material caused by weathering of the rock, change in state consistency, change in structure, and change in intergranular forces.

3.1.3. Landslide causes

The most common causes of the landslide are due to many mechanisms that as the triggers such as physical, morphological, geological, and human. Dai, Lee & Ngai (2002) has summarised landslide causes can be described as the following;

- Morphological causes: Vegetation removal, Deposition loading slope or its crest;
- Human causes: Mining/Mining waste containment, deforestation, and excavation.

3.1.4. Impact of landslide

Landslide activity gives effect to many supplies around the environment. Dai, Lee & Ngai (2002) has summarised increasing of landslide activity are due to the following;

- Continued deforestation of landslide-prone areas;
- Increasing urbanisation and development in landslide-prone areas; and
- Increased regional precipitation caused by changing climate patterns.

3.1.5. Economic impact of landslide

Impact on landslide also involves in economic perspectives. Keefer (1984) has summarised some of the economic impacts due to landslide derived as the following;

- Repair, or maintenance resulting from damage to property or infrastructure due to landslides;
- Landslide mitigation measures;
- Reduced land value; and
- Effect on water quality/sedimentation.

3.1.6. Landslide classification

With many cases that occur for the past years involving the landslides, many researchers have been conducting studies and there is a type of landslides can be classify and it is still ongoing. Based on the definition mentioned earlier, landslide classified from two terms, which are the material type, and the type of movement.

3.1.7. Type of materials

In most of the landslide cases, some materials can be prone for landslide to occur. Novotny (2013) has summarised the materials can be as the following;

- Rock: hard, firm mass that was intact and in its natural place before the initiation of movement;
- Soil: an aggregate of solid particles that consist of mineral and rocks that transported or formed by the weathering of rock in place. Liquids or glasses filling the pores of the soil from part of the soil;
- Earth: material in which 80% or more of the particles are smaller than 2mm, the upper limit of sand-sized particles;
- Mud: material in which 80% or more of the particles are less than 0.06mm, the maximum limit of silt sized particles; and
- Debris: contains a large proportion of coarse material, approximately 65% of the particles are greater than 2mm.

3.1.8. Type of movements

The second term that used is the type of movement of the materials down the slope. There is five unique type of movements analysed from previous case studies. The most common type of movements that classify landslides are fall, topple, slide, spread, and flow. The combination of type of materials and type of movements will classify each type of landslide for each combination (Ortigao & Sayao, 2004). Summary of all the combination that valid for landslide classification seen in Table 4. This project will be focusing on the classification of the landslide on Bingham Canyon mine. This information used for numerical analysis and kinematics investigation.

Table 4.

Summary of landslides classifications (Hungr, Leroueil & Picarelli, 2013)

Movement type	Rock	Debris	Earth
Fall	1. Rock fall	2. Debris fall	3. Earth fall
Topple	4. Rock topple	5. Debris topple	6. Earth topple
Rotational sliding	7. Rock slump	8. Debris slump	9. Earth slump
Translational sliding	10. Block slide	11. Debris slide	12. Earth slide
Lateral spreading	13. Rock spread	–	14. Earth spread
Flow	15. Rock creep	16. Talus flow	21. Dry sand flow
		17. Debris flow	22. Wet sand flow
		18. Debris avalanche	23. Quick clay flow
		19. Solifluction	24. Earth flow
		20. Soil creep	25. Rapid earth flow
			26. Loess flow
Complex	27. Rock slide-debris avalanche	28. Cambering, valley bulging	29. Earth slump-earth flow

3.2. ROCK AVALANCHE

Rock Avalanches classified as a complex landslide. It is complex due to more than one type of landslide included in rock avalanches. Rock avalanches happen due to a rock slide from the crown and then followed by a debris flow at the run out to the toe. Rock avalanche is one of the most violent natural catastrophic of landslides (Shea & Vries, 2008). The velocity of travel of rock avalanches is extremely fast sliding and flowing from crown to toe. Kennecott failure considered as a large-scale rock avalanche deposit. The size can be characterised by a scar which deposition from the crown occurred, a path along the landslide that partly depositional, and a distal zone of deposition (Ortigao & Sayao, 2004). The depth of scar may depend on the size of the slide, the depth of weak zones, and the nature of the rock. Blasio (2011) has summarised the progressive stages of development of a rock avalanche as the following:

- Rocky surface moves very slowly before massive failure. Slow creep may indicate instability of possible catastrophic failure;
- Rock slab slides and may partially travel in ballistic flight with steep terrain;
- The mass rapidly disintegrates, free fall, shockwave energy created by the free fall mass. Disintegration mechanisms probably comprise the bending of the rock slab beyond the tensile stress, and crushing along force chains in granular medium;
- The fragmented rock flows rapidly;
- The mass reaches lower slope angle; and
- The landslide comes to a stop, Peculiar structures in the deposit may be revealing of the internal dynamics.

3.3. RUN OUR KINEMATICS

Run out can be defined as the flow behaviour of materials after a certain event (Pirulli & Pastor, 2012). In the context of this thesis project, landslide run out defined as the movement of the material debris that ejected from the top to bottom (Jakob & Hungr, 2005). Flowing landslides can be fast to extremely rapid to be able to reach areas far from their source. The authors suggest rockslide avalanches as the type of landslide that happens at Bingham Canyon mine (Manefay failure). The structure genesis of rockslide avalanches seen in Figure 9.

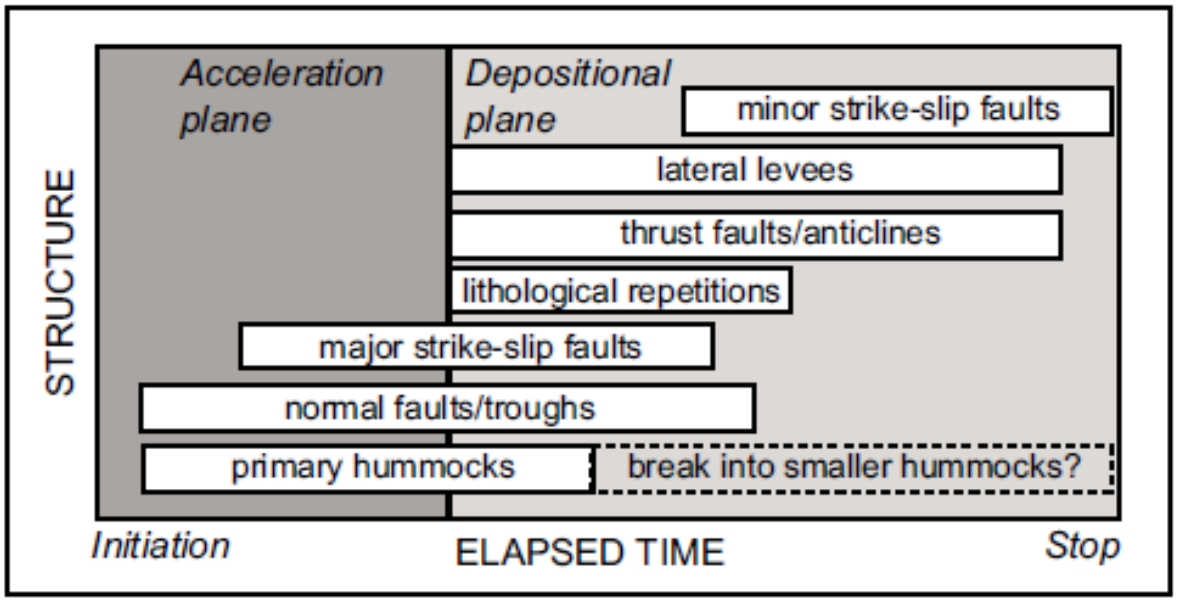

Figure 9. Structural genesis of rockslide avalanches (Shea & Vries, 2008)

As shown in Figure 9, the structure starts with hummocks appearing at the initiation of the accelerated. The structure with minor strike-slip faults ends the genesis of rockslide avalanches (Whittall, 2015). Based on the structure genesis of the landslide, some of the variables that will be introduces are the volume of debris that flows, how wide the spread of the flow, the velocity of the flow, farboschung, and the length of the run out (Prochaska, 2008). Hence, these kinematics variables will be analyse using MPM for Bingham Canyon mine failure.

Farboschung can be defined as the apparent friction coefficient as shown in Figure 10. The difference of farboshung and real friction angle is the measurement of height and length (McDougall & Hungr, 2004). They measure height and length using the uppermost point of the scar and distant tip of the deposit can be symbolised as H and L for apparent friction coefficient. However, the real friction coefficient measured from the centre of gravity of the deposit and deposit that collapsed, which are Hg and Lg.

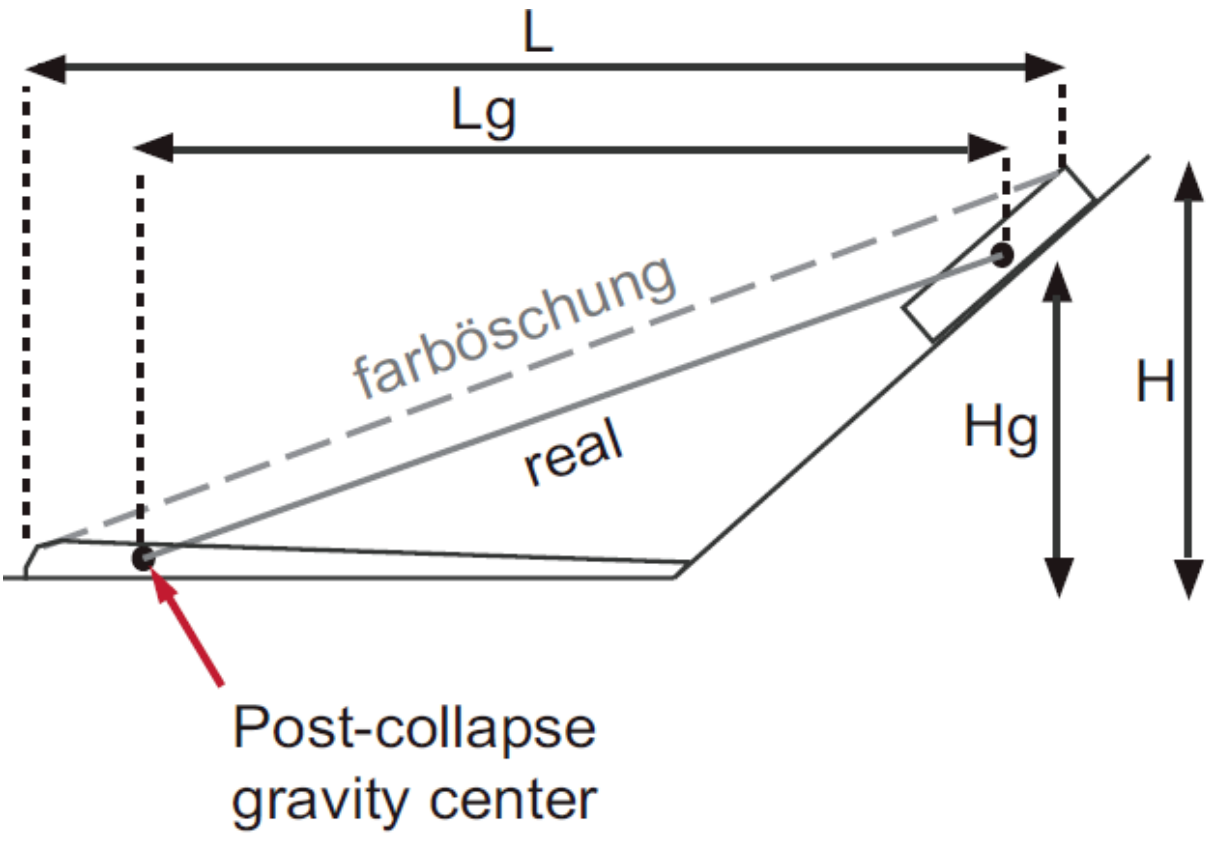

Figure 10. Comparison of apparent friction coefficient (farboschung) with real friction coefficient (Shea & Vries, 2008).

Theoretically, other than farboshung, there is some fundamental parameter need to be determined. This allows the authors gives insight and better understanding of the slope failure at Bingham Canyon mine. Illustration of the slope stability parameters seen in Figure 11.

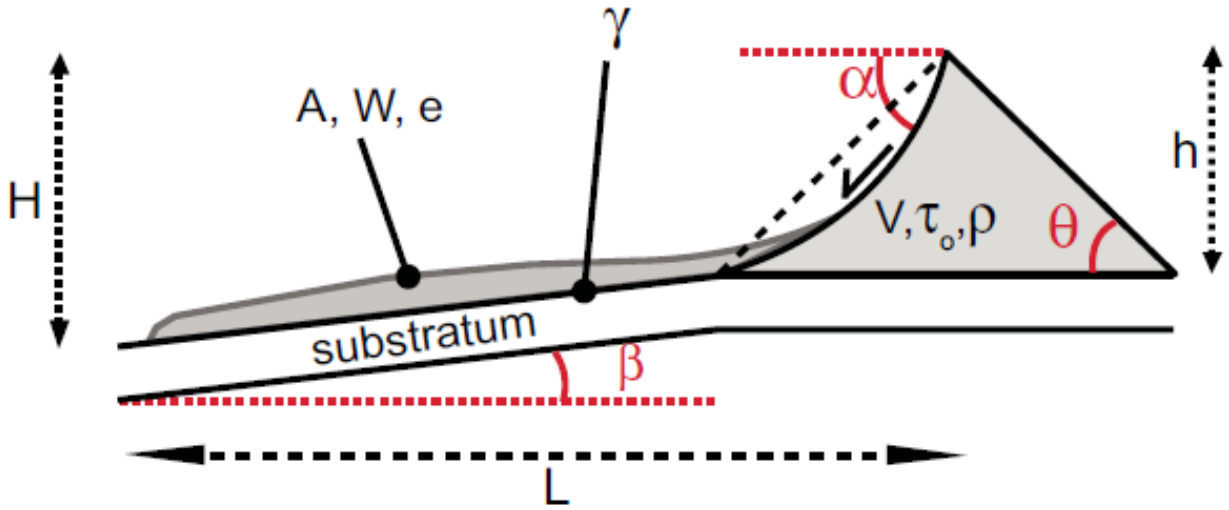

Figure 11. Fundamental parameters of slope stability failure (Shea & Vries, 2008)

The variables that involve in slope failures can be summarised in Table 5.

Table 5.

Fundamental parameters on slope stability

Type of variables	Symbols	Description
Deposit geometry and sliding environment	L	Avalanche run out
	e	Deposit thickness
	A	Covered area
	W	Deposit width
	H	Total fall height
	h	Fall height before arrival
	β	Depositional surface average slope
	α	Failure plane average slope
	V	Volume
Intrinsic material properties	ρ	Material density
	θ	Internal friction angle
	τ_o	Cohesion
Dynamic variables	ϒ	Basal friction angle
	u	Avalanche velocity
	g	Gravity

The authors will analyse the run out kinematics from MPM numerical modelling at Bingham Canyon mine.

3.4. 3D SLOPE STABILITY

In this numerical analysis, one of the factors that required to is the FOS (Factor of Safety). Research has shown that FOS is the main reason for the massive landslide to take place (Oritgao & Sayao, 2004). However, there is not enough geotechnical information or literature research has been done to quantify the FOS at Bingham Canyon mine failure. An iterative approach has been conducted to identify the FOS. Open software that used to determine the FOS such as Google Earth, TCX Converter, Excel, Matlab, QGIS, and Scoop. A 3D numerical analysis is recommended to create geotechnical and numerical modelling to give an accurate simulation at the run-out after the event. Lam & Fredlund (1993) summarised the advantages of conducting 3D analysis are the following;

- Gives more precise result;
- back analyses in slope failure that defined;
- using limit equilibrium methods;
- based on symmetrical force; and
- Gives higher FOS than 2D analyses due to more restriction applied for the parameters.

In comparison, Albataineh (2006) has summarised the advantages of conducting 2D analysis are the following;

- Gives partial result (along the cross section);
- gives lower FOS than 3D analyses;
- simplification modelling with less restriction (constraints);
- less time to compute the analyses; and
- The slope numerical model is uniform.

The authors have decided to conduct 3D analyses on Bingham Canyon mine due to the complex geometry of the landslide. Progressive landslide event that gives different outcomes, and to observe the mass failure movement and run-out in 3D using MPM for accurate simulation and analyses.

3.5. LIMIT EQUILIBRIUM METHOD

Limit equilibrium is one of the methods that used by many researchers. The method used mostly in slope stability analysis. This method is useful due to its flexibility on choosing the parameters, including the ability to associate complex geometries and variable soil and water pressure conditions (Huang & Tsai, 2000). The method utilises the slices acted on the force that applied to the sliding surface. Hence, limit equilibrium method will simplify complex 3D slope stability analysis (Michalowski, 2010). There are many methods incorporated with the limit equilibrium analysis in finding the factor of safety of particular slope stability case. The method that the authors were used is the simplified bishop method to analysis the 3D factor of safety in Bingham Canyon mine.

3.5.1. Simplified Bishop's method

Bishop founded simplified bishop method in 1955. The concept of the method is similar to Fellenius methods, which dependent on each interslice of the slope surface that generate many vertical intercolumns (Albataineh, 2006). Both methods initially applied to two-dimensional slope stability cases. It is applicable for analysing three-dimensional slope stability cases. Few assumptions that made for simplified bishop method, which is the following;

- Vertical intercolumns shear forces are negligible;
- Horizontal force is neglected and;
- Vertical force equilibrium of each column and the overall moment equilibrium are the requirements to determine all the unknowns.

Simplified bishop method typically used in rotational slope failure. It gives the factor of safety that derived from the summation of moments about the common points by using an axis for point of references. However, the method proved very conservative, due to its neglect of internal shear stresses from non-rotational geometry (Fredlund & Krahn, 1977). The author suggests that the potential sources of errors using this method are the influence of internal strength for non-rotational surfaces and influence of lateral asymmetry. Hence, simplified bishop method gives accurate results of 3D and 2D FOS for rotational and symmetric sliding surfaces with its firm characteristics on non-rotational and asymmetric surfaces because it neglects internal strength (Hungr, Salgado, & Byrne, 1989). Simplified bishop method used for Bingham Canyon mine slope failure three-dimensional analysis.

3.6. MPM (MATERIAL POINT METHOD)

3.6.1. Introduction

The Material Point Method (MPM) is one of the numerical methods in most engineering applications. MPM developed in the early 1950s (Nairn, 2003). The basic illustration of MPM seen in Figure 12 & 13. As shown in Figure 12, the object that will be analysed with MPM overlapped with the yellow grid. The object then converted or transformed into a red sphere that is unique, called as material elements as shown in Figure 13. The object then ready to be analysed dependent on the direction of each sphere will move, the gridlines surrounding each sphere will move according to the movement of the sphere.

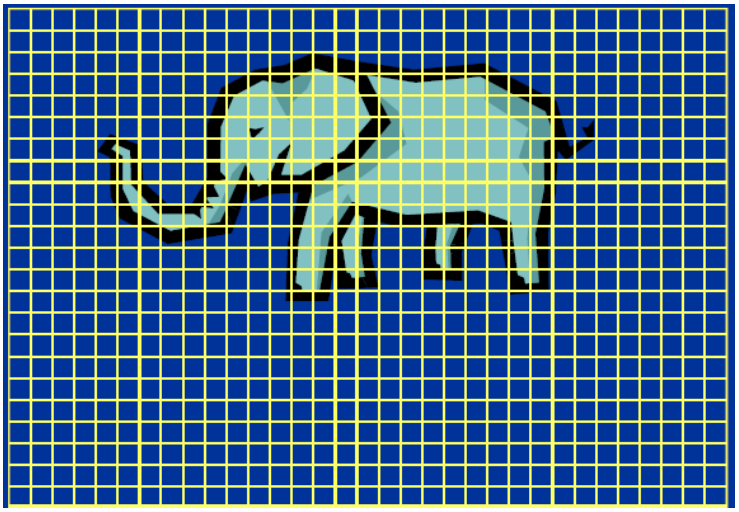

Figure 12. Illustration of initial MPM analysis in 2D (Brannon, 2014)

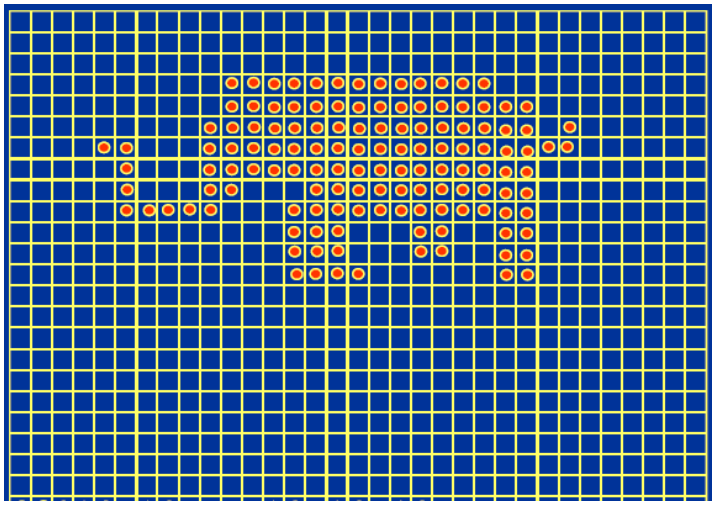

Figure 13. Illustration of MPM analysis in 2D (Brannon, 2014)

The idea of using this method is by using the advantages of Eulerian and Lagrangian formulation that used in other numerical methods such as Finite Element Method (FEM). Soga et al (2016) summarised the benefit of using MPM for numerical analysis due to the following;

- It is the most suitable methods for modelling landslide problems;
- It can be utilised on failure analysis in a large-scale that involves large deformations;
- The method is based on continuum description of material flow using Eulerian-Lagrangian approach;
- It gives easier instructions to follow compare to FEM;
- It can incorporate to soil constitutive models; and
- It is mesh-free methods.

MPM output simulation dependent on properties of the materials, unique material elements for the modelling, and the time it takes to run the simulation. The Kinematic approach of the run-out will be the properties that will be analysed using MPM on Bingham Canyon mine failure.

3.6.2. Eulerian-Lagrangian

Eulerian formulations defined as the equations are solved on a fixed grid, with the material moves through the mesh (Pastor, 2009). However, in Lagrangian methods, the mesh is attached to the material that being simulated. This results from the mesh to moves and distorts as each material moves (Shandyba, 2015). The illustrations of Eulerian and Lagrangian description seen in Figure 14.

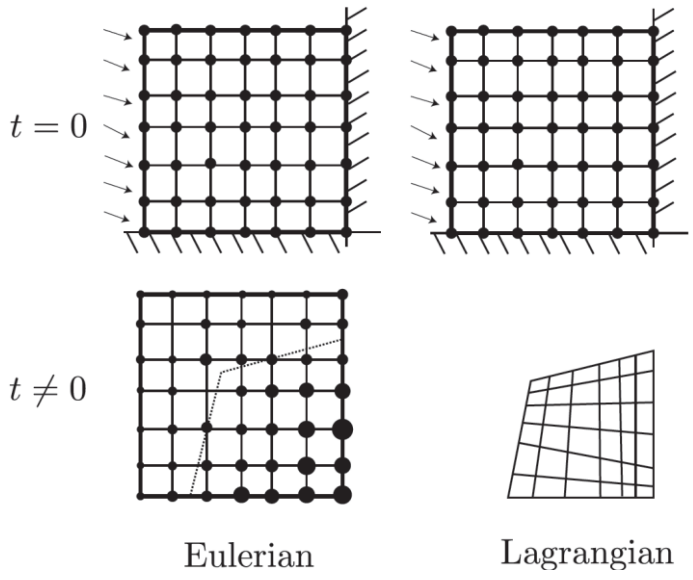

Figure 14. Illustration of Eulerian and Lagrangian description (Nguyen & Cardiff University, 2014)

As shown in Figure 14, the Eulerian formulation has a fixed grid with a highly distorted motion of the materials, which gives the materials moves from point to point based on the size of the grid (Nairn, 2003). However, using Eulerian formulation gives few disadvantages such as the difficulties with history-dependent materials due to the past material locations not tracked. The other disadvantage of using this formulation is defining the material boundaries (Nguyen & Cardiff University, 2014). Hence, the Eulerian formulation is very conservative due to its movement that static based on the grid/mesh shape.

Lagrangian formulation is mostly suitable to analyse the motion of fluids. The advantage of using the Lagrangian formulation that it is mesh-free that gives the material elements to move freely without bounded by the grid (Zhang & Chen, 2007). However, the difficulties of the formulation are the unknown flow lines that give more difficult and challenging computation due to the boundary is not restricted to the initial location. Hence, Lagrangian formulation provides free motion analysis with difficulties to control the movement/flow (Soga et al, 2016).

MPM formulation based on the combination of the advantages of both Eulerian and Lagrangian formulation. Eulerian formulation gives a fixed boundaries and grid where the equation balance of momentum solved as shown in Figure 15.

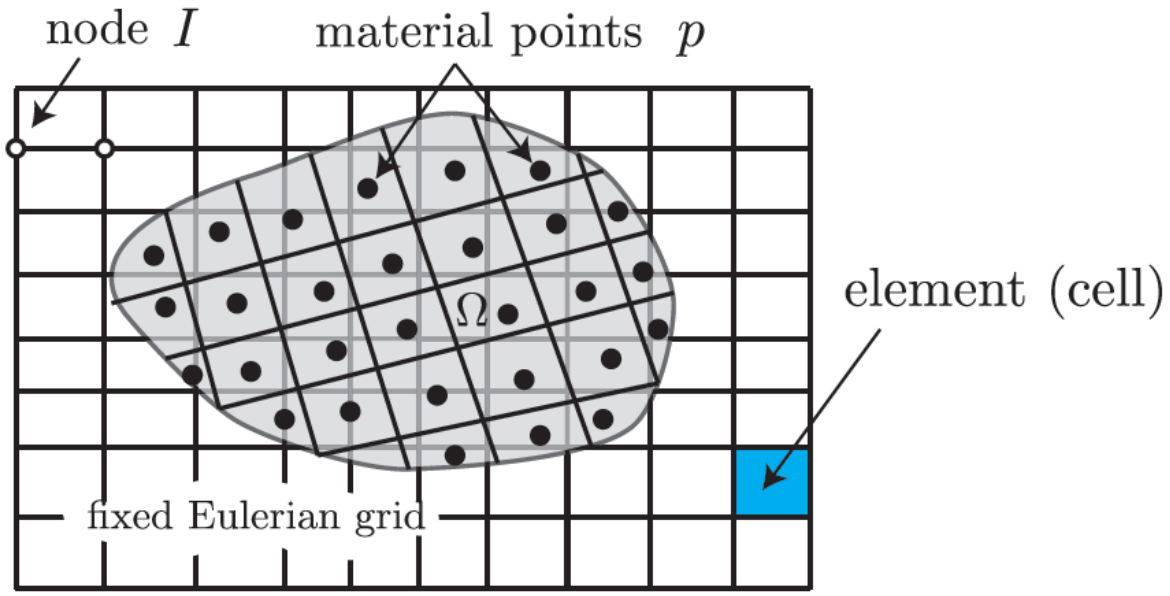

Figure 15. Illustration of MPM with Lagrangian material points over Eulerian grid (Nguyen & Cardiff University, 2014)

Furthermore, Lagrangian formulation provides a unique property for each material element. The moving material points with the integration of time and fixed Eulerian grid (McDougall & Hungr, 2004). It gives less time computing due to the fixed grid will give distortion-free of each material points as shown in Figure 16. Hence, MPM is the numerical analysis that used to investigate the landslide event at Bingham Canyon mine due to its suitability to analyse large-scale deformation with the utilisation of Eulerian-Lagrangian description/formulation.

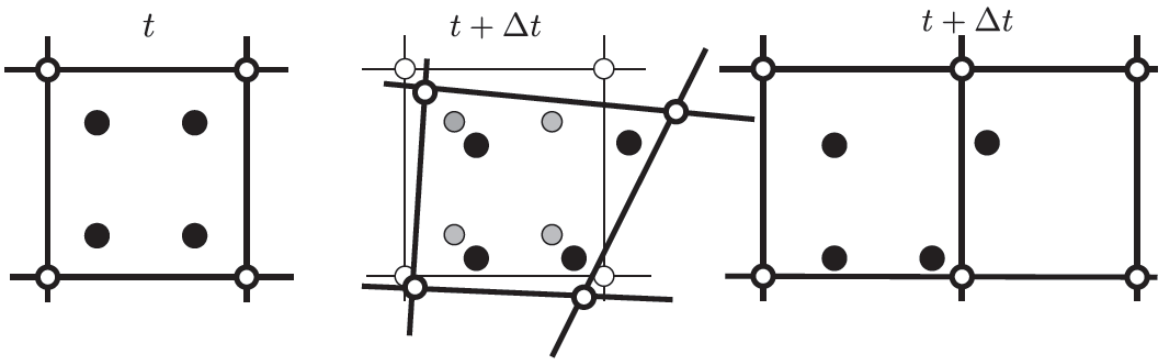

Figure 16. Illustration of movement in MPM with integration of time (Nguyen & Cardiff University, 2014)

3.6.3. FEM vs MPM

In definition, FEM defined as a numerical method that involves discretisation of mathematical model to simple geometry that called finite elements. As mentioned above, FEM usually called updated Lagrangian due to the particles move without any constrictions (Bhandari et al, 2016). Zhang & Chen (2007) has summarised the advantage of using FEM are the following;

- It is suitable for solving fluid flow conditions;
- It allows the use of variable approximation order in each element;
- Naturally, account for inhomogeneity in problems; and
- It addresses easier on small-scale problems.

However, some of the disadvantages of using FEM are the following;

- Mesh distortion in solving large-deformation problems;
- Not valid for post-failure behaviour due to the difficulties to define each particle; and
- Complex re-meshing of variables cause additional errors in simulating the problems on large-scale.

MPM or mesh-free techniques defined as a hybrid Eulerian-Lagrangian approach, which uses moving, unique material points and computational nodes that are moving around a background mesh in each time step as shown in Figure 17. The deformation determined by Newton's laws.

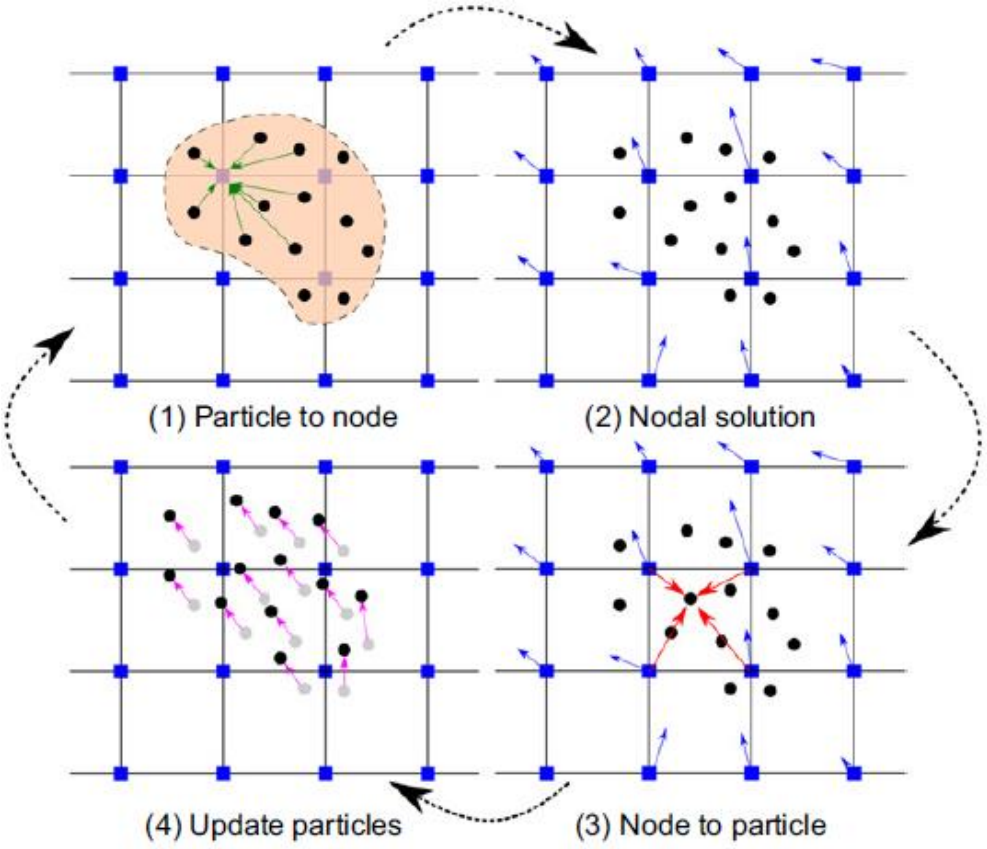

Figure 17. MPM cycle (Soga et al, 2016)

Bhandari et al (2016) has summarised the advantages of using MPM over MPM are the following;

- MPM can be seen as updated Lagrangian FEM which material points serve as integration points not dependent on Gauss points of an element of the grid;
- Mesh distortion from Lagrangian FEM eliminated;
- It is easier to solve free surface problem;
- Boundary conditions can be applied quickly;
- Adding material points during calculations is relatively easy as there is no dependent between the grid and the material points; and
- MPM is more suitable to solve complex geometries problem due to its simplicity to construct the mesh automatically and not dependent on the geometries.

However, the disadvantages of using MPM over FEM are the following;

- Efficiency of MPM is lower than FEM because the accuracy of the mappings is less compare to FEM that always has a structured movement;
- It may introduce new visualisation challenges with its meshless nature;
- Higher computational time is required to define higher dimensional shape functions; and
- Computational cost is greater than FEM.

After much consideration, the authors decided to use MPM for numerical modelling/analysis in three dimensions due to its less restriction on each material points on the failure event at Bingham Canyon mine. It will be the authors challenges on developing a three-dimensional MPM analysis with limited information and past literature review on the same topic. Furthermore, the 3D MPM analysis at Bingham Canyon mine landslide failure event will gives/simulate the run-out of the particles or mass that ejected during the event.

3.7. NAIRNMPM

NairnMPM is an open software for the users to have the experience of putting MPM theoretical approach into practice. John Nairn develops the software with the current ongoing development of the software. NairnMPM allows the users to analyse and simulate their model in 2D and 3D. However, only NairnFEA (Finite Element Analysis) can do 2D analyzation. NairnMPM is object oriented C++ code that can run on many platforms. John Nairn has developed a custom script language for the software to execute the MPM simulation. The script language was expanded to Extensible Markup Language (XML) for users to design the script for MPM simulation. The overview input command file has listed as follows:

- Main header: this section defines the type of analysis to run. This includes analysis command, annotation commands, and processors command;
- MPM header: This section defines many settings and features for MPM calculations. This includes MPM methods and simulation timing, MPM archiving options, LeaveLimit command, and ExtrapolateRigid command;
- MPM background grid: this can be defined as the grid that created for MPM calculations to improve the accuracy;
- Creating and defining the material points: In MPM, a group of material points discretises the objects. Each material point assigned to a material type that relevant to the objective of

the users. Some of the examples of the material models are linear elastic small strain, hyperelastic, softening, viscoelastic, phase transition, membrane, and rigid;

- Using explicit cracks;
- Multimaterial MPM: this can be defined as a mode where the calculation involves more than one model that contacts;
- Boundary conditions: this defined as the outer grid of the whole simulations. This is required to prevent the particles from escaping from the grid that may cause an error; and
- Gravitation field: this defined as the gravitation field to be applied for MPM calculation.

4. GEOTECHNICAL MODELLING

General information of Bingham Canyon mine is required to construct a geotechnical modelling. The purpose of geotechnical modelling is to simulate the slope failure and factor of safety. Geotechnical modelling is also required for further numerical analysis using MPM to observe the kinematics of the massive landslides. However, there is so little information to have an accurate result on the factor of safety at the slope (Manefay failure). The authors suggest a list of assumptions to achieve FOS lower than one in this modelling further in this section.

The first step is to get the coordinates of the area of failure around Bingham Canyon mine. As shown in Figure 18, the boundaries marked with green colour. Both first and second failures marked with the yellow and red circle. The coordinates obtained with path tool from google earth, marked with blue colour.

Figure 18. Bingham Canyon mine from google earth

The longitude, latitude, and altitude obtained from google earth used as an input for topography software called QGIS. As shown in Figure 19, a topography of Bingham Canyon mine can be observed with the red zone is higher z value compare to blue one. The purpose of using this free open software is to obtain the DEM (Digital Elevation Model) file. DEM file defined as the file contains the elevation (z-coordinates) of every x and y coordinates given. DEM file from QGIS can be obtained from the contour file in that area, then converted to DEM file, as an input for FOS analysis software, Scoop 3D.

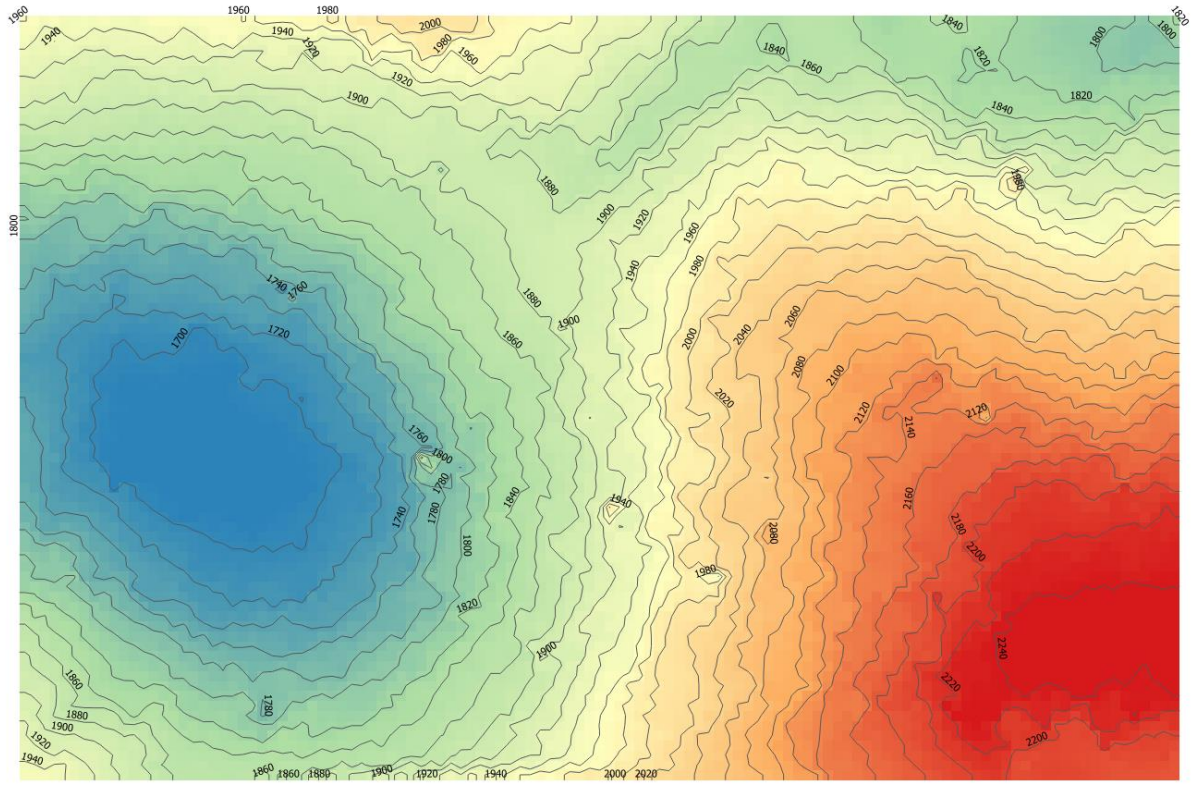

Figure 19. Topography file with contours from QGIS

Scoop3D is an open software to help analyse the FOS based on the topography. There are two main input files required to be able to estimate the FOS, which are the main parameter input file, and the DEM file. As shown in Figure 20, DEM file obtained from QGIS as mentioned above can be visualised.

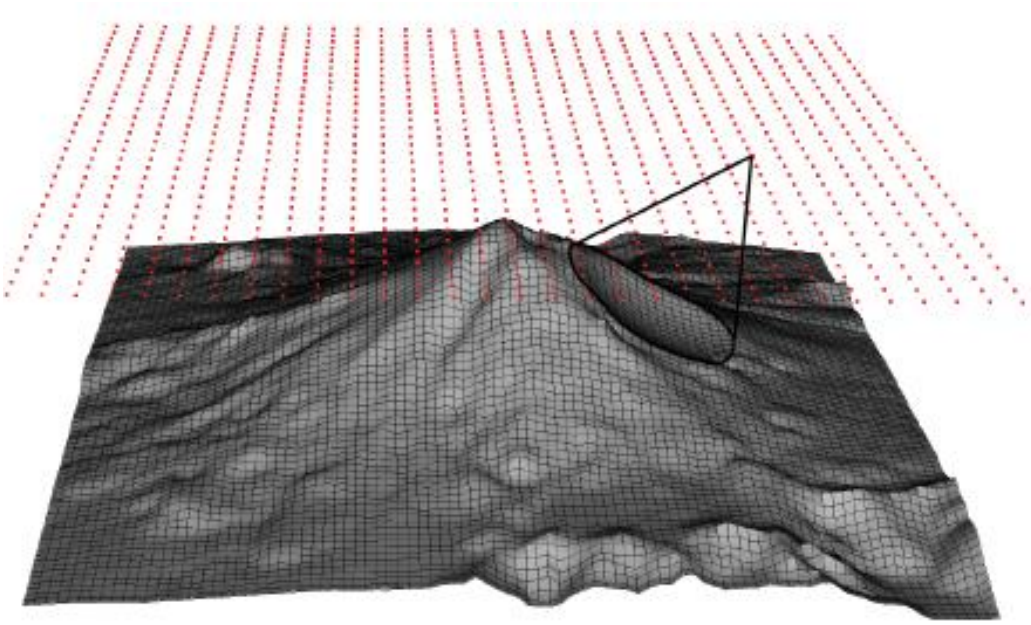

Figure 20. Visualisation of DEM file in Scoop3D (Reid et al, 2015)

The main parameter input file can be obtained by background researches that had been observed. However, there is no visualisation in Scoop3D to enable the authors to visualise the output. Hence, another software is required to visualise and observe its accuracy with the event that occurred at Bingham Canyon mine. Due to the difficulties in visualising the output results, many iterations has been made to increase the accuracy of the FOS calculation with limited geotechnical information. In Figure 21, the visualisation of 3D analyse and search using Scoop 3D can be shown.

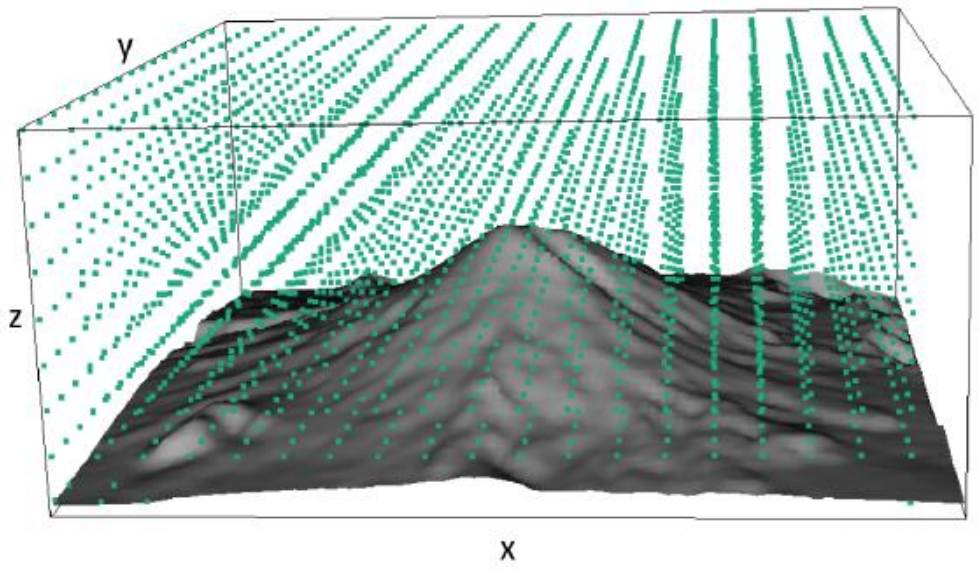

Figure 21. Visualisation of 3D search lattices using Scoop3D (Reid et al, 2015)

For the material properties input in Scoop3D, there is no exact information to find the material properties on the Manefay fault. However, there is some information on other faults at Bingham Canyon mine. Hence, the cohesion and internal friction angle properties will be similar to the Brooklyn fault as shown in Table 2. The unit weight properties of quartzite will be used for this analysis. It is also assumed that the material properties are homogeneous, and there are no groundwater features as it is proven that rainfall did not cause the failure. The input for material properties shown in Figure 22.

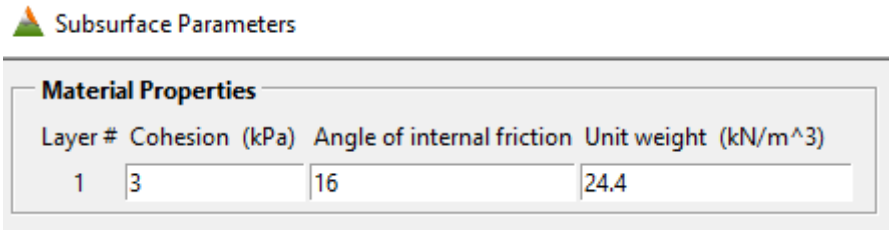

Figure 22. Material properties on Scoop3D (Reid et al, 2015)

The other properties that required is the search type. Scoop3D have two search types on analysing FOS called box search and single surface search. The illustration of box search seen in Figure 23. The boundaries of the box area need to be define before the script run in Scoop3D. However, using box search will give an inaccurate estimation of the area that provides lower FOS. There are difficulties to visualise the box area in every run. Many errors have made by using the box search, and it gives inaccurate result when no errors occurred. Therefore, box search not recommended to analyse the FOS in Bingham Canyon mine.

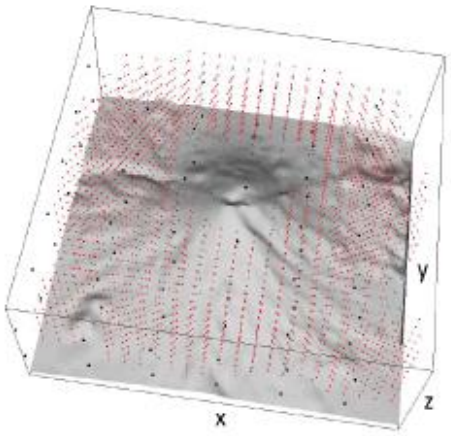

Figure 23. Illustration of box search in Scoop3D (Reid et al, 2015)

On the other hand, single surface search provides accurate results to find FOS. It gives simple instructions. Figure 24 illustrated the single surface search. The single surface search dependent on a sphere that created. As shown in Figure 24, it is required to define the centre coordinates of the sphere, with the radius and slip directions of the sphere. When the Scoop3D runs, the sphere will be generated to touch the topography, and then it will give the results of that single surface cut by the sphere. However, the difficulty of this search type is similar to the box search; it is hard to visualise the coordinates of the sphere. Many iterations made to optimise the sphere to execute the single surface search. Therefore, a single surface search used to analyse the FOS in Bingham Canyon mine.

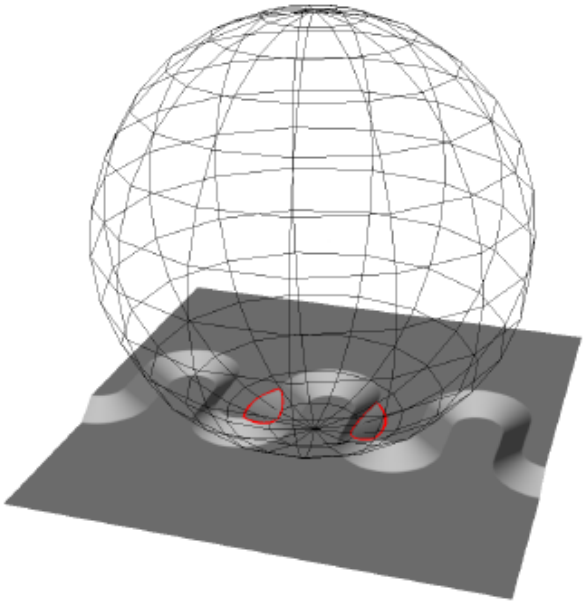

Figure 24. Illustration of single surface search in Scoop3D (Reid et al, 2015)

The search method that used in Scoop3D is bishop's simplified method. This approcah used due to its simplicity and gives more accurate results on FOS in three dimension as mentioned at above section. The illustration of Bishop's simplified method seen in Figure 25.

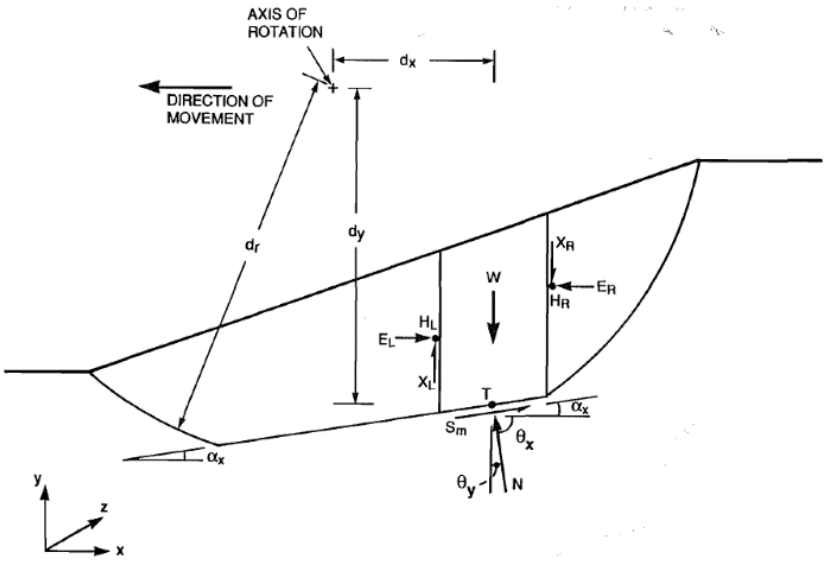

Figure 25. Illustration of Bishop's simplified method in Scoop3D (Lam & Fredlund, 1993)

4.1. SCOOP3D SINGLE SURFACE OPTIMISATION

As mentioned earlier, iterations made to obtain the best FOS result. The variables that included are the centre coordinates of the sphere, the radius, and the slip surface. As the geotechnical modelling purpose is to simulate the landslide event, optimising the FOS will be required for further numerical analysis/modelling with MPM. The variables from Scoop3D that can be controlled will be the slip direction, radius, and the z-coordinates of the sphere. By optimising these variables, the authors obtain the optimised FOS and volumes.

4.1.1. Slip direction vs FOS

Slip direction defined as the maximum range of angles to analyse for each trial surface. Because the slip surface is spherical, a potential failure may occur with rotation in any direction. As shown in Figure 26, the slip direction changes the FOS. It is shown that as the slip direction increases, FOS will decrease to a certain limit then it will increase back again. By using this knowledge, the lowest FOS optimised.

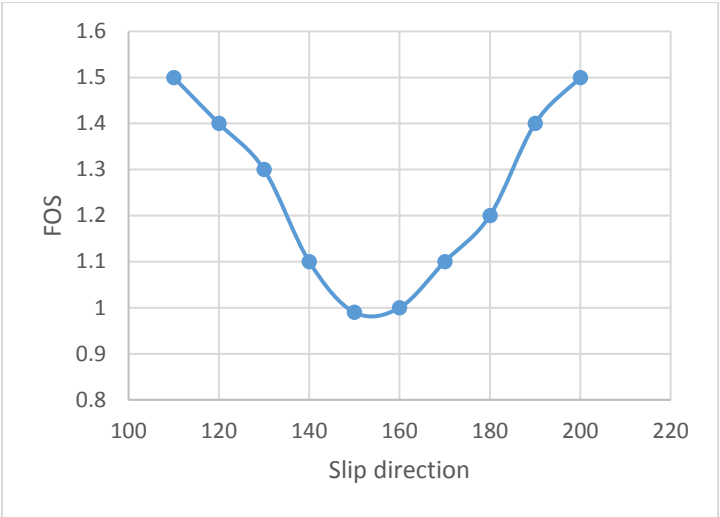

Figure 26. Slip direction vs FOS

4.1.2. Elevation z vs FOS vs volumes

Elevation z is the z-coordinates of the centre of the sphere located to optimise the slice that touches surface topography. As shown in Figure 27, the increase of the z-coordinates will give increasing FOS due to there will be more materials will be sliced to analyse. On the other hand, increasing z-coordinates will decrease the volume of mass moved for the event. Hence, the elevation z-coordinates is optimised in Scoop3D by considering the balance between the FOS and the volumes.

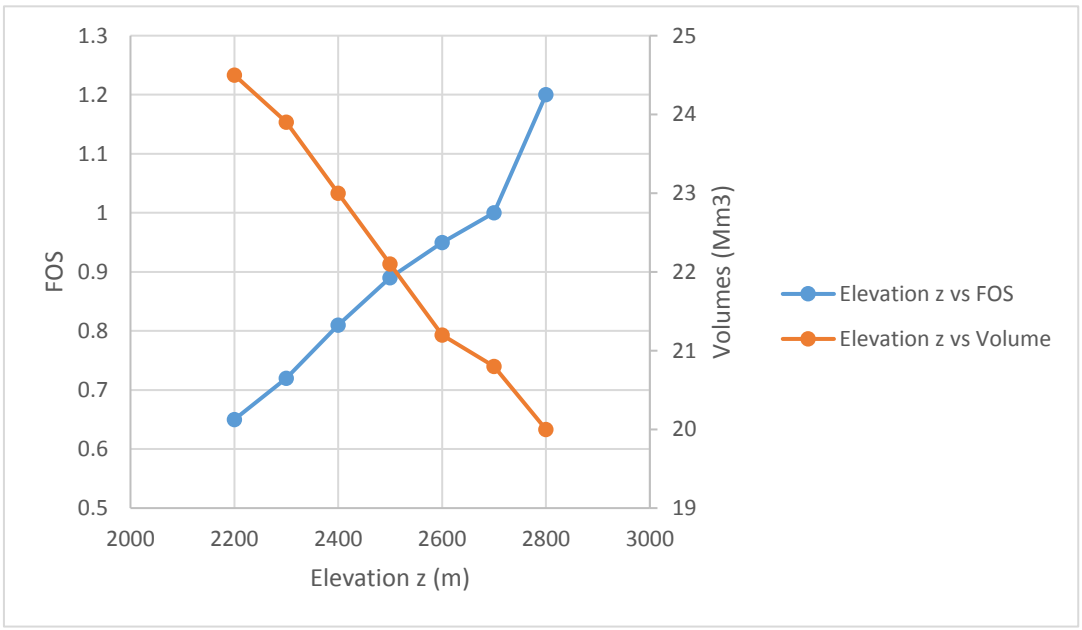

Figure 27. Elevation z vs FOS vs Volumes

4.1.3. Radius r vs FOS vs volumes

Radius r is the length of the sphere that created for single surface search. The changing of the radius r will affect both the FOS and volumes during the Scoop3D run. As shown in Figure 28, increasing radius r will reduce the FOS as there will be more mass will be analysed, differ from the elevation z that depending on the position of the sphere. On the other hand, as the radius increases, the volume will increase as well due to the mass that analysed will be larger. Hence, the radius r optimised in Scoop3D by considering the balance between the FOS and the volumes.

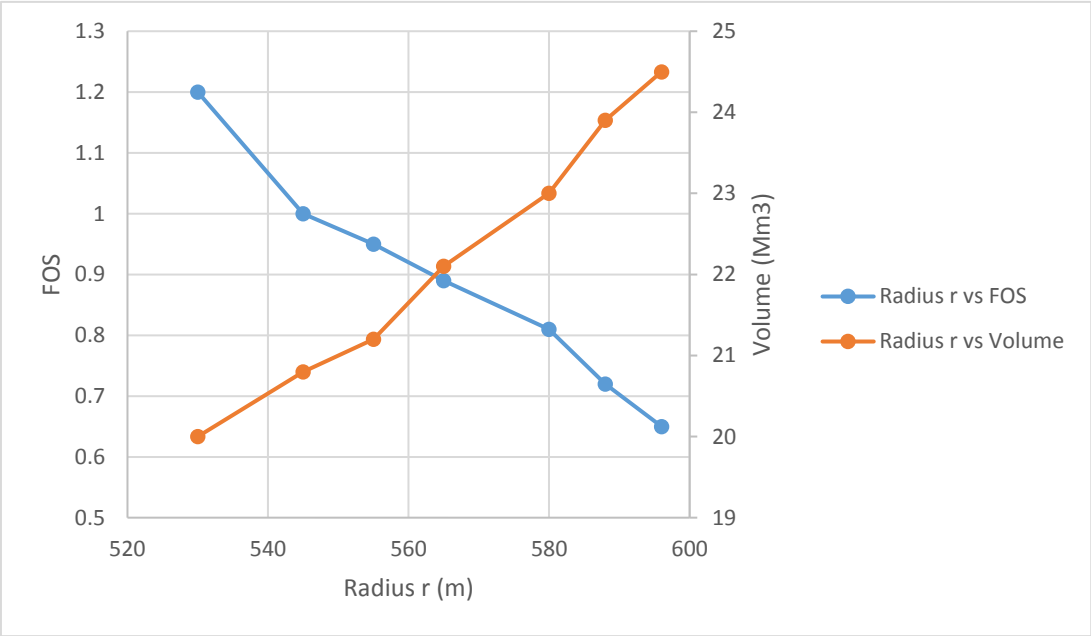

Figure 28. Radius r vs FOS vs Volumes

5. NUMERICAL MODELLING

5.1. INTRODUCTION

As mentioned above section, the run-out of landslide at Bingham Canyon mine will be modelled and analysed by MPM. There are some challenges occur during the modelling, which are the limited resources to perform the MPM modelling and analysis in 3D, and also the familiarity with the algorithms and codes for input in each material element. Using DEM files obtained from geotechnical modelling as the input for MPM, need to be modified using mathematical computational software called MATLAB, to create the material properties for each material element included in DEM file. The input material consists of the material type, name, ID, thick, angle, etc. The input for the material strings is crucial to carefully simulate and calibrate the simulation during the analysis to give more accurate results on describing the run-out behaviour at Bingham Canyon mine as shown in Figure 29.

```
<mp elem='1' mat='1' angle='0' thick='1'>
<pt units='m' x='10' y='10' z='1950' />
<vel units='mm/sec' x='0' y='0' z='0' />
<mass units='kg' m='82000000' />
</mp>
<mp elem='2' mat='1' angle='0' thick='1'>
<pt units='m' x='10' y='30' z='1945.4' />
<vel units='mm/sec' x='0' y='0' z='0' />
<mass units='kg' m='82000000' />
</mp>
<mp elem='3' mat='1' angle='0' thick='1'>
<pt units='m' x='10' y='50' z='1930.1' />
<vel units='mm/sec' x='0' y='0' z='0' />
<mass units='kg' m='82000000' />
</mp>
<mp elem='4' mat='1' angle='0' thick='1'>
<pt units='m' x='10' y='70' z='1930.1' />
<vel units='mm/sec' x='0' y='0' z='0' />
<mass units='kg' m='82000000' />
</mp>
<mp elem='5' mat='1' angle='0' thick='1'>
<pt units='m' x='10' y='90' z='1921.4' />
<vel units='mm/sec' x='0' y='0' z='0' />
<mass units='kg' m='82000000' />
</mp>
```

Figure 29. Input strings for each material points

5.2. BASE MATERIAL ELEMENT

The base of the numerical modelling is the first materials that created using DEM of the second failure. The second failure is treated to be the stiff properties of the material, and the input for each material elements are modified using MATLAB before converting it to MPM software. The

MATLAB code for the base material points can be seen in Appendices B. The base MPM modelling seen in Figure 30.

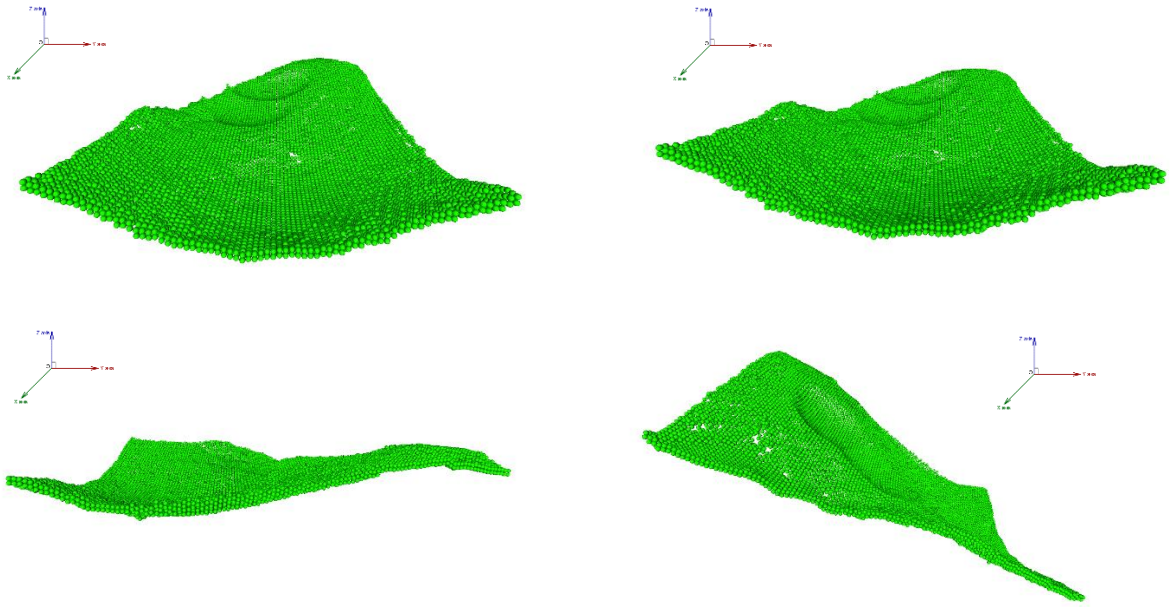

Figure 30. MPM analysis for the base simulate Bingham Canyon mine failure

As shown in Figure 30, it can be seen that the base material elements were able to identify both of the failure surfaces at post event in comparison with the topography files obtained. However, there are some difficulties determining the material type. Similar input has been approached with previous research using the same method; it gives an error result. Hence, more consultation and time is required to improve the material input for the base.

5.3. FAILURE SURFACES MATERIAL ELEMENT

After the base material elements generated, the failure surfaces created in the same manner. Back analysis and modification of MATLAB coding used during the process of creating the strings of each material elements. The MATLAB code for the failure surfaces material points seen in Appendices B. The failure surfaces MPM modelling seen in Figure 31.

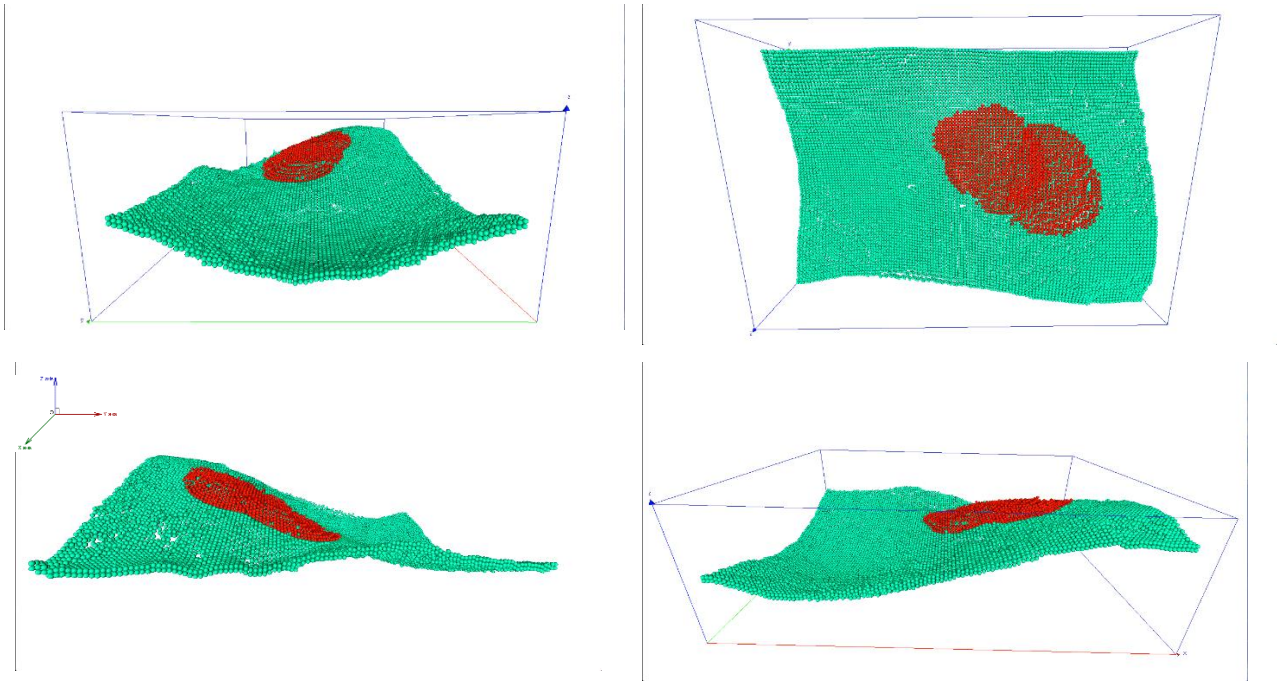

Figure 31. MPM analysis for the failure surfaces simulate Bingham Canyon mine failure

As shown in Figure 31, both the base and failure surfaces material elements labelled as green and red colours. The failure surfaces material elements were able to locate accurately according to the DEM's coordinates. Furthermore, MATLAB code involved generating numbers of material elements required at each coordinate for every single material points at both failure surfaces. However, a minor error has occurred on defining the material name input for both surfaces. There are three types of materials: Base, Failure 1, and Failure 2. MPM gives an error 3D visualisation to achieve three different material name. Furthermore, the authors chose to use the same material name for both failure surfaces. Hence, more consultation and time is required to improve the material input for the failure surfaces.

6. RESULT AND ANALYSIS

6.1. GEOTECHNICAL ANALYSIS

6.1.1. First failure

The input for single surface search to simulate and FOS analysation seen in Figure 32. This input obtained from the optimisation of the variables for Scoop3D as mentioned above section.

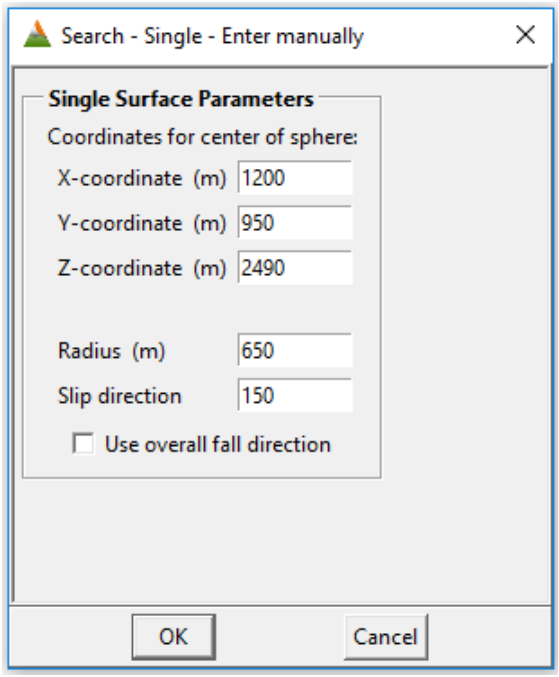

Figure 32. Single surface parameters for failure 1 (Reid et al, 2015)

The output file for the first failure seen in Figure 33. The volumes of the first failure are approximately 24Mm3 volumes with 0.98 for FOS with 3D Bishop's search method.

```
++++++++++++++++++++++++++++++++++++++++++++++++++++++++++++++++++++++++++++++++++
IV. RESULTS:
------------
3D POTENTIAL FAILURE
Bishop's 3D factor of safety:                                          0.9877
Ordinary 3D factor of safety:                                          0.9179
Volume (m ^3):                                                      2.40819E+07
Horizontal surface area (m ^2):                                     3.62075E+05
Slip surface area (m ^2):                                           4.16035E+05
Weight (kg):                                                        5.87598E+08
Number of active columns:                                                   938
        x-center         y-center          z-center     radius
       1200.0000          950.0000         2490.0000   6.50000E+02
Slip direction, relative to search lattice:                            150.0000

Associated 2D potential failure:
Bishop's 2D factor of safety:                                          1.0110
Cross-sectional area ( m ^2):                                       6.38273E+04
Horizontal length ( m ):                                            7.69346E+02
Arc length ( m ):                                                   8.67337E+02
Number of active columns:                                                    54
------------
```

Figure 33. Output files from Scoop3D for failure (Reid et al, 2015)

With the same output, the topography for the first failure seen in Figure 34. It is seen that the location of the first failure is accurate following the real event that happened at Bingham Canyon mine.

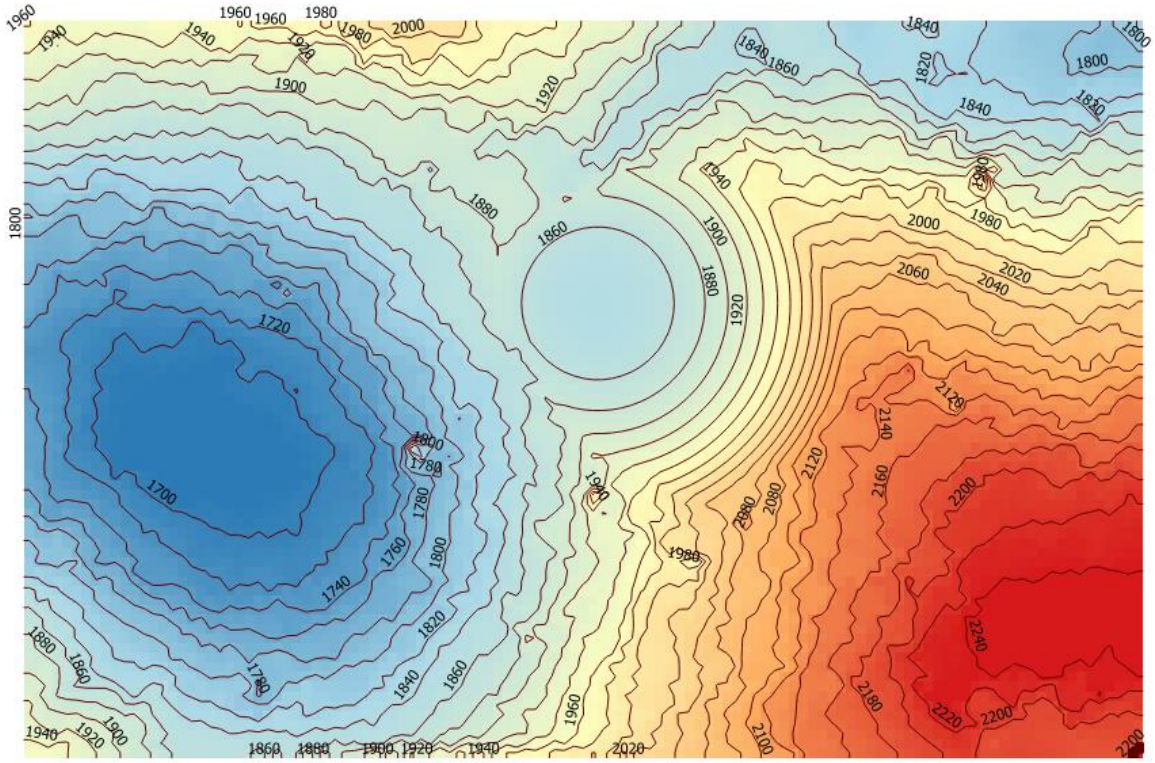

Figure 34. Topography at failure 1

Hence, 3D representation for the geotechnical modelling seen in Figure 35. With FOS lower than one, it can be seen that the model is accurate according to the event that took place in Bingham Canyon mine.

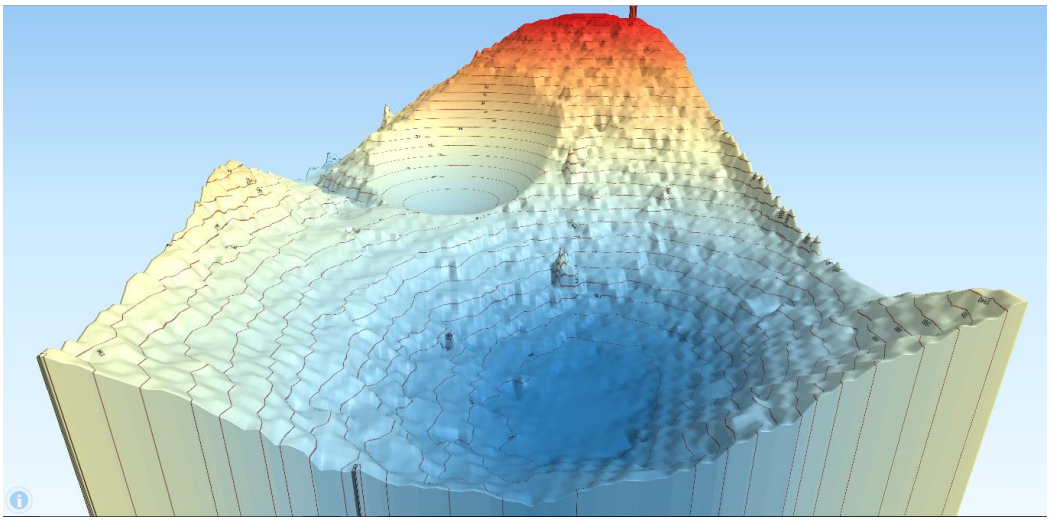

Figure 35. 3D representation of failure 1

6.1.2. Second failure

The input for single surface search to simulate and FOS analysation seen in Figure 36. This input obtained from the optimisation of the variables for Scoop3D as mentioned above section. Based on the input, the authors optimised the location of the second sphere to touch the result from the first failure to increase the accuracy.

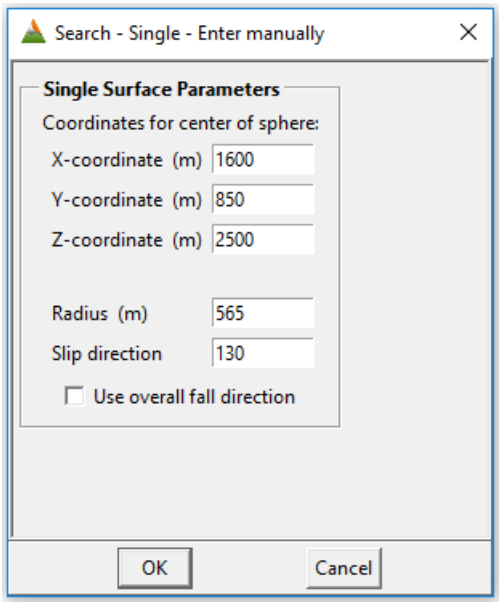

Figure 36. Single surface parameters for failure 2 (Reid et al, 2015)

The output file for the first failure seen in Figure 37. The volumes of the second failure are approximately 22Mm3 volumes with 0.89 for FOS with 3D Bishop's search method. In comparison, the second failure gives lower FOS rather than the first one due to some of the mass that move from the first failure acted as support for the mass that moved at the second failure.

```
++++++++++++++++++++++++++++++++++++++++++++++++++++++++++++++++++++++++++++++++++
IV. RESULTS:
F < foscut found and newDEM_out file created?                          yes
------------
3D POTENTIAL FAILURE
Bishop's 3D factor of safety:                                        0.8983
Ordinary 3D factor of safety:                                        0.8370
Volume (m ^3):                                                   2.21736E+07
Horizontal surface area (m ^2):                                  2.88109E+05
Slip surface area (m ^2):                                        3.40915E+05
Weight (kg):                                                     5.41036E+08
Number of active columns:                                              753
        x-center         y-center          z-center     radius
       1600.0000          850.0000         2500.0000   5.65000E+02
Slip direction, relative to search lattice:                        130.0000

Associated 2D potential failure:
Bishop's 2D factor of safety:                                        0.8651
Cross-sectional area ( m ^2):                                    6.24801E+04
Horizontal length ( m ):                                         6.03018E+02
Arc length ( m ):                                                6.93308E+02
Number of active columns:                                              43
------------
```

Figure 37. Output files from Scoop3D for failure 2 (Reid et al, 2015)

With the same output, the topography for the second failure seen in Figure 38. It is shown that the location of the second failure is overlapping the first failure zone, which is accurate according to the real event that happened at Bingham Canyon mine.

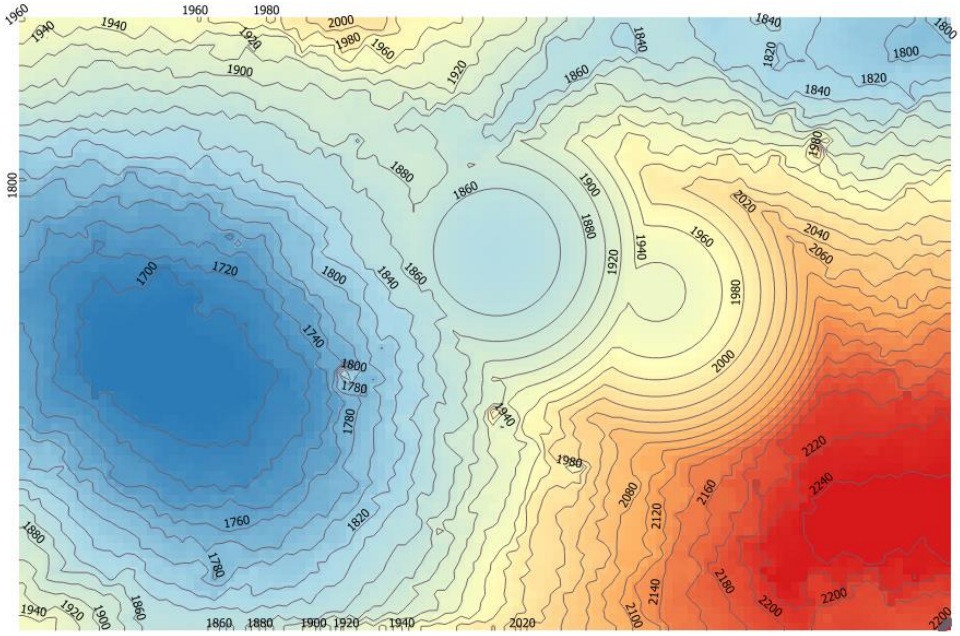

Figure 38. Topography at failure 2

Hence, 3D representation for the geotechnical modelling shown in Figure 39. With FOS lower than one, it shown that the model is accurate according to the event that took place in Bingham Canyon mine.

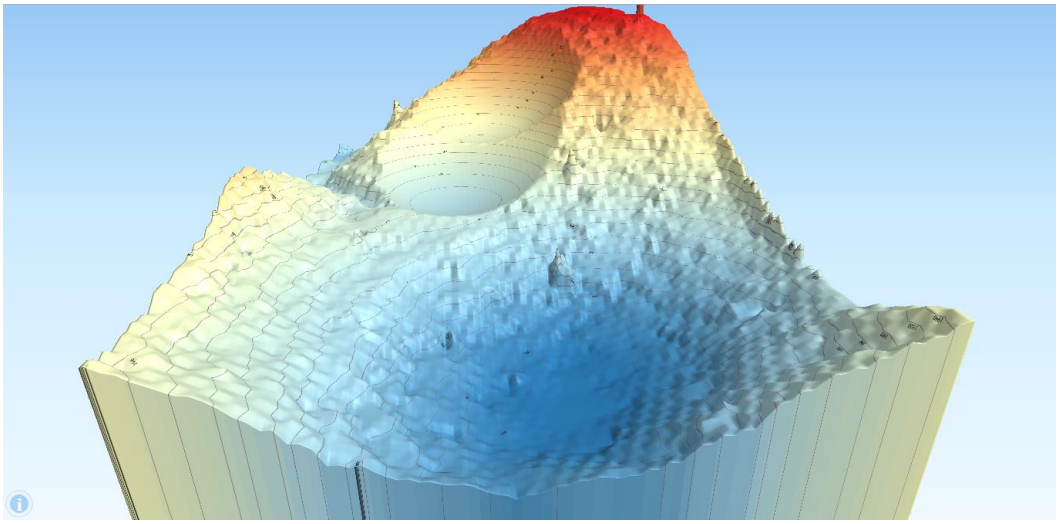

Figure 39. 3D representation of failure 2

As seen in Figure 39, the authors simulated a geotechnical model from the original DEM file with optimised input parameters of the single surface search and 3D bishop's simplified search method. This gives 24Mm3 volumes with 0.98 for FOS on the first failure. Furthermore, the second failure gives 22Mm3 volumes with 0.89 for FOS. This output will be a good indication for the authors to build and design the numerical modelling and analysis with MPM to observe the kinematic behaviour of the mass that moves during the landslide event in Bingham Canyon mine. However, MPM gives an error 3D visualisation to achieve three different material name. In addition, the authors chose to use the same material name for both failure surfaces.

6.2. NUMERICAL ANALYSIS

This section provides a brief justification of the MPM followed by the simulation of both slides. The simulation runs on a desktop computer Intel i7-2600k, with eight cores, and CPU @ 3.4 GHz. The computations for each slide takes roughly 2 hours. The geometric discretization used in the simulation of the Bingham Canyon Mine slides is described in Table 6. Based on previous results, the geotechnical parameters of both slides are identical as shown in Table 7. The parameters are based on past research by (Pankow et al, 2013). Both slides are of roughly similar mass.

Table 6.

Geometric model details used in MPM simulation of Bingham Canyon mine slides

Cell Size (m)	40
Material point size (m)	1
Material point per cell	4
Material points representing the base layer	146,653
Material points representing the first slide	3,510
Material points representing the second slide	3,169
Number of nodes	54,684

Table 7. Geotechnical parameters of the first and second slides

Unit Weight Υ (kN/m^3)	24.4
Modulus E (MPa)	600.0
Shear Strength □ (kPa)	2.0
Poisson's ratio v	0.33
Friction μ	0.02

With all the numerical input has been applied, the MPM simulation model in cross-section and the panoramic view can be seen in Figure 40. This model used to analyse the geotechnical properties of the velocity and kinetic energy.

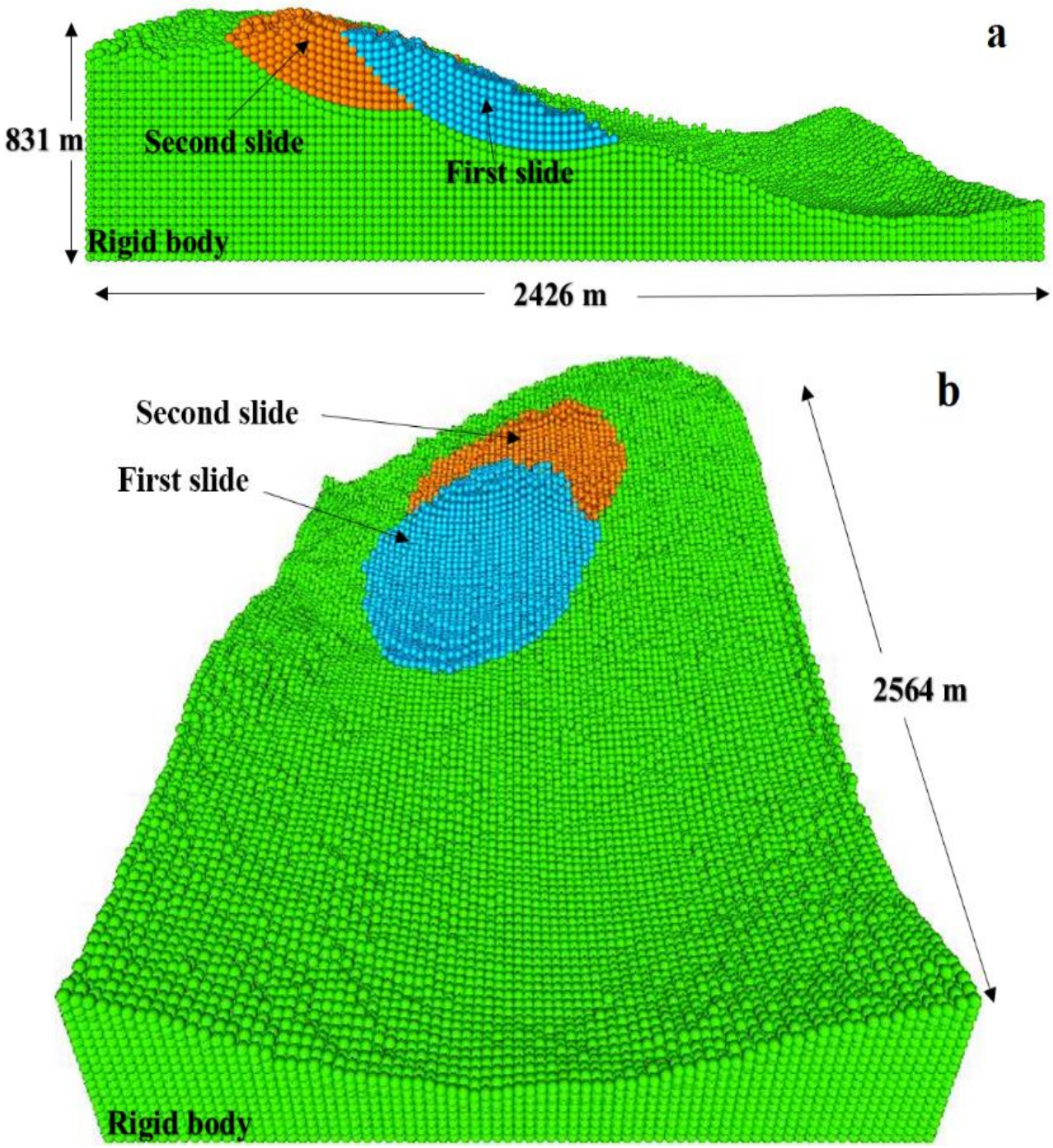

Figure 40. MPM model: (A) cross-section, and (B) panoramic view

6.2.1. Kinetic energy analysis

The kinetic energy computed for the first slide presented in Figure 41, which shows the progression of the energy during run-out. The kinetic energy increases with time until the slide hits the northwestern pit wall at t=20 s, reaching values of up to 10^7 Joule. At t=40 s, the sliding mass reaches the bottom of the pit. Beyond this time, the energy decreases and the slide almost stop at t=60 s. Then, between t=60 s and 90 s, the rate of energy decrease slows, while the last of the sliding mass forms a new topographic configuration. The energy practically dissipated after 90 s.

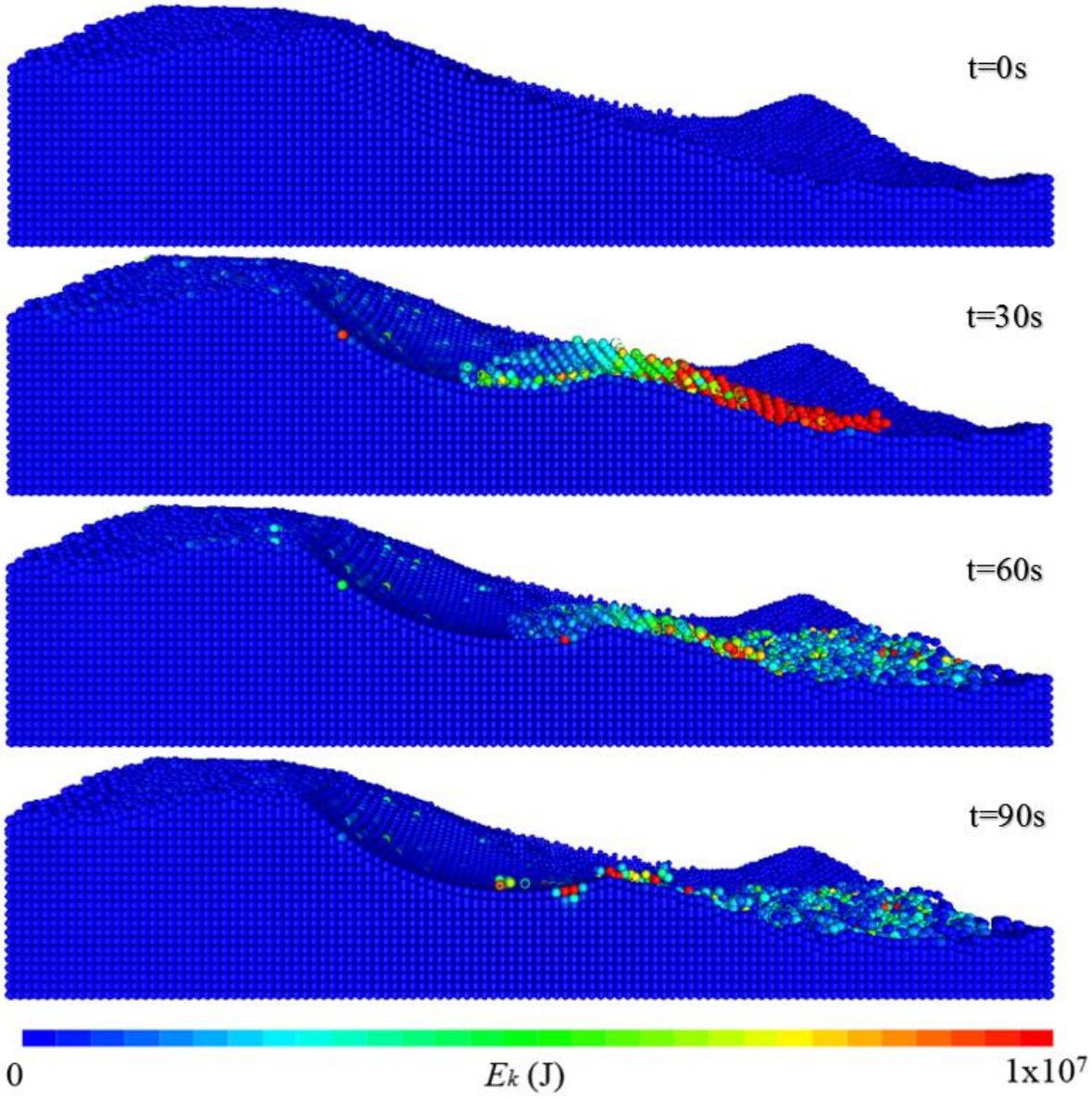

Figure 41. Kinetic energy of the first slide

The kinetic energy computed for the second slide presented in Figure 42. Similar to the first slide, the second slide gives a maximum kinetic energy of 10^7 Joule at t=30 s due to the fall of the sliding material from its original position to the void created by the first slide. The major findings comparing the first result show in Figure 41, to the second result is the value of kinetic energy is constant on the second failure while there is a decrease in the kinetic energy on the first slide both at t=30 s. The slide almost stops at t=80 s, as the rate of energy decrease slows.

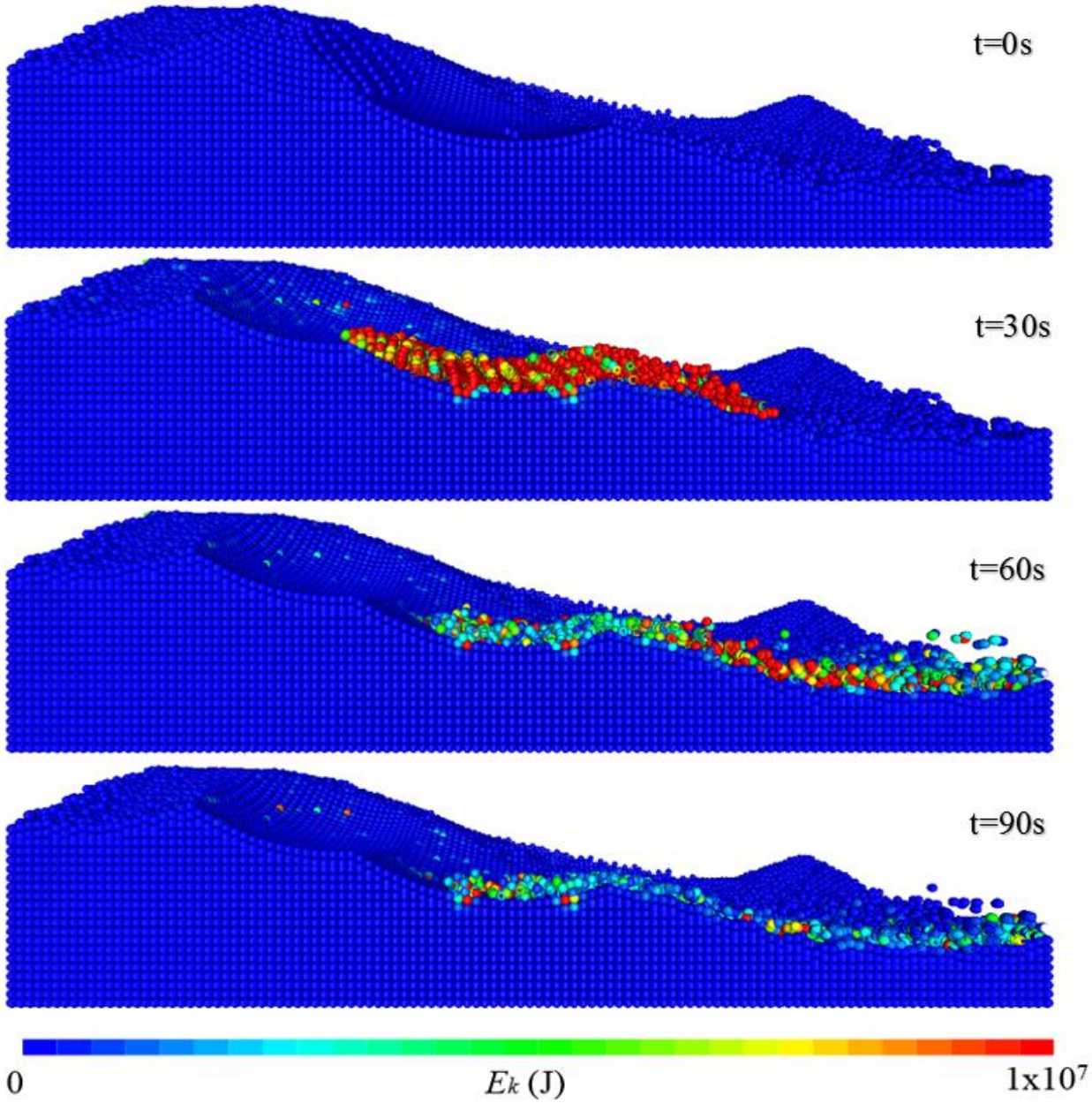

Figure 42. Kinetic energy of the second slide

6.2.2. Velocity analysis

Further analysis done based on the mean velocity of the slides. Comparisons of the MPM two-dimensional and three-dimensional velocities of both slides shown in Figure 43. The results compared in Figure 43 with computations using the Landslide Force History (LFH) obtained by (Hibert el al, 2014). It seen that for both slides, the MPM and LFH results match reasonably well. The seismic records analysed by (Pankow et al, 2013) indicate that the slides had durations of about 90 s, in very close with the computations obtained herein.

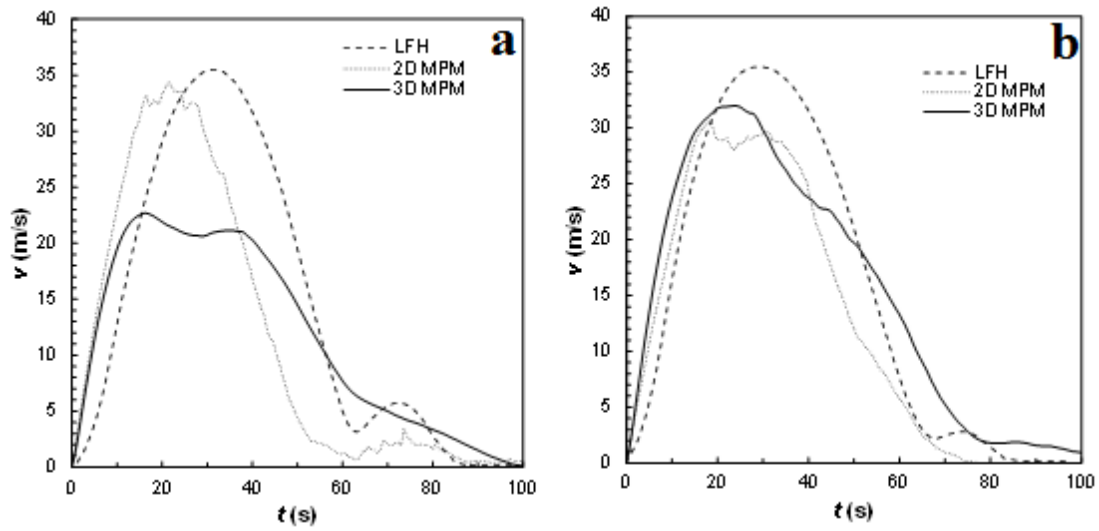

Figure 43. Velocity with time for: (A) first slide, and (B) second slide

The computed peak velocities for the second slide are within 5 m/s, while for the first slide, the two-dimensional MPM and LFH peak velocities are in close agreement. The three-dimensional MPM peak velocity for the first slide is about 15 m/s lower than the other two computed results. This happens because the particles sliding down the northeastern pit wall hit the north-western pit wall, reversing the movement and slowing the slide. This observation highlights the importance of considering three-dimensional effects in complex cases. This reversal of movement is not present in the second slide since the movement is smoother compared with the first slide.

Finally, a comparison between the photograph from Figure 7 and MPM simulated geometry at the end of the second slide shown in Figure 44. Debris left behind after the slides seen in the simulation. The MPM model also reproduced how the debris flow covered the bottom of the pit. However, some differences are also apparent. The numerical model considered herein relies on the 2007 topography of the pit, while the slides occurred in 2013. It is clear that the pit was

actually larger prior to the slides than it was in 2007. As results, Figure 44 shows a larger buried area.

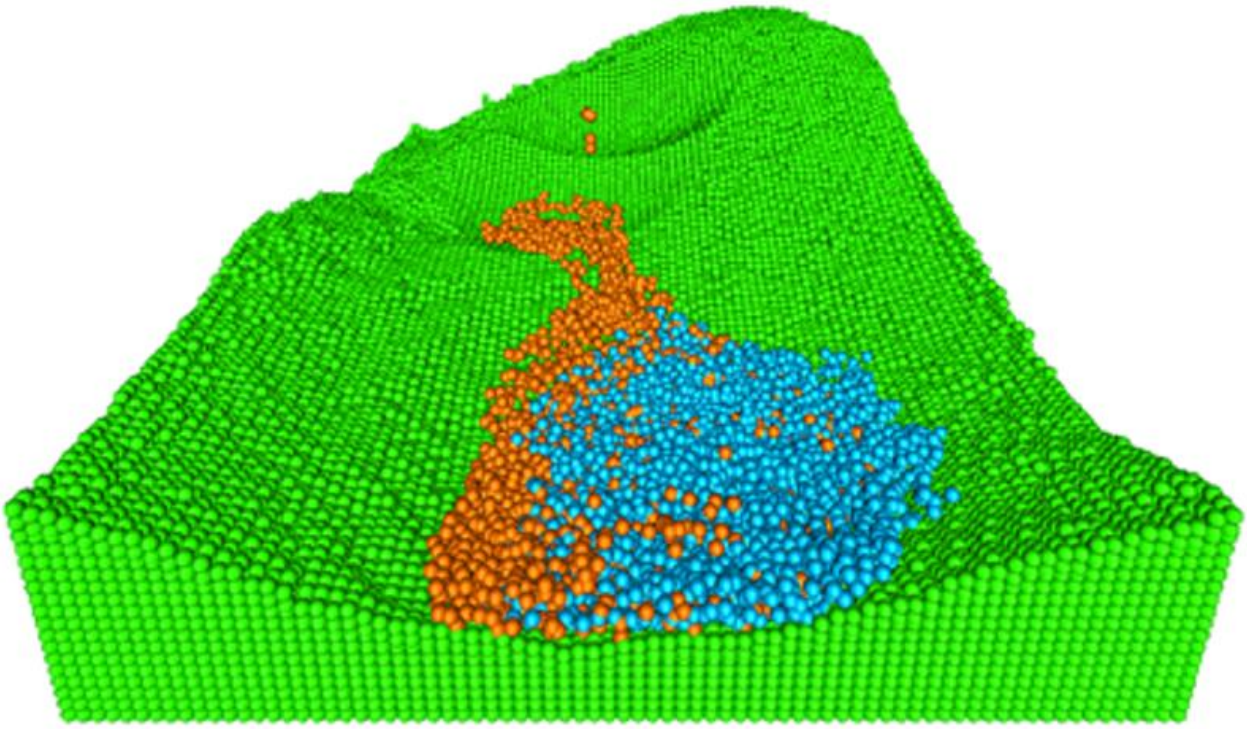

Figure 44. MPM simulated geometry at the end of second slide

7. SENSITIVITY ANALYSIS

As one of the aims and objectives of this project, the author seeks to observe and analyse the geotechnical properties using the applied MPM on the real case study by using the parameters that used as shown in Table 8. The parameters that will be analysed includes yield, modulus, Poisson's ratio, masses of the slide failures, and the friction as shown in Table 9. The Sensitivity analysis covers the visual interpretation with the changes in each of the parameters, and also further study is conducted in graphical interpretation to observe in details the velocity, force, and kinetic energy.

Table 8.

Initial parameters setup

Initial Parameters						
Type	***File Name***	***Yield***	***Modulus***	***P. Ratio***	***Mass***	***Friction***
Fail 1	TestTest_no_elem18	1	600	0.33	23510	0.02
Fail 2	TestTest_Fail2_03	1	600	0.33	26033	0.02

Table 9.

Parameter criteria for sensitivity analysis

Sensitivity Criteria		
Parameters	***1***	***2***
Yield	50%	-50%
Modulus	50%	-50%
Poisson's	0.35	0.4
Mass	10%	-10%
Friction	5%	-5%

As shown in Table 9, there will be two tests simulated for each parameter, and it applies to both visual and graphical sensitivity analysis. These analyses conducted to get a comprehensive understanding of the geotechnical properties that gives influence in the movement of the slide failures in tridimensional MPM. This will give more accurate results compare to past research that only done in a two-dimensional approach of MPM or any numerical analysis. The List of sensitivity analysis matrix seen in Table 10. There are 20 simulations in total includes ten simulations in each slide failure. In the section below for visual analysis, the author will be focusing on the first failure only. The second failure viewed in Appendix C.

Table 10.

Matrix of Sensitivity analysis

Sensitivity Analysis						
File Name	***Fail No.***	***Yield***	***Mod***	***P. Ratio***	***Mass***	***Fric***
ST_F1_Y1	1	**1.5**	600	0.33	23510	0.0200
ST_F1_Y2		**0.5**	600	0.33	23510	0.0200
ST_F1_M1		1	**900**	0.33	23510	0.0200
ST_F1_M2		1	**300**	0.33	23510	0.0200
ST_F1_P1		1	600	**0.37**	23510	0.0200
ST_F1_P2		1	600	**0.4**	23510	0.0200
ST_F1_Ma1		1	600	0.33	**25861**	0.0200
ST_F1_Ma2		1	600	0.33	**21159**	0.0200
ST_F1_F1		1	600	0.33	23510	**0.0210**
ST_F1_F2		1	600	0.33	23510	**0.0190**
ST_F2_Y1	2	**1.5**	600	0.33	26033	0.0200
ST_F2_Y2		**0.5**	600	0.33	26033	0.0200
ST_F2_M1		1	**900**	0.33	26033	0.0200
ST_F2_M2		1	**300**	0.33	26033	0.0200
ST_F2_P1		1	600	**0.37**	26033	0.0200
ST_F2_P2		1	600	**0.4**	26033	0.0200
ST_F2_Ma1		1	600	0.33	**28636**	0.0200
ST_F2_Ma2		1	600	0.33	**23430**	0.0200
ST_F2_F1		1	600	0.33	26033	**0.0210**
ST_F2_F2		1	600	0.33	26033	**0.0190**

7.1. VISUAL INTERPRETATION

As mentioned in above section, the analysis will be focusing on the first failure only due to the similar behaviour that occurs on the second failure, which is seen in Appendix C. The summary of the interpretation of the first failure shown in Table 11. The interpretation of the visual approach covers the speed to pit wall and to depositional zone, the flow behaviour, dispersion, simulation time that capped at 100 seconds, leftovers of the failure particles at the failure surface zone, and the average quantity of the leftovers at the failure surface zone.

Table 11.

Visual interpretation for first failure

Interpretation for Failure 1							
File Name	***Speed to Pit Wall***	***Speed to Depositional Zone***	***Flow Behaviour***	***Dispersion***	***Simulation Time (secs)***	***Leftovers at Failure Surface Zone***	***Quantity of Leftovers***
ST_F1_Y1	Slow	Slow	Compact	No	80	No	No
ST_F1_Y2	Fast	Fast	Fluid	Yes	100	Yes	Many
ST_F1_M1	Fast	Fast	Fluid	No	100	Yes	Few
ST_F1_M2	Slow	Fast	Fluid	No	90	No	No
ST_F1_P1	Medium	Fast	Fluid	No	100	Yes	Few
ST_F1_P2	Slow	Slow	Fluid	No	100	Yes	Many
ST_F1_Ma1	Medium	Medium	Fluid	No	100	Yes	Few
ST_F1_Ma2	Medium	Medium	Fluid	No	100	No	No
ST_F1_F1	Slow	Slow	Fluid	No	100	Yes	Few
ST_F1_F2	Fast	Fast	Fluid	No	100	No	No

7.1.1. Yield (ST_F1_Y1 and ST_F1_Y2)

As mentioned above there is two yield value that tested, which are 1.5 and 0.5 as shown in Figure 45. It was observed that if the increasing yield will affect the speed of the failure surface to move, and will compact the whole failure particles throughout the simulations. However, the lower yield cause the flow behaviour become fluid like and there are many leftovers at the failure surface. Therefore, changing the yield value gives changes on the flow behaviour and simulation time.

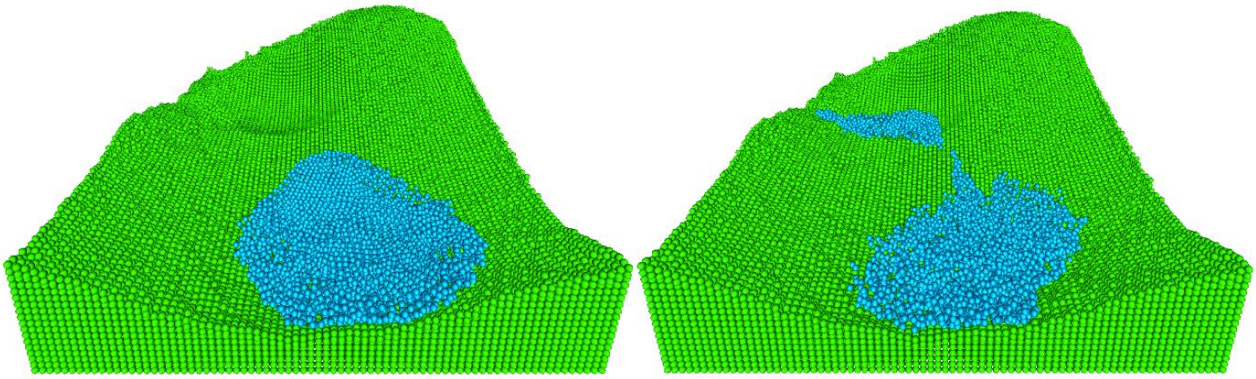

Figure 45. Failure 1 yield interpretation

7.1.2. Modulus (ST_F1_M1 and ST_F1_M2)

Two modulus value that tested is 900 and 300 as shown in Figure 46. It was observed that the increasing modulus will cause the failure materials to move faster throughout the simulation, with

few leftovers occur due to the reducing velocity of some of the failure materials that was hitting the pit wall. However, by decreasing the modulus, it will reduce the speed of the movement of the failure materials, which enough to give enough momentum for all of the materials to move to the depositional zone. Therefore, by changing the modulus, it will provide an impact on the speed, and momentum of the failure materials.

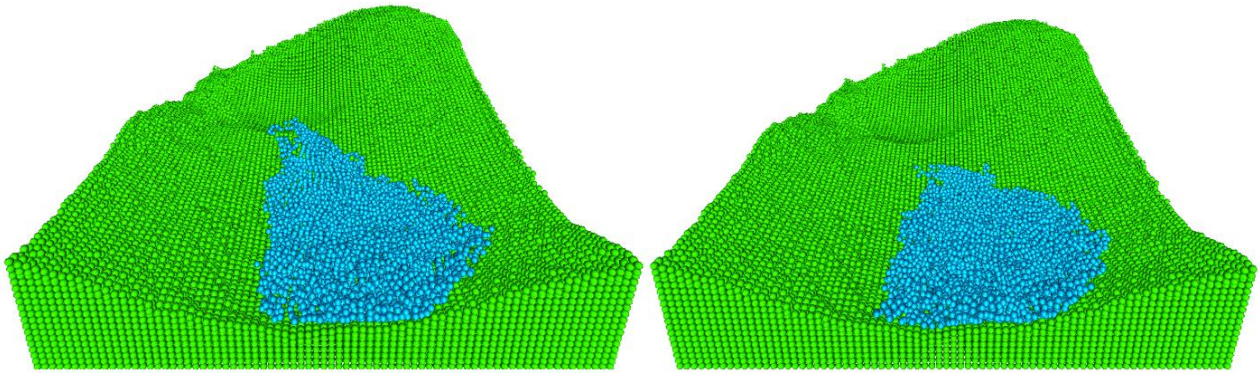

Figure 46. Failure 1 modulus interpretation

7.1.3. Poisson's ratio (ST_F1_P1 and ST_F1_P2)

There is two increasing value that used for analysing the effects of changing the Poisson's ratio, which is 0.37 and 0.40 as shown in Figure 47. It observed that the increasing Poisson's ratio will not give many differences in the behaviour and movement of the failure materials, except for the number of the leftovers at the second value tends to give more throughout the simulation. Therefore, there is not much difference by changing the Poisson's ratio that further investigation may be required.

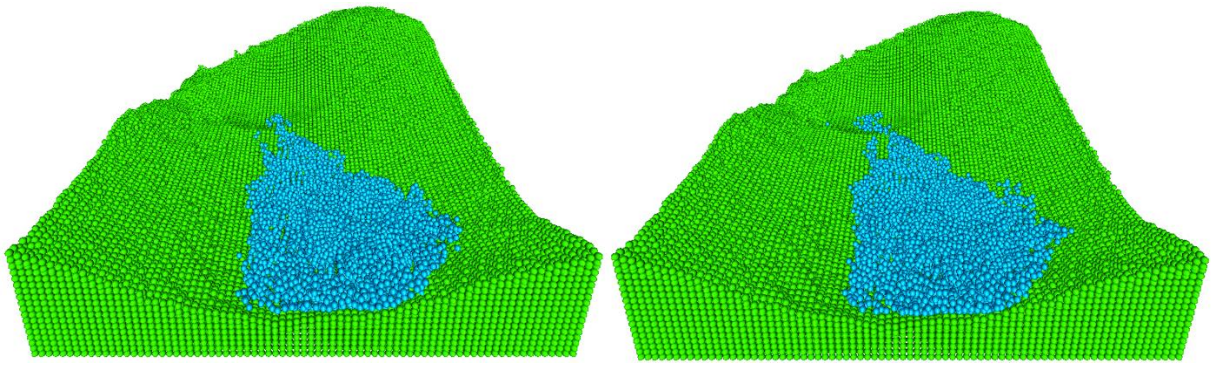

Figure 47. Failure 1 Poisson's ratio interpretation

7.1.4. Mass (ST_F1_Ma1 and ST_F1_Ma2)

Two failure materials mass values that used are 25861kg and 21159kg respectively as shown in Figure 48. It observed that both of the simulations give similar results. However, there are few

leftovers failure materials on the first simulations due to the increasing mass, will increase the speed and momentum, that gives more impact on the pit walls. This result to decrease in velocity after an impact that gives more leftovers failure materials on the failure zone. Therefore, changing in masses will only affect the speed of the failure materials that move towards the depositional zone.

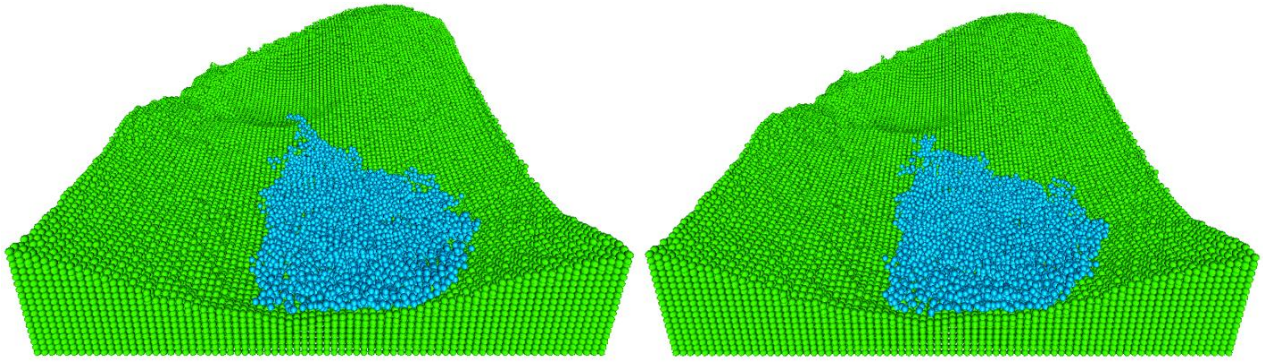

Figure 48. Failure 1 mass interpretation

7.1.5. Friction (ST_F1_F1 and ST_F1_F2)

Two failure materials friction values that used are 0.0210 and 0.0190 respectively as shown in Figure 49. It observed that higher friction would reduce the speed of the movement of the failure materials, which gives few leftovers in the failure zone. However, lower friction will give faster movement with no leftovers at the failure zone. Therefore, the change in friction gives impacts on the movement speed of the failure materials.

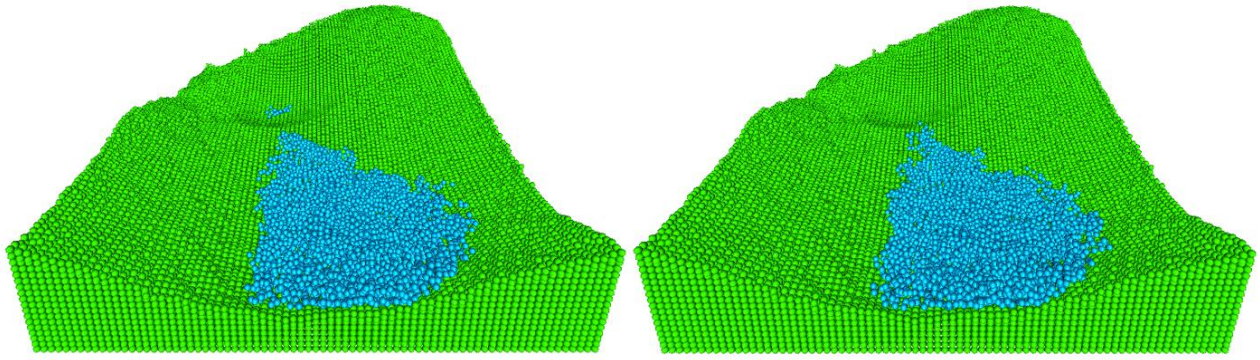

Figure 49. Failure 1 friction interpretation

7.2. GRAPHICAL INTERPRETATION

Further approach from the visual interpretation observed to gain new findings and analysis on the kinematics of the run-out, for both the first and second slide. The variables that involved similar to the visual interpretation in observing the velocity of the run-out from both first and second slide. The kinematics then compared with the visual interpretation to observe if both findings match to each other.

7.2.1. Yield

The velocity for both failures slides by the modification of the yield shown in Figure 50. It observed that the adjustment of the yield gives impact on the velocity for both first and second slide with the comparison of the results from Figure 43. The trend of the velocity is decreasing for Y1 and increasing for Y2. It observed that the increasing of yield on the first slide gives inconsistent velocity throughout the event, with a reasonable trend. However, the yield modification of the second slide provides consistent results. Hence, both slides are similar to the visual representation that observed in Figure 45.

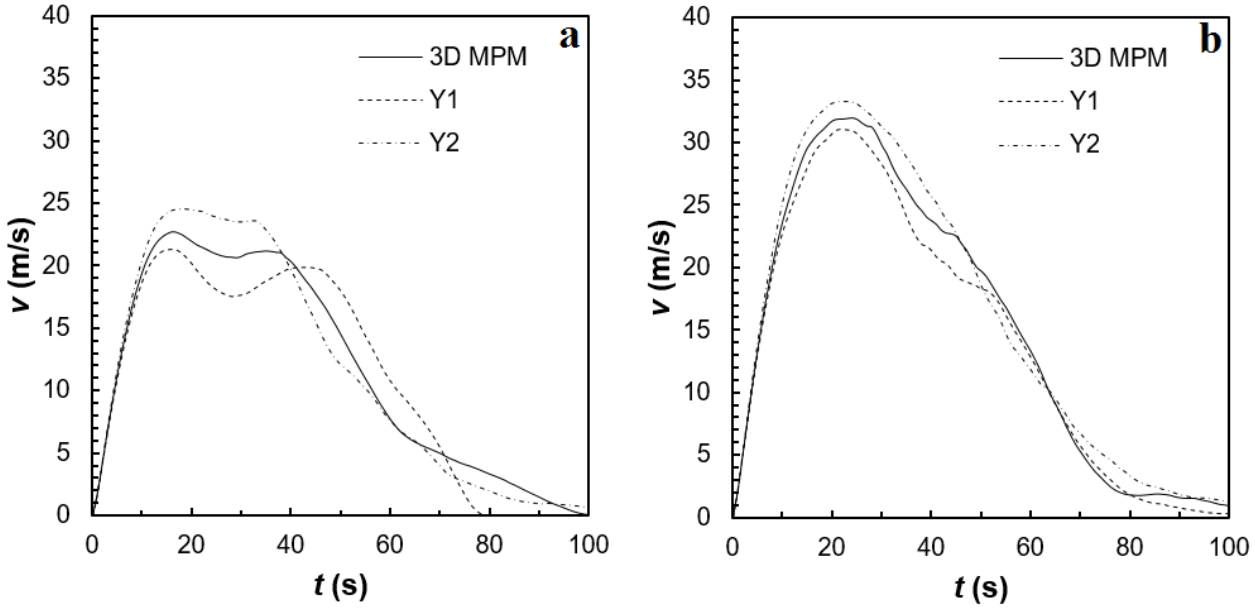

Figure 50. Velocity with yield modification for: (a) first slide, and (b) second slide

7.2.2. Modulus

The velocity for both failures slides by the modification of the modulus shown in Figure 51. It is found that the change of the modulus gives impact on the velocity for both first and second slide with the comparison of the results from Figure 43. The trend of the velocity is decreasing for M1 and increasing for M2. It is found that the increase of modulus decreases the velocity of the slides with a consistent trend. However, it gives longer time for the slides to finish for both first and second slides. Therefore, both slides are similar to the visual representation that observed in Figure 45.

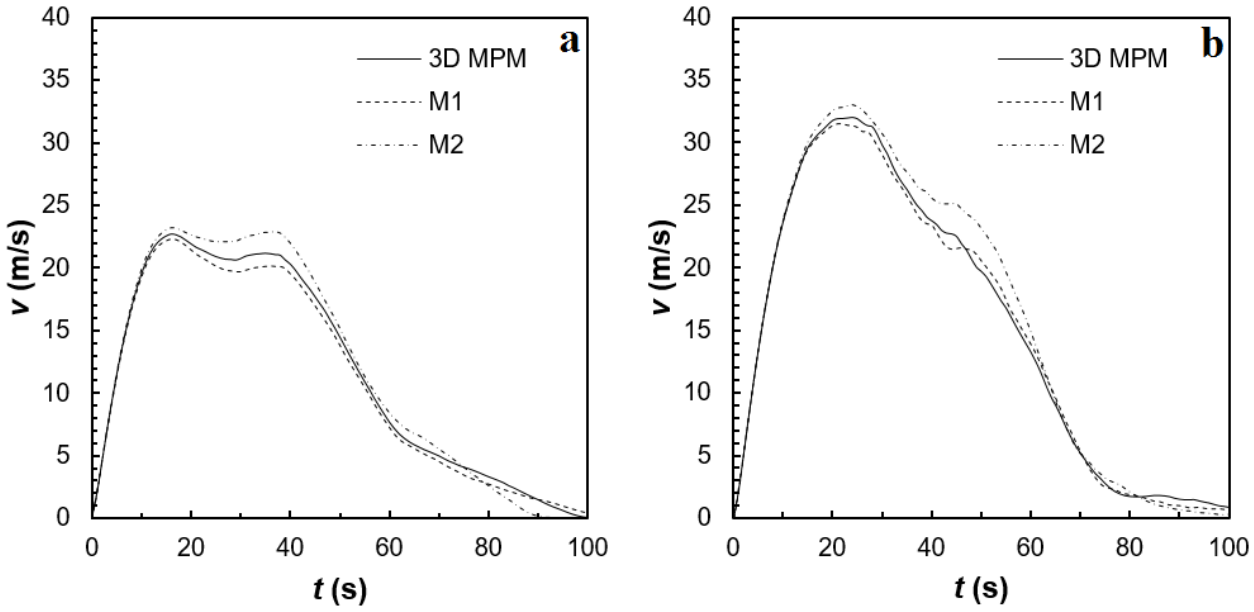

Figure 51. Velocity with modulus modification for: (a) first slide, and (b) second slide

7.2.3. Poisson's ratio

The velocity for both failure slides by the modification of the Poisson's ratio shown in Figure 52. It is observed that the modification of Poisson's ratio gives little impact on the velocity for both first and second slide with the comparison of the results from Figure 43. The trend of the velocity is decreasing with increasing of the Poisson's ratio for both P1 and P2. The increase the Poisson's ratio gives impact on t=40s to t=50s. However, it gives consistent trend for both first and second slide. Therefore, both slides are similar to the visual representation that observed in Figure 45.

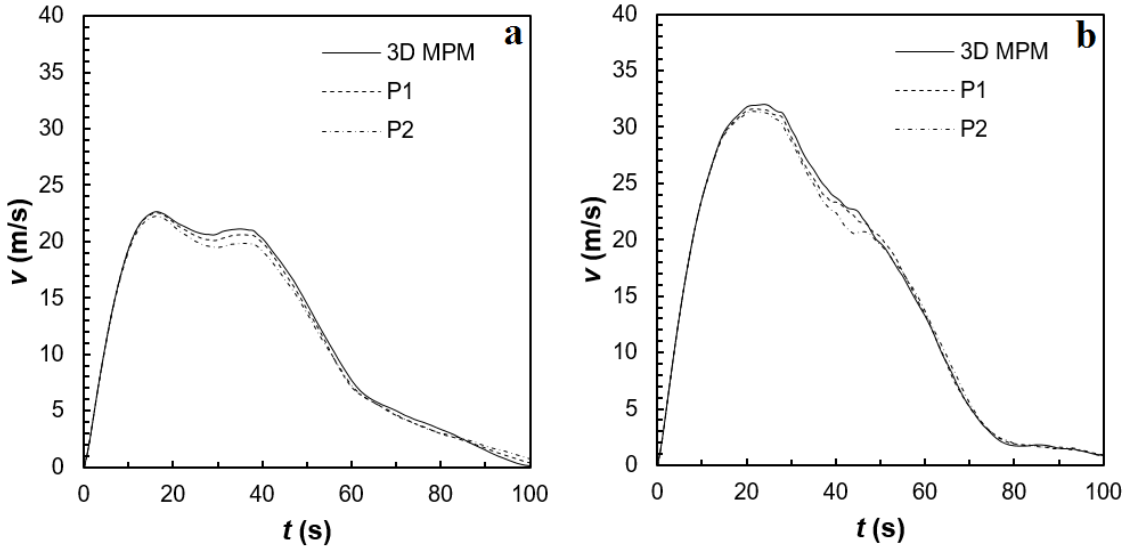

Figure 52. Velocity with Poisson's ratio modification for: (a) first slide, and (b) second slide

7.2.4. Mass

The velocity for both failure slides by the modification of the mass shown in Figure 53. The modification of mass gives little impact on the velocity for both first and second slide with the comparison of the results from Figure 43. The trend of the velocity is similar for both Ma1 and Ma2. However, there were only 10% changes in mass as shown in Table 9. Hence, it is recommended to modify the mass further to give more possible findings for future research.

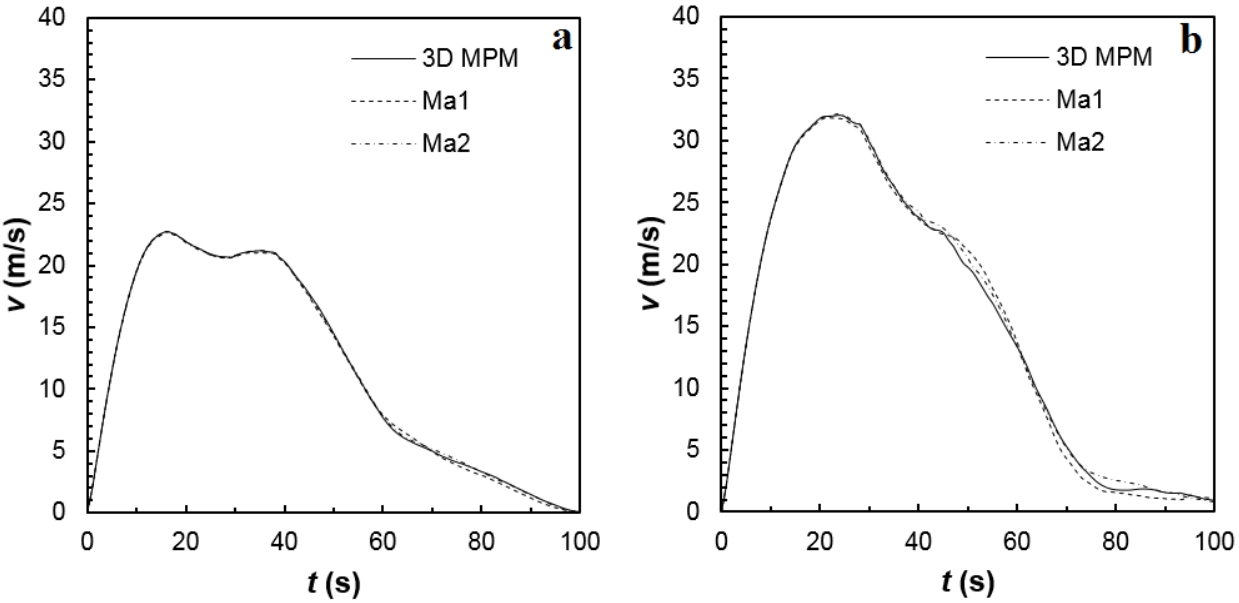

Figure 53. Velocity with mass modification for: (a) first slide, and (b) second slide

7.2.5. Friction

The velocity for both failure slides by the modification of the friction of the failure slides shown in Figure 54. It is observed that the modification of friction gives little impact on the velocity to both first and second slide with the comparison of the results from Figure 43. The trend of the velocity is similar for both F1 and F2. However, there were only 5% changes in mass as shown in Table 9. The little changes decided by the author due to the effects of friction gives large impact on the base results obtained in Figure 40. Hence, it is recommended to modify the friction further to give the possible findings for further research.

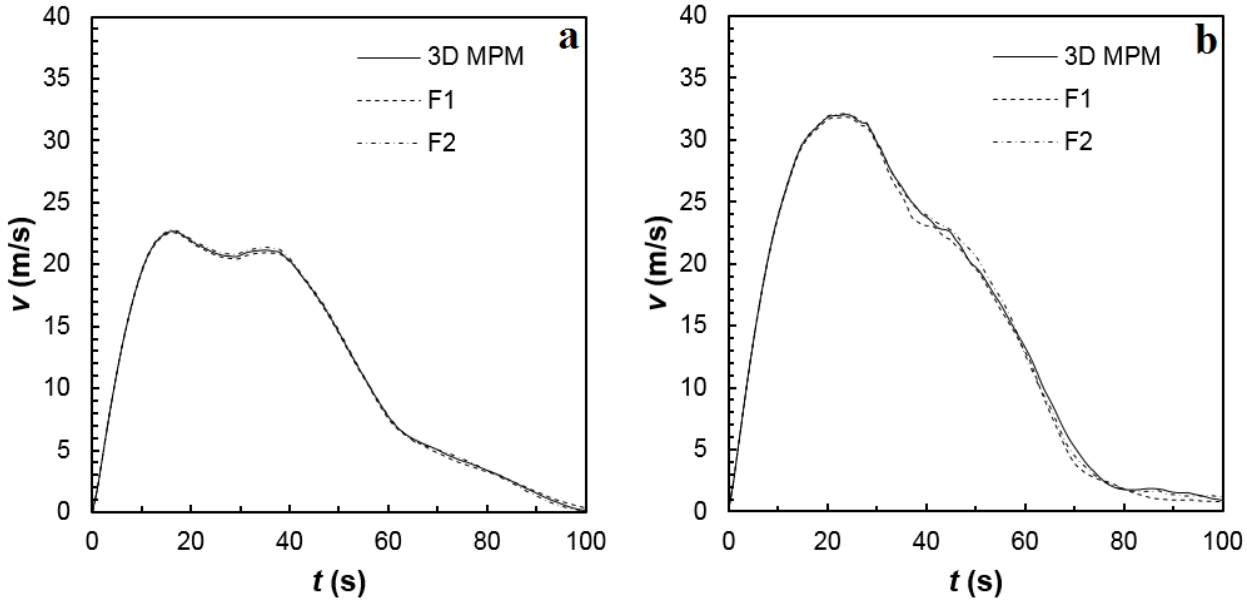

Figure 54. Velocity with friction modification for: (a) first slide, and (b) second slide

7.3. REAL SCALE INTERPRETATION

Another significant finding that discovered involves the application of three-dimensional analysis to the actual case study for further analysis and validation. As shown in Figure 18, the initial input of the numerical and geotechnical modelling starts from the digitisation of the real scale case study at Bingham Canyon mine. The digitisation gives coordinates and topography of the area as a result. After achieving a satisfactory analysis of three-dimensional analysis, kinematics analysis, and visual interpretation, it is required to trace the movement of the landslide that simulated by NairnMPM, and then compare it to the real scale orientation from Google Earth.

7.3.1. Trajectory analysis

The simulation's slide trajectory line applied to the real scale shown in Figure 55.

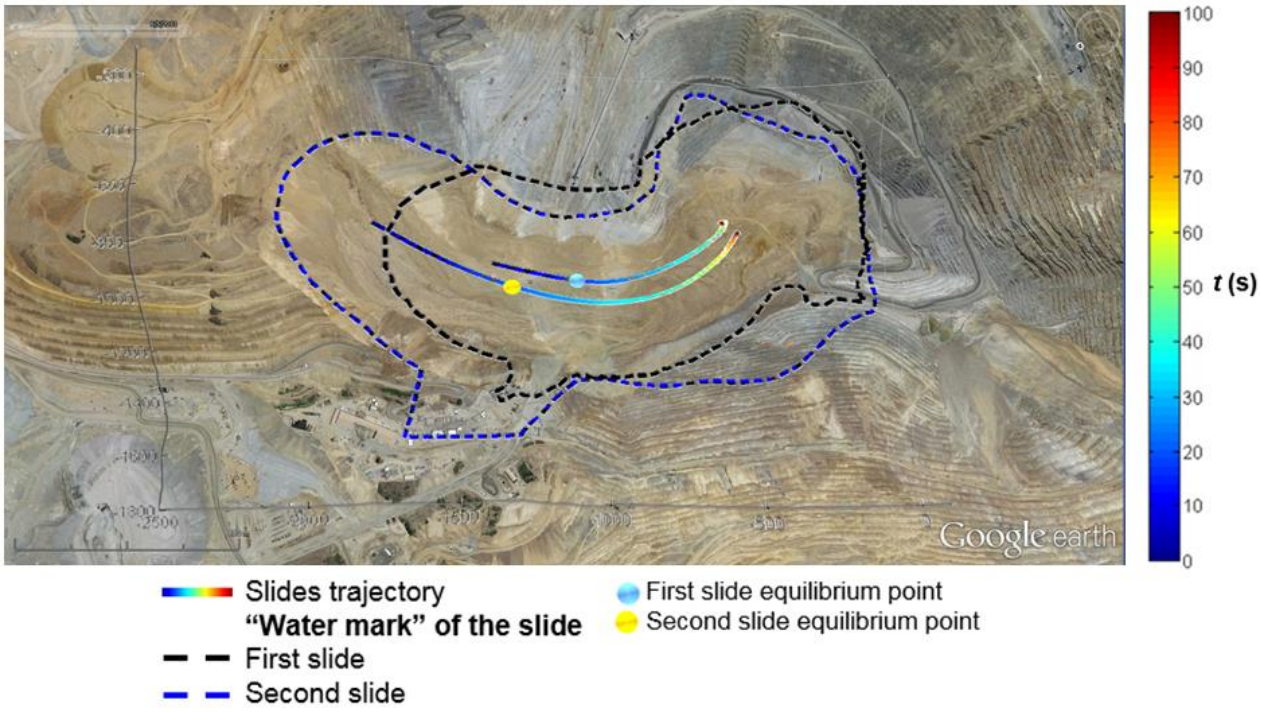

Figure 55. Trajectory line from simulation to real scale

As shown in Figure 55, the path line of the first slide shown as a black colour, during the second slide in blue colour. Both slides give similar pathway that analogous to the past research that shown in Figure 7. Each line and trajectory line have been georeferenced to fit the real scale from Google Earth, to observe how numerical modelling and analysis able to solve and be a major part of case study analysis. Panoramic view of the slide trajectory seen in Figure 56.

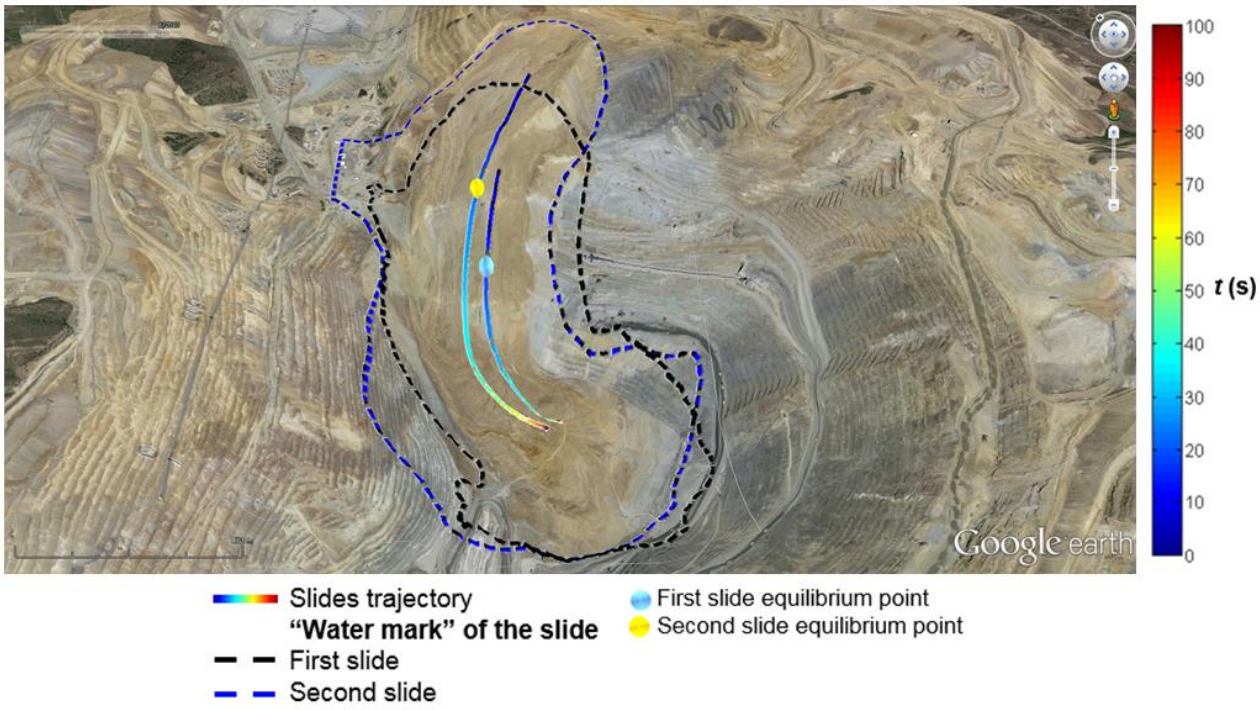

Figure 56. Panoramic view of slide trajectory from simulation to real scale

As shown in Figure 56, the panoramic view gives a better visual representation of the path line of both slides failure from the crown to the toes of the landslide. In addition, it gives more accurate results compare to the previous research done by (Hilbert, Ekstrom & Stark, 2014) using the LFH methods. Additionally, the conducted numerical approach was treated as a supporting evidence of their main findings; due to the limitation of LFH methods, that focuses on the seismicity monitoring that placed throughout the entire mine. However, MPM three-dimensional approach uses the real scale data to be treated as initial input for modification, and further manipulation to achieve the results that satisfactory as the findings.

7.3.2. Safety analysis

Bingham Canyon mine is one the largest open-pit mine in the world. Having the landslide event to occur makes it be the largest landslide that happens in the world. The event took place in April 2013 causes losses of profit in the corresponding mining industry that runs the mine on site. The loss profit comes from the decreasing mining and processing capacity each day and the significant amount of cost that spent to rehabilitate the area that caused by the landslide. Regarding to safety, numerical modelling seems to be able to predict the run-out and the zone of an impact that affected by the landslide. Safety assessment is required for the areas that potentially affected by the landslide. The possible area that affected by the landslide illustrated in Figure 57.

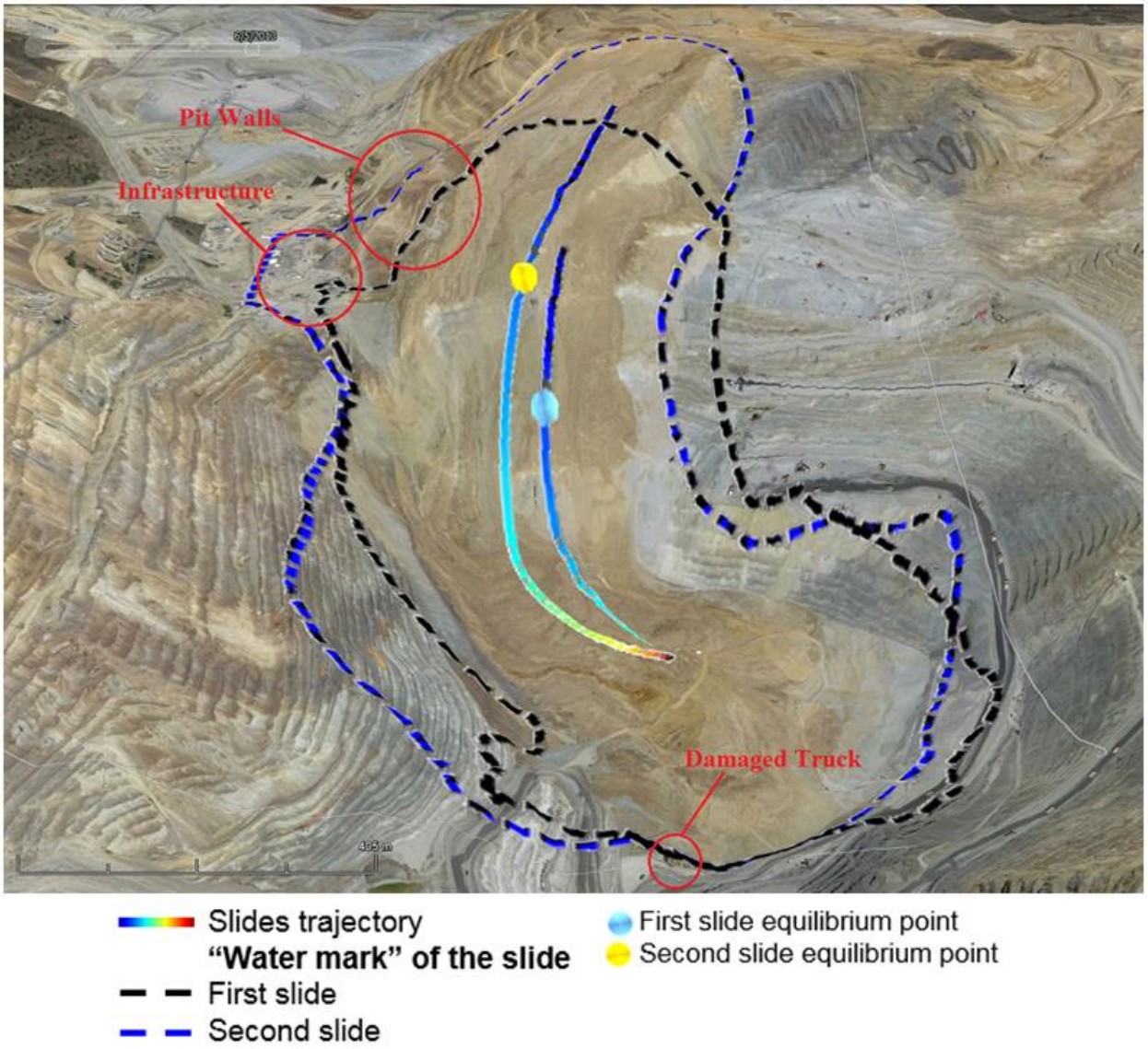

Figure 57. Areas that affected by the landslide

As shown in Figure 57, three-dimensional MPM is capable to identifing the areas that affected by the landslide zone from the slide trajectory line. The three major areas that damaged and achieved by three-dimensional MPM includes:

- damaged truck;
- infrastructure; and
- pit walls.

As mentioned in Section 1.3, it is important to assess further for potential hazards that may happen after a large event took place to improve the safety, taking into account the hazards and vulnerabilities as part of safety assessment to minimise risk, and to be able to predict future hazards accurately using many approaches including numerical analysis.

8. RISK ASSESSMENT

8.1. INTRODUCTION

The completion of this research project is dependent on each component of the project completed on time and to a high standard. Given the large period associated with the project, it is crucial that a risk assessment be undertaken, outlining any possible hazards that may prevent the completion of individual components or the project as a whole. The risk assessment will cover hazards affecting the completion of the final project and will cover possible hazards that encountered while on site collecting data. Figure 58 shows a risk management matrix, based on the impact and cause of each potential hazard. Table 12 and 13 shows the categories of impact and consequence.

Impact	Consequences				
	A - Insignificant	B - Minor	C - Moderate	D - Major	E - Severe
1 - Almost Certain	M	H	H	E	E
2 - Likely	M	M	H	H	E
3 - Possible	L	M	M	H	E
4 - Unlikely	L	M	M	M	H
5 - Rare	L	L	M	M	H

Figure 58. Risk management matrix (Risk Management Group, 2015)

Table 12.

Definition of hazard impact categories (Risk Management Group, 2015)

Level	Description	Definition
1	Almost certain	Occur in most circumstances
2	Likely	Probably occur in most circumstances
3	Possible	Could occur at some time
4	Unlikely	Not expected to occur
5	Rare	Occur at exceptional circumstances only

Table 13.

Definition of hazard consequence categories (Risk Management Group, 2015)

Level	Description	Definition
A	Insignificant	No impact on project completion
B	Minor	Slight time loss, minor reduction in project quality
C	Moderate	Major time loss, significantly reduced project quality
D	Major	Late submission of project - Loss of marks
E	Severe	Unable to complete project at all, or to a satisfactory standard

8.2. HAZARDS AFFECTING PROJECT COMPLETION

As seen in Table 14 are the identified hazards that could have an effect on project completion, the table shows the risk rating of each hazard as identified using the risk assessment matrix.

Table 14.

Hazards relating to project completion and their respective risk ratings

Hazard	Impact	Consequence	Risk Rating
Lost time due to sickness of injury	Possible	Minor	Moderate
Failure to protect commercially sensitive information	Unlikely	Major	Moderate
Failure of data storage	Possible	Severe	Extreme
Traffic delays	Likely	Major	High
Insufficient reference material	Possible	Major	High
Poor quality work	Unlikely	Major	Moderate

8.3. HAZARDS RELATING TO DATA COLLECTION FOR PROJECT

Seen in Table 15 are identified hazards relating to time spent in Brisbane on site. Table also shows the risk rating of each hazard as identified using the risk assessment matrix.

Table 15.

Hazards identified for data collection phase and their representative risk ratings

Hazard	Impact	Consequence	Risk Rating
Missing trip due to sickness or injury	Unlikely	Moderate	Moderate
Lost time due to injury to self on site	Possible	Minor	Moderate
Traffic delays	Possible	Major	High
Requested data not available	Unlikely	Major	Moderate
Supervisor not available for consultation	Unlikely	Major	Insignificant

8.4. FTA (FAULT TREE ANALYSIS)

A fault tree analysis (FTA) was also to be constructed for this project. An FTA is another risk assessment tool, which identifies models and evaluates the unique interrelationships of events leading to (Risk Management Group, 2015):

- Undesired events/states
- Unintended events/states
- Failure

The fault tree analysis separated into two broad events that would lead to the project research not being completed. These were failure to complete supplementary MINE4122/3 course work and failure to complete work on the project itself. Supplementary work included the project proposal, annotated bibliography, progress report, and consultation with supervisors, seminar, and the final submission of the research project. From these two broad categories, reasons for not completing the work or not it to satisfactory standard derived. The fault tree for this research project is seen in Figure 59.

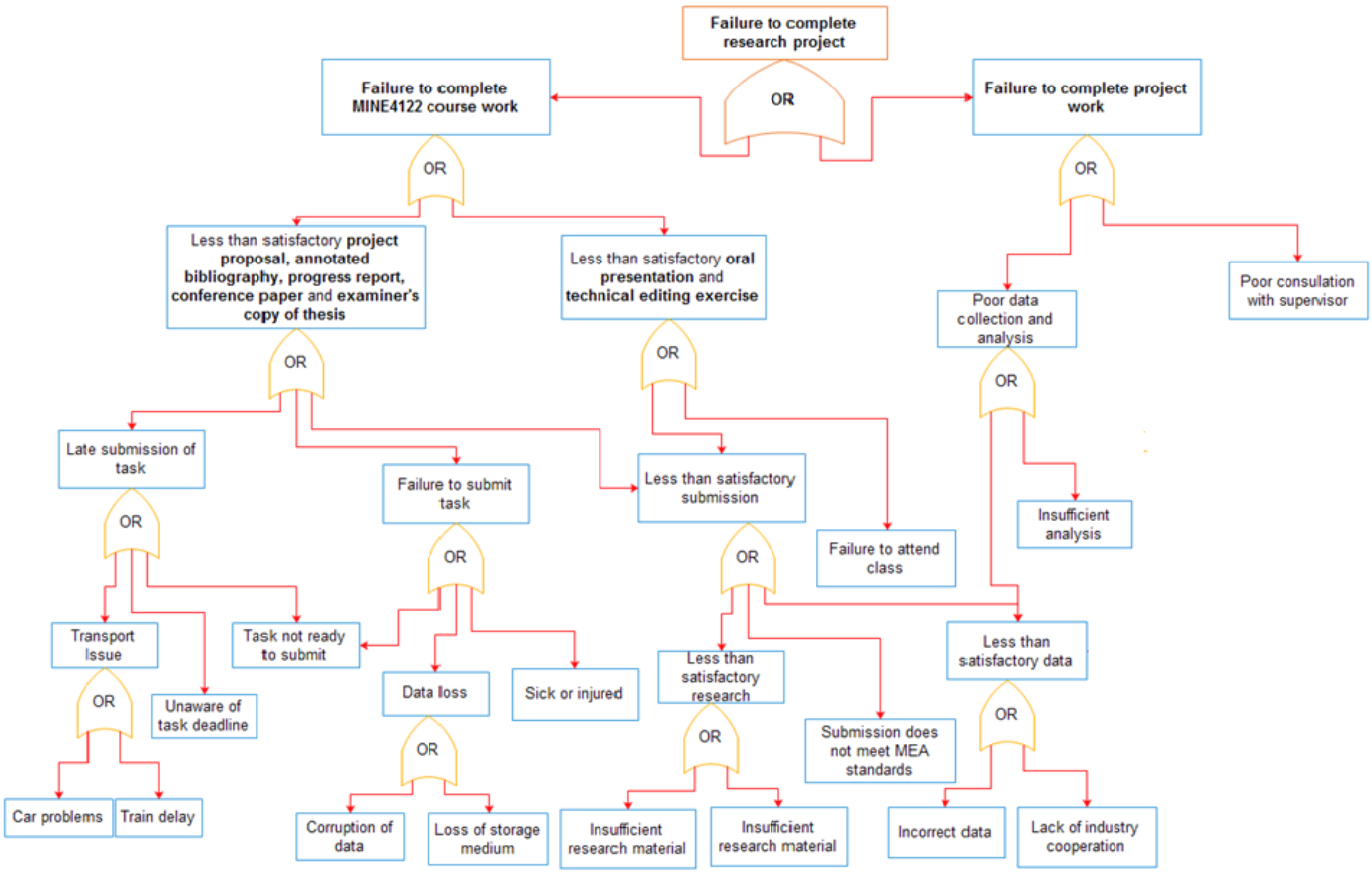

Figure 59. Fault tree analysis

8.5. CONTINGENCY PLANS

Based on the hazards identified using the hazard management matrix and the fault tree analysis, contingency plans were developed. Seen in Table 16 are contingency plans for hazards relating directly to project completion, and seen in Table 17 are contingency plans relating to the data collection phase of the project.

Table 16.

Control for identified hazards relating to project

Hazard	Risk Rating	Control
Lost time due to sickness of injury	Moderate	Ensure regular rest and healthy eat to stay in good health
Failure to protect commercially sensitive information	Moderate	Ensure thesis is not published to library
Failure of data storage	Extreme	Back files up to USB and computer hard drive
Traffic delays	High	Allow more time to gather the data
Insufficient reference material	High	Allow time for literature research and consultation
Poor quality work	Moderate	Apply self-work of high quality and proof read by peers

Table 17.

Control for identified hazards relating to data collection

Hazard	Risk Rating	Control
Requested data not available	Moderate	Ensure communication with the supervisor to ensure requested data will be available
Supervisor not available for consultation	Moderate	Ensure communication with the supervisor to arrange meetings based on their availability to ensure requested data will be available

9. CONCLUSION AND RECOMMENDATION

The relevance of this analysis relies on the potential of defining a framework of actions that may give insights on the preparation to attend the operative needs in a failed slope and mitigate its negative effects. The volumes of the first and second failure are approximately 24Mm^3 and 22Mm^3 with 0.98 and 0.89 for FOS respectively. These outputs will be a good indication for the authors to build and design the numerical modelling and analysis with MPM to observe the kinematic behaviour of the mass that moves during the landslide event in Bingham Canyon mine.

The kinetic energy computed for the first slide presented, which shows the progression of the energy during run-out. The kinetic energy increases with time until the slide hits the northwestern pit wall at t=20 s, reaching values of up to 10^7 Joule. Additionally, similar to the first slide, the second slide gives a maximum kinetic energy of 10^7 Joule at t=30 s due to the fall of the sliding material from its original position to the void created by the first slide. The major findings comparing the first result to the second result is the value of kinetic energy is constant on the second failure while there is a decrease in the kinetic energy on the first slide both at t=30 s.

The computed peak velocities for the second slide are within 5 m/s, while for the first slide, the two-dimensional MPM and LFH peak velocities are in close agreement. The three-dimensional MPM peak velocity for the first slide is about 15 m/s lower than the other two computed results. This happens because the particles sliding down the north-eastern pit wall hit the north-western pit wall, reversing the movement and slowing the slide. This observation highlights the importance of considering three-dimensional effects in complex cases. The reversal of movement is not present in the second slide since the movement is smoother compared with the first slide.

Sensitivity analysis conducted by changing the geotechnical properties of the failure surfaces to observe the changes that will affect the run-out of the landslide. The geotechnical properties that modified were yield, modulus, Poisson's ratio, masses of the failure particles, and friction. Sensitivity analysis conducted by analysing the graphical output from the changes of the geotechnical properties. This gives more findings on the kinematics of the run-out such as the velocity, and kinetic energy. The changing of yield and modulus gives large impact on the velocity on both first and second failures.

The trajectory analysis seem to be more accurate compare with the past research that has been done by Hilbert et al due to different approach input to obtain the input data. This gives different

results and analyses. Using the numerical approach, it resulted more accurate findings, and it is valid comparing to the past research in two-dimensional approach.

The tridimensional approach seem to be able to describe better due to complex topography than two-dimensional simplifications. Another major finding that discovered involves the application of three-dimensional analysis to the real case study for further analysis and validation. MPM seem to be suitable to solve real scale events. It can potentially use to improve risk assessment in the mining industry.

9.1. RECOMMENDATION

- it is required to use the updated DEM file for the case study due to the topography that used in this thesis is from 2007 for more accurate results and interpretation;
- more numerical methods on case study need to be conducted to validate and increase the accuracy of the result or replicate what actually happen on the event;
- using another search method for geotechnical modelling to compare the FOS results with the other search method;
- update the development of the software "*NairnMPM*" to increase the user efficiency to achieve the desired results;
- improve the input file for 3D mode in "*NairnMPM*" software, especially the input code of "matname" for 3D mode and "mpelem" for 2D mode;
- improve the material definition for "rigid body" to be visible and without any bugs/error for 3D mode;
- more choices of modification of input variables to gives more findings in sensitivity analysis;
- more kinematics observation such as force, momentum, etc;
- more approach on sensitivity analysis with the modification of input variables, such as friction and mass of the failure material points/particles; and
- practically used the numerical analysis to give insight in predicting the possible failure that might occur on site, to help assess the risk assessment and safety.

10. REFERENCES

AGU Blogosphere, 2013. Analysing the Bingham Canyon Mine Landslide Part 2: The Landslide Track [online]. Available from: < http://blogs.agu.org/landslideblog/2013/05/06/analysing-the-bingham-Canyon-mine-landslide-part-2-the-landslide-track/ > [Accessed: 06 Mar 2016].

Albataineh, N, 2006. Slope Stability Analysis using 2D and 3D Methods [online]. Available from < https://etd.ohiolink.edu/rws_etd/document/get/akron1153719372/inline > [Accessed: 06 April 2016].

Bhandari et al, 2016. Numerical modelling of seismic slope failure using MPM, *Computer and Geotechnics*, 75:126-134.

Blasio, F V D, 2011. Introduction to the Physics of Landslides [online]. Available from: < http://link.springer.com/book/10.1007%2F978-94-007-1122-8 > [Accessed: 06 Mar 2016].

Brannon, R M, 2014. A beginner's introduction to the material point method (MPM). Conference Training Lecture delivered at Computational Solid Mechanics Group, The University of Utah, 16 May.

Dai, F C Lee, C F, and Ngai, Y Y, 2002. Landslide risk assessment and management: an overview, *Engineering Geology*, 64:65-87.

Fredlund, D G, and Krahn, J, 1977. Comparison of slope stability methods of analysis, *Canadian Geotechnical Journal*, 14(3):429-439.

Gruen, G Heinrich, C A, and Schroeder, K, 2010. The Bingham Canyon Porphyry Cu-Mo-Au Deposit II Vein Geometry and Ore Shell Formation by Pressure Driven Rock Extension [online]. Available from: < http://economicgeology.org/content/105/1/69.full.pdf > [Accessed: 06 Mar 2016].

Highland, L M, and Bobrowsky, P, 2008. The Landslide Handbook, A Guide to Understanding Landslides [online]. Available from: < http://pubs.usgs.gov/circ/1325/pdf/C1325_508.pdf > [Accessed: 06 Mar 2016].

Hilbert, C Ekstrom, G, and Stark, C P, 2014. Dynamics of the Bingham Canyon Mine Landslides from Seismic Signal Analysis [online]. Available from: < http://onlinelibrary.wiley.com/doi/10.1002/2014GL060592/full > [Accessed: 06 Mar 2016].

Huang, C C, and Tsai, C C, 2000. New method for 3D and asymmetrical slope stability analysis, *Journal of Geotechnical and Geoenvironmental Engineering*, 126(10):917-927.

Hume, H R, 1983. Geotechnical Slope Stability Analysis, B&G Sector, Bingham Canyon Open Pit, Utah, with a Consequent Investigation of Methods for Delineating Rock Mass Fracture Domains [online]. Available from: < http://docs.lib.purdue.edu/dissertations/AAI8400369/ > [Accessed: 06 Mar 2016].

Hungr, O Salgado, F M, and Byrne, P M, 1989. Evaluation of a three dimensional method of slope stability analysis, *Canadian Geotechnical Journal*, 26(4):679-686.

Jakob, M, and Hungr, O, 2005. *Debris-flow Hazards and Related Phenomena*. pp 339-358 (Praxis: Germany).

Keefer, D K, 1984. Landslides caused by earthquakes, *Geological Society of America Bulletin*, 95:406-421.

Lam, L, and Fredlund, D G, 1993. A general limit equilibrium model for three-dimensional slope stability analysis, *Canadian Geotechnical Journal*, 30(6):905-919.

Landtwing et al, 2010. The Bingham Canyon Porphyry Cu-Mo-Au Deposit III Zoned Copper-Gold Ore Deposition by Magmatic Vapor Expansion [online]. Available from: < http://economicgeology.org/content/105/1/91.full.pdf > [Accessed: 06 Mar 2016].

Lanier et al, 1978. General Geology of the Bingham Mine, Bingham Canyon, Utah [online]. Available from: < http://economicgeology.org/content/73/7/1228.full.pdf > [Accessed: 06 Mar 2016].

McDougall, S, and Hungr, O, 2004. A model for the analysis of rapid landslide motion across three-dimensional terrain, *Canadian Geotechnical Journal*, 41:1084-1097.

Monde Geospatial, 2015. *Create contours and DEM using google earth and QGIS 2.10*, online video. Available from: < https://www.youtube.com/watch?v=bLbY3iMBW-A > [Accessed: 03 March 2016].

Michalowski, R L, and F.ASCE, 2010. Limit analysis and stability charts for 3D slope failures, *Journal of Geotechnical and Geoenvironmental Engineering*, 136(4):1-11.

Nairn, J A, 2003. Material point method calculations with explicit cracks, *CMES*, 4(6):649-663.

Nguyen, V P Cardiff University, 2014. Material point method: basics and applications contents [online], *ResearchGate*. Available from: < https://www.researchgate.net/publication/262415477_Material_point_method_basics_and_applications_Contents > [Accessed: 06 Mar 2016].

Novotny, J, 2013. Varnes Landslide Classification [online]. Available from: < http://www.geology.cz/projekt681900/vyukove-materialy/2_Varnes_landslide_classification.pdf > [Accessed: 06 Mar 2016].

Ortigao, J A R, and Sayao, A S, 2004. *Handbook of Slope Stabilisation*, pp 27-66 (Springer: Berlin).

Pankow et al, 2013. Massive landslide at utah copper mine generates wealth of geophysical data, *GSA Today*, 24(1):4-9.

Pastor et al, 2008. A depth integrated coupled SPH model for flow like landslides and related phenomena, *Wiley InterScience*, 33:143-172.

Pierce, M Gaida, M, and DeGagne, D, 2009. Estimation of Rock Block Strength [online]. Available from: <http://www.geogroup.utoronto.ca/wp-content/uploads/rockeng09/Session8/4360%20PAPER.pdf > [Accessed: 06 Mar 2016].

Pirulli, M, and Pastor, M, 2012. Numerical study on the entrainment of bed material into rapid landslides, *Geotechnique*, 62(11):959-972.

Prochaska et al, 2008. A study of methods to estimate debris flow velocity. *Springer-Verlag*, 5:431-444.

Prochaska et al, 2008. Debris flow run out predictions based on the average channel slope (ACS). *Engineering Geology*, 98:29-40.

Reid et al, 2015. *Scoops3D-software to analyse three-dimensional slope stability throughout a digital landscape,* pp 43-153 (USGS: Virginia). Available from: < http://pubs.usgs.gov/tm/14/a01/pdf/tm14-a1.pdf > [Accessed: 03 March 2016].

Rio Tinto, 2009. Kennecott Utah Copper's Bingham Canyon Mine Teacher Guide [online]. Available from: < http://www.kennecott.com/library/media/TeacherGuide.pdf > [Accessed: 06 Mar 2016].

Serna, M A L Farias, M, and Pedroso, D M, 2015. An assessment of the material point method for modelling large scale run-out processes in landslides [online], *Springer-Verlag Berlin Heidelberg 2015*. Available from: < http://link.springer.com/article/10.1007/s10346-015-0664-4 > [Accessed: 06 Mar 2016].

Shandyba, A B, 2015. Application of Lagrangian methods for optimization of interaction in aquatic systems [online], *ICE Virtual Library.* Available from: < http://www.icevirtuallibrary.com/doi/pdf/10.1680/teonratc.30046.0013 > [Accessed: 29 Apr 2016].

Shea, T, and Vries, B V T W D, 2008. Structural Analysis and Analogue Modelling of the Kinematics and Dynamics of Rockslide Avalanches [online]. Available from: < http://geosphere.gsapubs.org/content/4/4/657.short > [Accessed: 06 Mar 2016].

Soga et al, 2016. Trends in large deformation analysis of landslide mass movements with particular emphasis on the material point method, *Geotechnique*, 66(3):248-273.

Styles, T, 2011. Integrated numerical modelling and insar monitoring of a slow moving slope instability at Bingham Canyon mine, in *Proceedings of Slope Stability 2011: International Symposium on Rock Slope Stability in Open Pit Mining and Civil Engineering*, Vancouver, Canada, 18-21 Sep, pp 3-7 (ResearchGate).

Sutherlin, C, 2014. Lessons from Kennecott Utah copper's manefay slide. Conference Training Lecture delivered at 2014 Mine Design, Operations & Closure at Rio Tinto, Rio Tinto, April.

Whittall, J R, 2015. Runout Exceedance Prediction for Open Pit Slope Failures [online]. Available from: < https://open.library.ubc.ca/cIRcle/collections/ubctheses/24/items/1.0166590 > [Accessed: 11 Apr 2016].

Zhang, Z, and Chen, Q, 2007. Comparison of the eulerian and lagrangian methods for predicting particle transport in enclosed spaces, *Atmospheric Environment*, 41(25):5236-5248.

APPENDIX A - SCOOP INPUT FILE

FAILURE 1

title

Fail_1

lengthunits ceeunits gammaunits

m kPa kN/m^3

water

no

nmat

1

lnum cee phi gamt

1 3 16 24.4

eq

0

method

B

srch

single

xcen ycen zcen rad angle

1200 950 2490 650 150

remove foscut

N 10

isqout

1

irelfos

1

icritlattice

1

isubsurf zfrac

2 1

DEM file

C:\Users\alfre\Desktop\Scoop_200416\DEM_ori_200416.asc

output directory

C:\Users\alfre\Desktop\Scoop_200416\Fail_1_output\

FAILURE 2

title

Fail_2

lengthunits ceeunits gammaunits

m kPa kN/m^3

water

no

nmat

1

lnum cee phi gamt

1 3 16 24.4

eq

0

method

B

srch

single

xcen ycen zcen rad angle

1600 850 2500 565 130

remove foscut

M 10

isqout

1

irelfos

1

icritlattice

1

isubsurf zfrac

2 1

DEM file

C:\Users\alfre\Desktop\Scoop_200416\DEM_Fail_1_200416.asc

output directory

C:\Users\alfre\Desktop\Scoop_200416\Fail_2_output\

APPENDIX B – MATLAB CODE

MPM BASE MATLAB CODE

```
%% Extract the data
clear all;
filename = 'DEM_Fail_2_200416.asc';
M_struct = importdata(filename, ' ',6); % Reads data after line 6

% Added flipud here, flipping the Z upside down
Z = flipud(M_struct.data()); % Convert from struct to matrix data

%% Calculate x and y coordinates based on cell size
[row col] = size(Z);
c = 20; % cellsize

% X is row, and Y is column
X = [1:row]*c - c/2;
Y = [1:col]*c - c/2;

%% Create 3 coordinate data-points vectors in terms of T = [x; y; z;]
[s_rX s_cX] = size(X);
[s_rY s_cY] = size(Y);
Yrep = repmat(X, 1, s_cY); % Repeat Y by length of column X times, horz
Xrep = repmat(Y, s_cX, 1); % Repeat X by length of column Y times, vert
[u v] = size(Xrep);
Xrep = reshape(Xrep, 1, u*v); % Reshape Xrep to 1-by-N matrix
Zrep = reshape(Z, 1, row*col)'; % Reshape Z into N-by-1 matrix

%% Plots
% Surf plot
figure(1);
surf(Y,X,Z);
axis tight;

% Set scale and lock it
set(gca,'XTick',[0:300:max(Y)]);
set(gca,'YTick',[0:200:max(X)]);
set(gca,'ZTick',[0:50:max(max(Z))]);

% Scatter plot
figure(2);
scatter3(Xrep,Yrep,Zrep);
axis tight;

%% Extract Data to NairnFEAMPM string format
F = [Xrep' Yrep' (Zrep-20)]; % Data in [x y z] format
u = length(F);
str_mpelem = 9010:1:u*2; % Create mp elem string from 1 to the number of data
in F
str_mat = repmat([1],u,1);
str_angle = zeros(u,1);
str_thick = repmat([1],u,1);
str_ptu = 'm';
str_vel = 'mm/sec';
v_x= '0';
v_y= '0';
v_z= '0';
```

```
str_mass = 'kg';
str_kg = '82000000';

fname = 'NairnFEAMPM_Base_BL.txt';
fileID = fopen(fname,'w');
for k = 1:1:u
    FEAMP_str = ['<mp elem=''' num2str(str_mpelem(k)) ''' ' ...
        'mat=''' num2str(str_mat(k)) ''' '...
        'angle=''' num2str(str_angle(k)) ''' '...
        'thick=''' num2str(str_thick(k)) '''>' '\n'...
        '<pt units=''' str_ptu ''' '...
        'x=''' num2str(F(k,1)) ''' '...
        'y=''' num2str(F(k,2)) ''' '...
        'z=''' num2str(F(k,3)) ''' ' '/>' '\n'...
        '<vel units=''' str_vel ''' '...
        'x=''' v_x ''' '...
        'y=''' v_y ''' '...
        'z=''' v_z ''' ' '/>' '\n'...
        '<mass units=''' str_mass ''' '...
        'm=''' num2str(str_kg) ''' ' '/>' '\n'...
        '</mp> \n'];
    fstring = sprintf(FEAMP_str);
    fprintf(fileID,fstring);
    disp(fstring);
end
fclose(fileID);
```

MPM FAILURE 1 MATLAB CODE

```
clear all;
%% Extract the data
filename = 'DEM_Fail_1.asc';
M_struct = importdata(filename, ' ',6); % Reads data after line 6

% Added flipud here, flipping the Z upside down
Z = flipud(M_struct.data()); % Convert from struct to matrix data

%% Extract the data
filename = 'DEM_Ori.asc';
M_struct2 = importdata(filename); % Reads data after line 6

% Added flipud here, flipping the Z1 upside down
Z1 = flipud(M_struct2.data()); % Convert from struct to matrix data

%% Calculate x and y coordinates based on cell size
[row col] = size(Z);
c = 20; % cellsize

% X is row, and Y is column
X = [1:row]*c - c/2;
Y = [1:col]*c - c/2;

%% Create 3 coordinate data-points vectors in terms of T = [x; y; z;]
[s_rX s_cX] = size(X);
[s_rY s_cY] = size(Y);
Yrep = repmat(X, 1, s_cY); % Repeat Y by length of column X times, horz
Xrep = repmat(Y, s_cX, 1); % Repeat X by length of column Y times, vert
[num_elem v] = size(Xrep);
```

```
Xrep = reshape(Xrep, 1, num_elem*v); % Reshape Xrep to 1-by-N matrix
Zrep = reshape(Z, 1, row*col)'; % Reshape Z into N-by-1 matrix

%% Plots
% Surf plot
% figure(1);
% surf(Y,X,Z);
% axis tight;
%
% % Set scale and lock it
% set(gca,'XTick',[0:300:max(Y)]);
% set(gca,'YTick',[0:200:max(X)]);
% set(gca,'ZTick',[0:50:max(max(Z))]);
%
% % Scatter plot
% figure(3);
% scatter3(Xrep,Yrep,Zrep);
% axis tight;

%% Defining Material Failure Surfaces/Fill the Holes
A = round(abs(Z-Z1)./c);

% Get index of A that is greater than zero
ind = find(A > 0);
[ind_row, ind_col] = ind2sub(size(A),ind);

% Perform calculation, and construct X, Y, Z matrix of the Hole
X1 = ind_row*c - c/2;
Y1 = ind_col*c - c/2;
Z1 = Z(ind) + A(ind)*c;
B = [X1 Y1 Z1];

%% Extract Data to NairnFEAMPM string format
F = [B(:,2) B(:,1) B(:,3)]; % Data in [x y z] format
num_elem = length(F); % Number of elements needed to be created
num_start = 18019; % Start material numbering from...
num_end = num_start + num_elem;
str_mpelem = num_start:1:num_end; % Create mp elem string from 1 to the number
of data in F
str_mat = repmat([3],num_elem,1);
str_angle = zeros(num_elem,1);
str_thick = repmat([1],num_elem,1);
str_ptu = 'm';
str_vel = 'mm/sec';
v_x= '0';
v_y= '0';
v_z= '0';
str_mass = 'kg';
str_kg = '82000000';

fname = 'NairnFEAMPM_Fail1.txt';
fileID = fopen(fname,'w');
for k = 1:1:num_elem
    FEAMP_str = ['<mp elem=''' num2str(str_mpelem(k)) ''' ' ...
        'mat=''' num2str(str_mat(k)) ''' '...
        'angle=''' num2str(str_angle(k)) ''' '...
        'thick=''' num2str(str_thick(k)) '''>' '\n'...
        '<pt units=''' str_ptu ''' '...
        'x=''' num2str(F(k,1)) ''' '...
        'y=''' num2str(F(k,2)) ''' '...
```

```
        'z=''' num2str(F(k,3)) ''' ' '/>' '\n'...
        '<vel units=''' str_vel ''' '...
        'x=''' v_x ''' '...
        'y=''' v_y ''' '...
        'z=''' v_z ''' ' '/>' '\n'...
        '<mass units=''' str_mass ''' '...
        'm=''' num2str(str_kg) ''' ' '/>' '\n'...
        '</mp> \n'];
    fstring = sprintf(FEAMP_str);
    fprintf(fileID,fstring);
    disp(fstring);
end
fclose(fileID);
```

MPM FAILURE 2 MATLAB CODE

```
clear all;
%% Extract the data
filename = 'DEM_Fail_2.asc';
M_struct = importdata(filename, ' ',6); % Reads data after line 6

% Added flipud here, flipping the Z upside down
Z = flipud(M_struct.data()); % Convert from struct to matrix data

%% Extract the data
filename = 'DEM_Fail_1.asc';
M_struct = importdata(filename, ' ',6); % Reads data after line 6

% Added flipud here, flipping the Z1 upside down
Z1 = flipud(M_struct.data()); % Convert from struct to matrix data

%% Calculate x and y coordinates based on cell size
[row col] = size(Z);
c = 20; % cellsize

% X is row, and Y is column
X = [1:row]*c - c/2;
Y = [1:col]*c - c/2;

%% Create 3 coordinate data-points vectors in terms of T = [x; y; z;]
[s_rX s_cX] = size(X);
[s_rY s_cY] = size(Y);
Yrep = repmat(X, 1, s_cY); % Repeat Y by length of column X times, horz
Xrep = repmat(Y, s_cX, 1); % Repeat X by length of column Y times, vert
[num_elem v] = size(Xrep);
Xrep = reshape(Xrep, 1, num_elem*v); % Reshape Xrep to 1-by-N matrix
Zrep = reshape(Z, 1, row*col)'; % Reshape Z into N-by-1 matrix

%% Plots
% Surf plot
% figure(1);
% surf(Y,X,Z);
% axis tight;
%
% % Set scale and lock it
% set(gca,'XTick',[0:300:max(Y)]);
% set(gca,'YTick',[0:200:max(X)]);
% set(gca,'ZTick',[0:50:max(max(Z))]);
%
```

```
% % Scatter plot
% figure(3);
% scatter3(Xrep,Yrep,Zrep);
% axis tight;

%% Defining Material Failure Surfaces/Fill the Holes
A = round(abs(Z-Z1)./c);

% Get index of A that is greater than zero
ind = find(A > 0);
[ind_row, ind_col] = ind2sub(size(A),ind);

% Perform calculation, and construct X, Y, Z matrix of the Hole
X1 = ind_row*c - c/2;
Y1 = ind_col*c - c/2;
Z1 = Z(ind) + A(ind)*c;
B = [X1 Y1 Z1];

%% Extract Data to NairnFEAMPM string format
F = [B(:,2) B(:,1) B(:,3)]; % Data in [x y z] format
num_elem = length(F); % Number of elements needed to be created
num_start = 18879; % Start material numbering from...
num_end = num_start + num_elem;
str_mpelem = num_start:1:num_end; % Create mp elem string from 1 to the number
of data in F
str_mat = repmat([3],num_elem,1);
str_angle = zeros(num_elem,1);
str_thick = repmat([1],num_elem,1);
str_ptu = 'm';
str_vel = 'mm/sec';
v_x= '0';
v_y= '0';
v_z= '0';
str_mass = 'kg';
str_kg = '82000000';

fname = 'NairnFEAMPM_Fail2.txt';
fileID = fopen(fname,'w');
for k = 1:1:num_elem
    FEAMP_str = ['<mp elem=''' num2str(str_mpelem(k)) ''' ' ...
        'mat=''' num2str(str_mat(k)) ''' '...
        'angle=''' num2str(str_angle(k)) ''' '...
        'thick=''' num2str(str_thick(k)) '''>' '\n'...
        '<pt units=''' str_ptu ''' '...
        'x=''' num2str(F(k,1)) ''' '...
        'y=''' num2str(F(k,2)) ''' '...
        'z=''' num2str(F(k,3)) ''' ' '/>' '\n'...
        '<vel units=''' str_vel ''' '...
        'x=''' v_x ''' '...
        'y=''' v_y ''' '...
        'z=''' v_z ''' ' '/>' '\n'...
        '<mass units=''' str_mass ''' '...
        'm=''' num2str(str_kg) ''' ' '/>' '\n'...
        '</mp> \n'];
    fstring = sprintf(FEAMP_str);
    fprintf(fileID,fstring);
    disp(fstring);
end
fclose(fileID);
```

APPENDIX C – VISUAL INTERPRETATION ON SECOND FAILURE

YIELD +50% (LEFT) AND -50% (RIGHT)

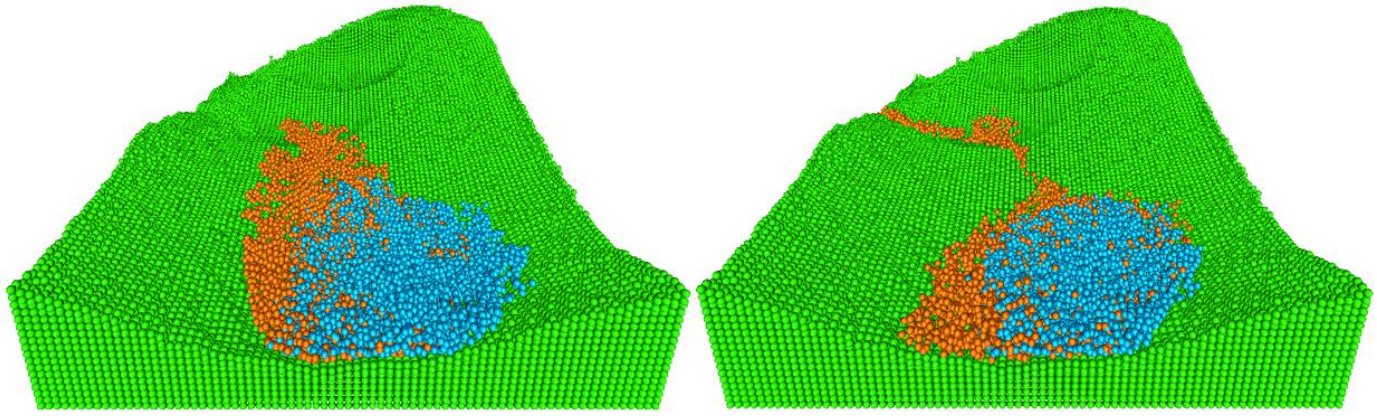

MODULUS +50% (LEFT) AND -50% (RIGHT)

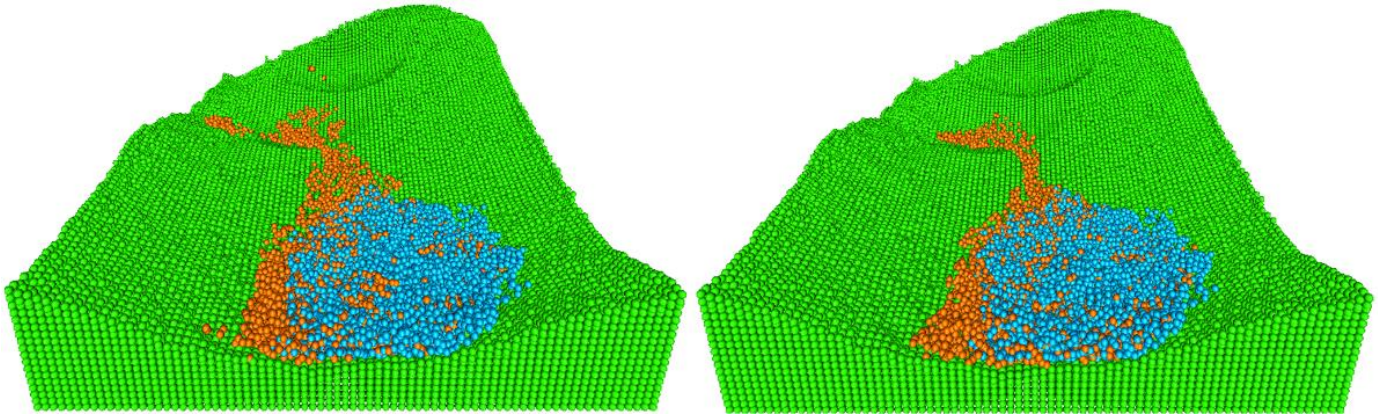

POISSON'S RATIO +50% (LEFT) AND -50% (RIGHT)

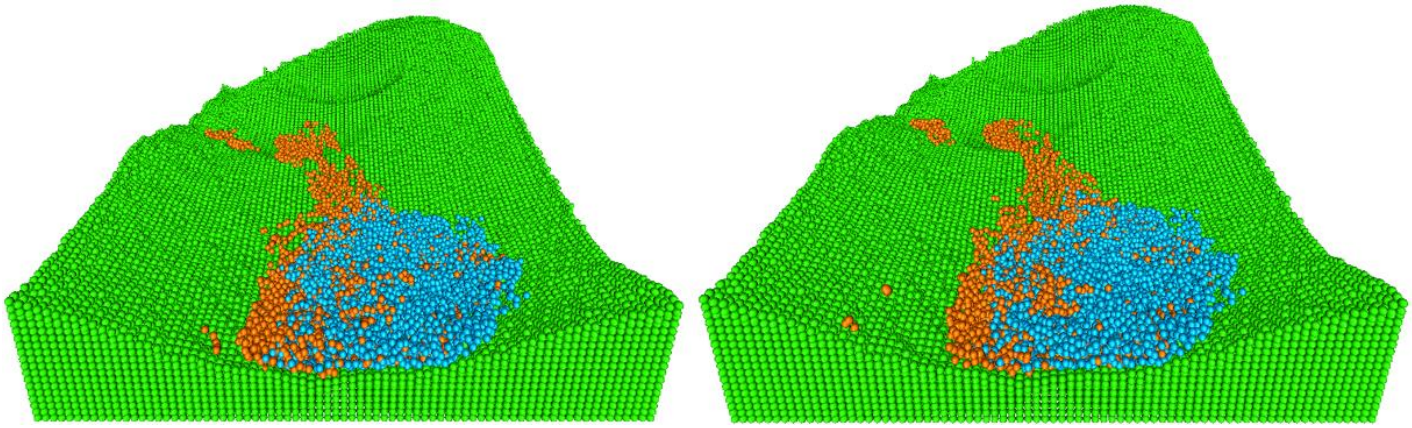

MASSES +10% (LEFT) AND -10% (RIGHT)

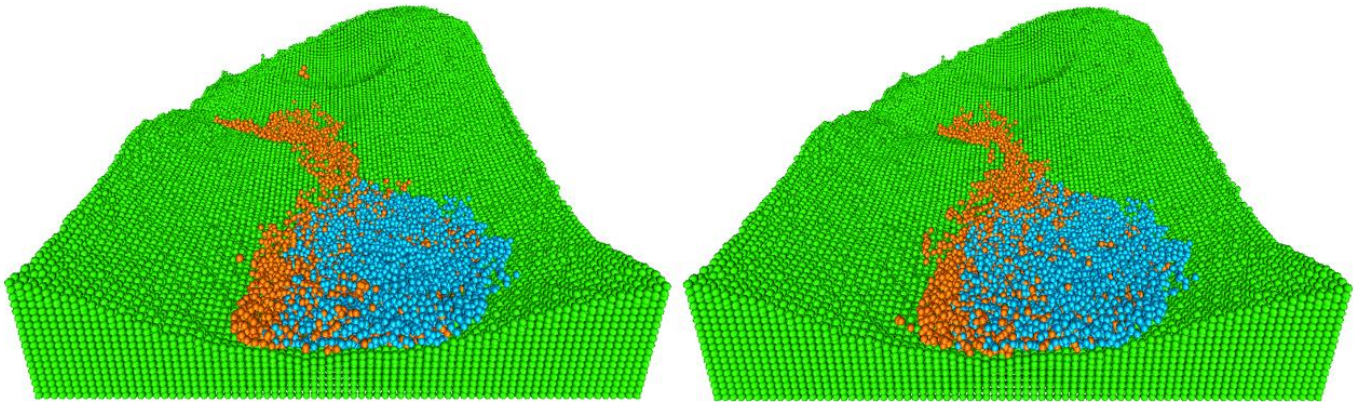

FRICTION +10% (LEFT) AND -10% (RIGHT)